UNIVERSITY OF CINCINNATI

Date: January 10, 2006

I, Andrew B. Thien,

hereby submit this work as part of the requirements for the degree of:

Master of Science

in:

Mechanical Engineering

It is entitled:

Pipeline Structural Health Monitoring Using Macro-fiber Composite Active Sensors

This work and its defense approved by:

Chair: Dr. Randall J. Allemang

Dr. Gyuhae Park

Dr. David L. Brown

Dr. Allyn W. Phillips

Pipeline Structural Health Monitoring Using

Macro-fiber Composite Active Sensors

A thesis submitted to the
Division of Research and Advanced Studies
of the University of Cincinnati

in partial fulfillment of the
requirements for the Degree of

MASTER OF SCIENCE

from the Department of Mechanical, Industrial, and Nuclear Engineering
of the College of Engineering

2006

by

Andrew B. Thien

B.S.M.E., University of Cincinnati, 2003

Committee Chair:	Dr. Randall J. Allemang, University of Cincinnati
Committee:	Dr. Gyuhae Park, Los Alamos National Laboratory
	Dr. David L. Brown, University of Cincinnati
	Dr. Allyn W. Phillips, University of Cincinnati

Abstract

The United States economy is heavily dependent upon a vast network of pipeline systems to transport and distribute the nation's energy resources. As this network of pipelines continues to age, monitoring and maintaining its structural integrity remains essential to the nation's energy interests. Numerous pipeline accidents over the past several years have resulted in hundreds of fatalities and billions of dollars in property damages. These accidents show that the current monitoring methods are not sufficient and leave a considerable margin for improvement. To avoid such catastrophes, more thorough methods are needed.

As a solution, the research of this thesis proposes a structural health monitoring (SHM) system for pipeline networks. By implementing a SHM system with pipelines, their structural integrity can be continuously monitored, reducing the overall risks and costs associated with current methods. The proposed SHM system relies upon the deployment of macro-fiber composite (MFC) patches for the sensor array. Because MFC patches are flexible and resilient, they can be permanently mounted to the curved surface of a pipeline's main body. From this location, the MFC patches are used to monitor the structural integrity of the entire pipeline.

Two damage detection techniques, guided wave and impedance methods, were implemented as part of the proposed SHM system. However, both techniques utilize the same MFC patches. This dual use of the MFC patches enables the proposed SHM system to require only a single sensor array. The presented Lamb wave methods demonstrated the ability to correctly identify and locate the presence of damage in the main body of the pipeline system, including simulated cracks and actual corrosion damage. The presented impedance methods demonstrated the ability to correctly identify and locate the presence of damage in the flanged

joints of the pipeline system, including the loosening of bolts on the flanges. In addition to damage to the actual pipeline itself, the proposed methods were used to demonstrate the capability of detecting deposits inside of pipelines. Monitoring these deposits can prevent clogging and other hazardous situations.

Finally, suggestions are made regarding future research issues which are needed to advance this research. Because the research of this thesis has only demonstrated the feasibility of the techniques for such a SHM system, these issues require attention before any commercial applications can be realized.

Acknowledgments

Many people were involved in the work to develop this thesis into its final form, and I am extremely thankful for their efforts in assisting me. Their help made this work possible, and I could not begin to take sole credit for the work and accomplishments presented in this thesis.

First, I would like to thank the Los Alamos National Laboratory for funding my work and giving me the opportunity be a part of its research efforts. In particular, I thank Dr. Gyuhae Park for his continual guidance as my mentor at the Engineering Institute. He always helped me maintain a sense of humor when I needed to lighten up, and beyond the realm of my research, our numerous conversations together kept me motivated and helped me with making decisions about my future path in life. Also, I thank Dr. Charles Farrar who initially gave me the opportunity to join the Engineering Institute as a part of the Los Alamos Dynamics Summer School. It's truly amazing to see what impact a single summer program has had on my life and career. I thank Dr. Anthony Puckett for his patience and assistance with my work. His breadth of knowledge and insight into my work was extremely helpful. In addition, I would like to thank the many others at the Lab who provided invaluable assistance and guidance, including Dr. John Schultze, Mandy Rutherford, Dave Allen, Jeff Hylok, Amy Askin, and Miles Buechler.

Second, I would like to thank those at the University of Cincinnati who have helped me over the course of my time there. In particular, I thank the members of my thesis committee: Dr. Randall Allemang, Dr. David Brown, and Dr. Allyn Phillips. I give special thanks to Dr. Allemang for his openness and willingness as my advisor to provide me with guidance regarding my academic interests. Even at his busiest times, he was always warming and open to chatting with me, and I am very thankful for his insight and leadership with the FSAE team. I

thank Dr. Brown for his incredible ability to challenge me to learn and grow as a student, and I thank Dr. Phillips for his inspiring energy and enthusiasm for his work, especially as a teacher. I also thank Dr. Ed Berger for his incredible talent as a teacher and his assistance outside the classroom, particularly when I was a teaching assistant for Structures-Motion Lab.

Finally, I would like to thank my friends and family for their unwavering support. I thank my parents for providing me with opportunities in life that they never even had themselves. They have always had the highest expectations of me and have inspired me to always give my very best effort to make the most of the gifts I have been given. I firmly believe that everything in life is given and not taken, and for no gift am I more thankful than for the time I have shared with my wife, Sarah. God alone knows where I would be if our paths had never crossed.

Table of Contents

List of Figures

List of Tables

Chapter 1 Introduction

1.1 Motivation

1.1.1 Importance of pipeline integrity to U.S. energy supply

The economy of the United States is heavily dependent upon an extensive network of distribution and transmission pipelines to transport the country's energy sources. The single largest source of energy in the United States is petroleum, which includes oil and natural gas. With 40% of the energy coming from oil and 25% coming from natural gas, petroleum accounts for 65% of the energy consumed in the United States. (Office of Pipeline Safety, 2005a) The transportation of petroleum and its products relies heavily upon a vast network of pipelines spread across the country. Countless industries rely heavily upon the pipeline infrastructure for the supply and distribution of required materials. In the United States alone, over two million miles (3.2 million-km) of oil pipelines are responsible for the transportation of crude oil and refined products, accounting for nearly 66% of the transportation of domestic products. In addition, there are over 1.4 million-miles (2.3 million-km) of natural gas pipelines in the United States. (U.S. National Energy Policy, 2001) Without pipelines, maintaining the current supply of energy to the industries and communities of the country would be nearly impossible.

As the extensive network of pipelines in the United States continues to age, monitoring and maintaining its structural integrity and reliability becomes more and more essential to the nation's energy requirements. (Posakony and Hill, 1992) Pipelines are susceptible to a wide variety of damage and aging defects. Some of the most common causes of failure in pipelines are corrosion, stress cracks, seam weld cracks, material flaws, and externally induced damage by

excavation equipment. In 2002 and 2003 combined, corrosion accounted for over 25% of all reported incidents involving transmission lines. In addition, failure of welded joints accounted for over 16%, and damage as a result of excavation accounted for over 15%. (Office of Pipeline Safety, 2005b) Over the same time span (2002 and 2003), the total cost of property damages from all incidents exceeded $147 million. Between 1986 and 2005, the total estimated property losses from reported incidents with natural gas or hazardous liquid transmission lines exceeded $1.6 billion. In addition, there was a total of 107 fatalities. (Office of Pipeline Safety, 2005c)

1.1.1 Bellingham and Carlsbad explosions

Two examples of particularly devastating pipeline accidents are the Bellingham explosion of 1999 and the Carlsbad explosion of 2000. The National Transportation Safety Board (NTSB) performed an investigation of each explosion, as it does for all pipeline incidents. Because of the severity of these two accidents, the NTSB released a comprehensive report of each explosion, including a detailed description of the cause of each explosion. (NTSB, 2002 and NTSB, 2003) According to the NTSB investigation, the cause of each accident was related to typical types of pipeline damage discussed above.

The Bellingham explosion occurred on June 10, 1999 in Bellingham, Washington. As a result of a rupture in a 16-in (41-cm) diameter pipeline, 237,000-gal (897,000-l) of gasoline were released into a creek which flows through a residential and industrial area in Bellingham, Washington. Approximately 1.5-hr after the rupture, the gasoline in the creek ignited, burning an area along 1.5-mi (2.4-km) of the creek, as seen in the photograph in Figure 1.1. The ensuing fire resulted in the deaths of two ten-year-old boys who suffered first and second degree burns over 90% of the surface of their bodies. In addition, an eighteen-year-old man fainted as a result of the intense gasoline vapors and drowned in the creek before it ignited. The estimated total of

property damage was $45 million. A photograph of the ruptured pipeline can be seen in Figure 1.2.

According to the NTSB, the primary cause of the rupture was excavation damage to the gasoline pipeline. This damage occurred in 1994 during a nearby modification project which was unrelated to the gasoline pipeline. (NTSB, 2002) A secondary cause of the rupture was the inability of the operator to accurately evaluate the results from a magnetic flux inspection, which was performed at regular intervals every five years for this pipeline. Therefore, the rupture and ensuing explosion could have been prevented if a reliable damage detection system had been implemented with the pipeline to continuously monitor its structural integrity.

Figure 1.1: Aerial view of resulting fire damage from Bellingham explosion (NTSB, 2002)

Figure 1.2: Actual rupture in the pipeline (NTSB, 2002)

The second example is the Carlsbad explosion, which occurred on August 19, 2000 near Carlsbad, New Mexico. A rupture in a 30-in (76-cm) diameter natural gas transmission pipeline resulted in the release of natural gas directly into the environment. The ensuing explosion of the released gas burned for 55-min, as seen in the photograph in Figure 1.3. The rupture site was near a point where the pipeline crosses the Pecos River on a service bridge, as shown in Figure 1.4. At the time of the explosion, twelve individuals were camping approximately 675-ft (205-m) from the rupture site under the service bridge. Six of the individuals were found dead at the scene, and the other six had sought refuge in the nearby river. They were rushed to the burn center at a local hospital. All six of these victims later died at the hospital, leaving a total of twelve fatalities. The estimated total of property damage was $998,000. This value is much lower than the $45 million from the Bellingham explosion because the Carlsbad explosion occurred in a remote area of New Mexico. If the accident had occurred in a more developed

region, the property damages surely would have exceeded several million dollars in addition to causing far more fatalities.

According to the NTSB, the primary cause of the rupture was a "significant reduction in the pipe wall thickness due to severe internal corrosion." (NTSB, 2003) The internal corrosion at the actual location of the fracture from the rupture is shown in Figure 1.5. A secondary cause of the rupture was the inability of the pipeline operator to "prevent, detect, or control internal corrosion." (NTSB, 2003) Therefore, the rupture and ensuing explosion with this example, as with the Bellingham example, could have been prevented if a reliable damage detection system had been implemented with the pipeline to continuously monitor its structural integrity.

Figure 1.3: Fire from rupture which lasted approximately 55-min. The support structure of suspension bridge seen in lower left corner of fireball is 85-ft (26-m) tall (NTSB, 2003)

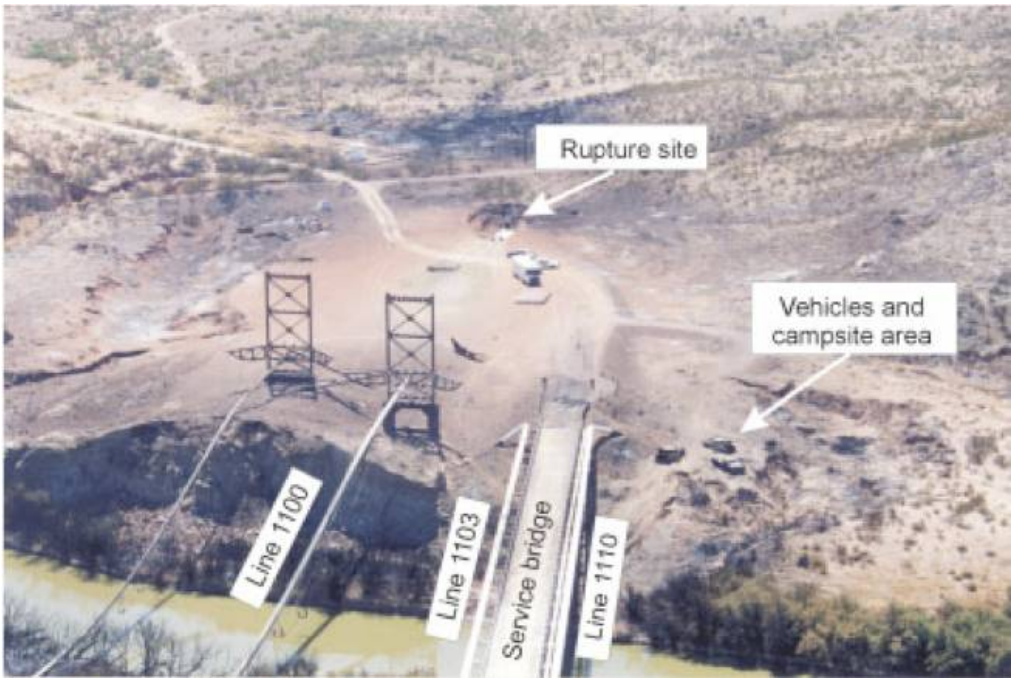

Figure 1.4: Accident location, including rupture site and camping area (NTSB, 2003)

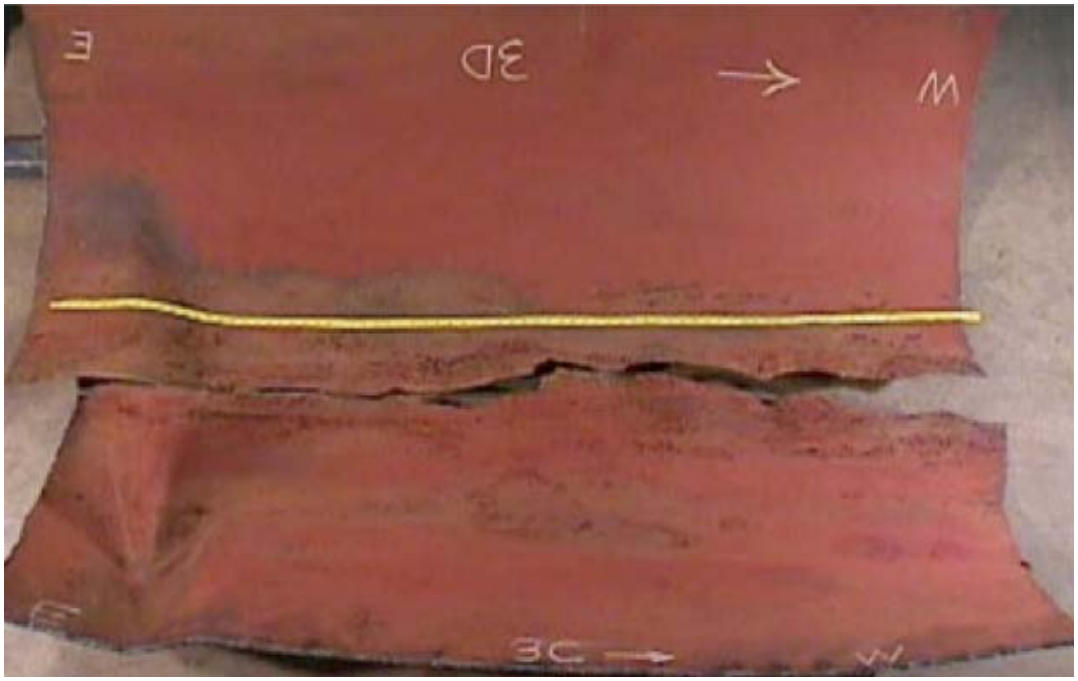

Figure 1.5: Corrosion seen at fracture location (NTSB, 2003)

1.1.2 Current approach in industry

In the pipeline industry, a single method for detecting or monitoring damage in a pipeline does not currently exist. Instead, industries typically implement a combination of several different techniques. For the oil and natural gas pipeline industry, destructive and non-destructive inspection techniques are commonly used together to ensure the integrity of transmission lines. These techniques typically require the pipeline system to be temporarily taken out of operation. The most common destructive technique is a hydrostatic test. For oil pipelines, a hydrostatic test involves pressurizing the pipeline to a point greater than the maximum operating pressure. The pressure is then observed for several hours to determine if any leaks are present. Because a hydrostatic test could potentially cause a leak or rupture, all the hazardous materials in the pipeline must be replaced with water to prevent environmental damage. Because of service interruptions and water removal difficulties, hydrostatic testing is not used with natural gas pipelines. (Tucker, et al. 2003)

When the geometry of the pipeline permits, non-destructive techniques are primarily used to ensure the structure's integrity. Such techniques commonly involve sending a magnetic flux or ultrasonic inspection device down the inside of the pipeline. The size of the device available limits the smallest size pipe that can be tested, and the radius of bends also limits the ability to use a particular device. These devices perform best in oil pipelines because petroleum products act as a good coupling between the instrument and the pipe wall. Accordingly, these techniques do not require oil pipelines to be emptied, contrary to hydrostatic testing. However, natural gas pipelines are more complicated because a gas does not provide good coupling for the testing device. Therefore, operators of natural gas pipelines have turned to direct assessment procedures for the determination of the integrity of their systems.

As evidenced by the documented cases of pipeline accidents, the current approaches used in industry to monitor the structural integrity of pipelines is not 100% effective. Even though pipelines are one of the safest modes of energy transportation, there is still justification for seeking improvements. The associated costs of property damage from accidents are quite significant, not to mention the enormous loss from each and every fatality. Also, the implementation of both destructive and non-destructive inspection techniques requires the pipeline to be taken temporarily out of service, which adds to the costs to an operator. Therefore, the development of a more reliable, cheaper monitoring system would have countless advantages for pipeline operators.

1.2 Solution

1.2.1 SHM for pipelines

The solution proposed in the research of this thesis for a more reliable, economical monitoring system involves a damage detection process known as structural health monitoring (SHM). In general, SHM refers to the discipline of damage detection as applied within the areas of aerospace, civil, and mechanical engineering. The process of SHM involves the use of an array of sensors distributed over a structure to make periodic observations of the system's dynamic response. The observations are evaluated to determine if damage is present in the system, and statistical analysis is then used to determine the current status of the system's health. After an extreme event, such as a bridge experiencing an earthquake, a SHM system can be implemented "for rapid condition screening and to provide, in near real time, reliable information regarding the integrity of the structure." (Farrar, et al. 2005) Ultimately, the output from a SHM system provides the operator with an assessment of the ability of the structure to

safely and reliably perform its designated function given the accumulation of damage from prior service and the potential for future operation to create additional damage.

In the case of the research of this thesis, the structure of interest is a pipeline system. There are numerous elements to a pipeline system, including the main body of the individual pipe segments, flanged and welded joints, valves, fittings, and pumping stations. Specifically, this thesis places emphasis on monitoring the structural integrity of the main body of the pipeline segments and of the flanged joints between the segments. To implement an SHM system with a pipeline, an array of sensors deployed at various locations along the axis of the pipeline is used to make observations regarding the damage state of the structure. The sensor array must be designed such that damage features corresponding to the structural integrity of the pipeline can be efficiently extracted from the observations. Ideally, the damage features should at least include the most common causes of pipeline incidents outlined in the previous section, including corrosion damage and excavation damage.

Because all materials and structures have inherent flaws and defects, a definition of damage is first needed before making an attempt to perform damage detection. Worden et. al (2004) defines damage as the condition of a structure under which it is "no longer operating in its ideal condition but can still function satisfactorily, i.e. in a sub-optimal manner." This definition of damage is extended in Farrar, et al. (2005) as a change in a structure, intentional or unintentional, which adversely affects the ability of the structure to perform its intended function. These adverse changes in the system can be material or geometric properties of the system, but they can also be changes to the boundary conditions or system connectivity. The relative time scale associated with damage must also be considered. Some forms of damage accumulate over long periods of operation. An example of such damage with pipeline systems is

internal corrosion, fatigue cracking, and deterioration of flanged joints. However, damage can also accumulate on relatively short time scales when the structure experiences a discrete event, whether scheduled or unplanned. With pipelines, such examples include damage incurred during a hydrostatic test, from nearby excavation projects, or from ground movement involved in an earthquake or landslide.

1.2.2 Advantages of SHM over NDE techniques

Because of the risk with hydrostatic testing of further damaging the pipeline, there is a clear advantage of non-destructive techniques over destructive ones. As outlined in the previous section, the use of non-destructive techniques with pipelines typically involves a damage detection discipline commonly referred to as non-destructive evaluation (NDE). The advantages of NDE techniques are obvious. Most importantly, there is very little risk of the structure incurring damage during a particular test. In addition, the various NDE techniques typically yield very detailed results regarding the status of the structure.

Although NDE techniques have several advantages over destructive testing methods, there are still some key disadvantages to these techniques. The primary disadvantage with forms of NDE involving pipelines is that the sensing mechanism used is typically only temporarily installed to the pipeline structure. This installation method poses two problems. First, the testing is only performed at scheduled intervals because the sensing mechanism is not permanently available. Therefore, the method relies on a predetermined schedule for testing. For damage which occurs on a large time scale, such as corrosion, this schedule is usually sufficient to detect the damage before it poses a threat to the structural integrity of the pipeline. However, with short time scale events, such as excavation or an earthquake, the testing schedule may allow the pipeline to operate under dangerous conditions, as demonstrated with the excavation damage

which led to the Bellingham explosion. With the pipeline involved in the Bellingham incident, the tests for damage were performed at a scheduled interval of 5 years. The second complication from temporary sensor installation arises from the need to obtain direct access to the structure in order to perform the NDE. Because pipelines are typically installed underground, direct access to the pipeline might require extensive excavation. In urban areas, this excavation process can become especially expensive if access to the pipeline requires digging beneath a roadway. Furthermore, there is always the chance of the excavation process itself causing damage to the pipeline.

Another major disadvantage of NDE techniques is that, depending on the particular technique used, they require that the pipeline be taken temporarily out of service. This aspect of the testing increases the potential cost of NDE techniques. The most common NDE techniques implement a sensing mechanism which is sent down the interior of the pipeline. With oil pipelines, the contents of the pipeline provide coupling between the transducer and the pipe material, so the contents need not be removed. With natural gas pipelines, however, the gas provides poor coupling, which may require that the pipeline be filled with a coupling material, such as water. Because of this rather expensive complication, NDE techniques are not commonly used with natural gas pipelines. In addition, geometry of the pipeline limits the ability to use certain NDE techniques. The sensing mechanism is limited by the size in which it can be efficiently packaged, meaning that the techniques can only be used with pipes with a diameter larger than approximately 3-in (8-cm). The geometry of pipe bends and fittings can also limit the compatibility of these techniques. Such was the case with the monitoring process used with the pipeline involved in the Carlsbad incident. The geometry of the pipeline prevented the implementation of internal NDE techniques, forcing the operator to use less reliable

techniques. Therefore, the corrosion went undetected and resulted in the eventual failure and explosion of the natural gas pipeline.

The implementation of a SHM system with pipelines addresses each of the issues with NDE described above. The most significant advantage is that the sensor array for a SHM system could be permanently installed on the pipeline structure. With a permanent installation, the pipeline operator could likely perform damage detection measurements as often as he wishes with much less financial repercussions. Therefore, the potential of a short time duration event going undetected would be much less likely. In the event of an earthquake or other natural disaster, the operator could check the structural integrity of the pipeline system immediately following the event. Accordingly, the operator could potentially take all severely damaged pipelines out of service before a leak could accumulate sufficient material to cause an explosion. In addition, a permanently installed system would enable the operator to perform an inspection following any excavation project in the vicinity of a pipeline.

A permanent installation would also eliminate the need to perform excavation in order to obtain direct access to the pipeline. If the sensor array was permanently installed on the pipeline structure, then the need to obtain temporary access to the pipe would no longer exist, leading to reduced costs. Finally, the SHM system proposed in this thesis would have fewer limitations regarding the geometry of the pipeline. A 2.5-in (6.4-cm) diameter pipe was used in some of the experimental procedures, and the proposed methods are compatible with even smaller pipe sizes. In fact, the proposed methods could potentially be adapted to applications outside of transmission and distribution pipelines, such as chemical plant pipe networks and the tubes in industrial heat exchangers. (Alleyne, et al. 1996)

One important disadvantage of SHM techniques is that, in their current form, they are not as robust as NDE techniques. As presented in the following chapter, NDE techniques are extremely reliable and accurate. Recent research has proven the ability of newly developed techniques to use focused guided waves to yield very accurate scans of a pipeline from a single axial location along the pipe. In order for the proposed SHM system of this research to be cost effective, a simpler transducer mechanism is used than is typically used in NDE techniques. Accordingly, the proposed techniques are not capable of locating or characterize the damage as accurately as NDE techniques. However, the proposed SHM system can be used as a first level alert to the operator. In the event that the SHM system detects the presence of a threat to the structural integrity of the pipeline because of damage, NDE techniques can then be used to yield a detailed evaluation of the current status of the pipeline, including an accurate description of the damage location and prognosis. Therefore, the number of NDE tests required would be reduced by implementing a SHM system with pipelines, which in turn would limit the associated cost of monitoring the structural integrity of the pipeline.

1.3 Means of applying an SHM system to pipelines

1.3.1 Guided waves and impedance methods

To incorporate a SHM system into a pipeline structure, a testing method is needed which can be implemented while the pipeline is in service. As discussed above, a large disadvantage with current NDE techniques is the requirement for the pipeline to be taken out of service so that the testing mechanism can be sent down the interior of the pipeline. Such testing is completed on a regular schedule. A SHM system must be capable of continuously monitoring the pipeline structure, even while it is in service. Accordingly, the sensor array for the SHM system must be

permanently mounted to the structure, making the ideal location of the sensor array on the exterior of the pipeline so that it can remain in service during testing.

In order to monitor the entire length of the pipeline, the sensor array must be capable of sensing damage over a long range. If the sensor array is mounted to the exterior surface of the pipeline and portions of the pipeline are installed underground, then sending a testing mechanism down the length of the pipe is not feasible. Therefore, a new method of testing is required to perform the damage detection.

One such testing method which is a solution for developing a SHM system for a pipeline is the use of ultrasonic, guided waves. Damage detection with guided waves involves exciting a pulse of ultrasonic waves in the wall of a pipe with an actuator. The waves are sent down the length of the pipe and received by a sensor at a second location on the pipe. In general, changes in the features of the wave propagation are used to monitor the pipeline for damage. Therefore, an extended length of the pipeline can be monitored using actuators and sensors which are permanently located at discrete locations along the length of the pipeline. As previous research has shown, guided wave techniques are extremely successful at detecting damage in the main body of a pipeline system. A more detailed review of the theory of guided waves is covered in Chapter 2.

Guided waves are not very efficient at detecting damage in flanged joints, so a second testing method is needed to ensure the integrity of the entire pipeline system. Impedance methods have been implemented in pipeline research for detecting damage in flanged joints. (Park, et al. 2001) These methods involve monitoring the mechanical impedance of a structure at relatively high frequencies. The use of a relatively high frequency range makes the impedance measurements more sensitive to local changes in the system than to global changes. Therefore,

the impedance methods can be used to detect and locate damage to the flanged joints of a pipeline system. In particular, impedance methods are extremely appealing for the SHM system proposed in the research of this thesis because the exact same sensor array can be used for both guided wave and impedance methods. This dual use implies that only a single sensor array is required to implement both methods, enabling the proposed SHM system to effectively monitor the structural integrity of the entire pipeline.

1.3.2 MFC patches

There are currently NDE techniques available which implement guided wave techniques. These techniques are the topic of much research in the area of pipeline monitoring, as discussed in Chapter 2. These techniques typically use a transducer ring to actuate and sense the propagation of guided waves in pipelines. The transducer ring is temporarily mounted to the exterior surface of the pipeline. Because the transducers are dry coupled to the pipeline, direct access to the pipe's exterior surface is needed, which may require excavation and removal of any coating or insulation material. The techniques are capable of scanning extended lengths of the pipeline, but attenuation of the wave propagation and geometry changes can limit the actual length achievable. Therefore, a permanent installation of these techniques would require numerous transducer rings along the length of a pipeline. Because the transducer rings are quite expensive compared to the costs of currently implemented NDE techniques, a permanent installation of transducer rings for guided wave testing is not financially feasible.

An alternative to the transducer ring involves the use of permanently bonded piezoelectric materials. Until recently, however, only piezo-ceramic materials were available for use as transducers. Because thin patches made of the piezo-ceramic materials are extremely brittle, they can only be bonded to flat surfaces. While this bonding arrangement is appealing to

numerous applications involving plate-like structures, it is not as appealing with the curved surfaces of pipelines. Therefore, the use of piezo-ceramic materials with pipelines is limited to bonding the patches to the pipeline flanges. While this transducer location is acceptable for detecting damage to the flanged joints of a pipeline system, it is not ideal for detecting damage in the main body of a pipeline. (Park, et al. 2001)

Recently developed Macro Fiber Composite (MFC) patches are a promising alternative to traditional, brittle piezo-ceramic transducers. The MFC patches are very appealing for pipeline applications because the patches are extremely flexible and have performance characteristics which are similar to traditional piezo-ceramic materials. In addition to being flexible, MFC patches are much more rugged and durable than piezo-ceramics. Another important factor is that MFC patches are much cheaper than the individual transducers from the rings used in the NDE techniques discussed above.

The MFC patch was developed at the NASA Langley Research Center. (Wilkie, et al. 2000) The MFC patch is a planar transducer made of several layers. The core of the MFC patch is comprised of several, piezoelectric fibers which are aligned in the same direction and embedded in epoxy, as seen in Figure 1.6. The piezoelectric fibers are unidirectional and have a rectangular cross section. The layer of fibers is encapsulated between two Kapton® layers, each of which contains an etching of an interdigitated electrode pattern (Williams, 2004). The fiber composition of the MFC makes it extremely flexible. The flexible nature of the MFC enables it to be bonded directly to the curved surface of a pipe, as seen in the photograph in Figure 1.7. In addition, the Kapton® layers provide protection to the fibers, making the MFC patch extremely durable. The patches could potentially withstand the environmental applications involved with pipelines located underground.

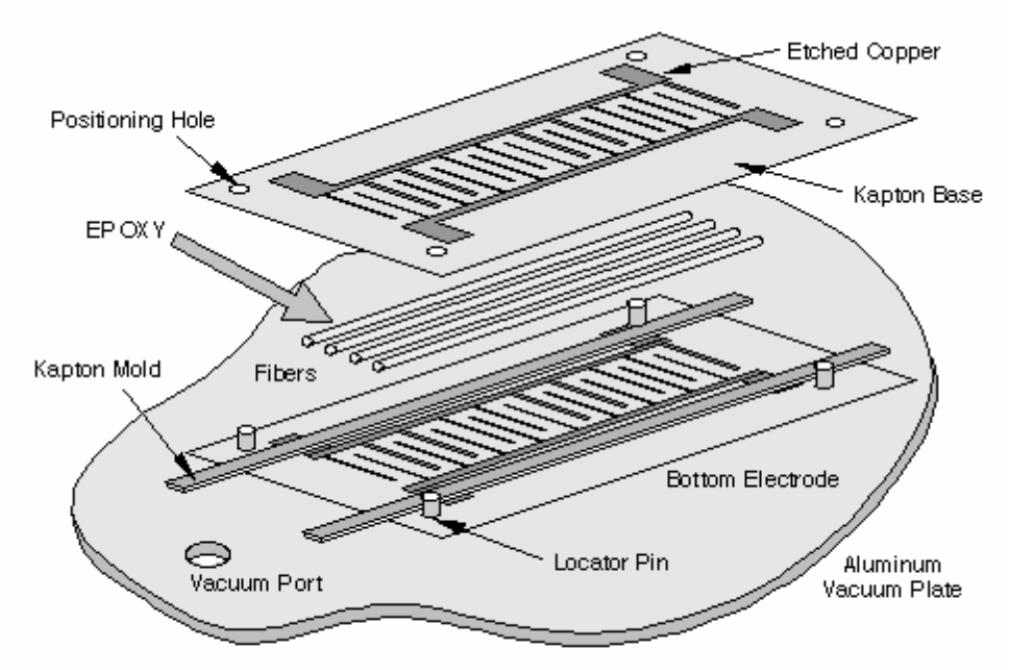

Figure 1.6: Composition of an MFC patch (Williams, 2004)

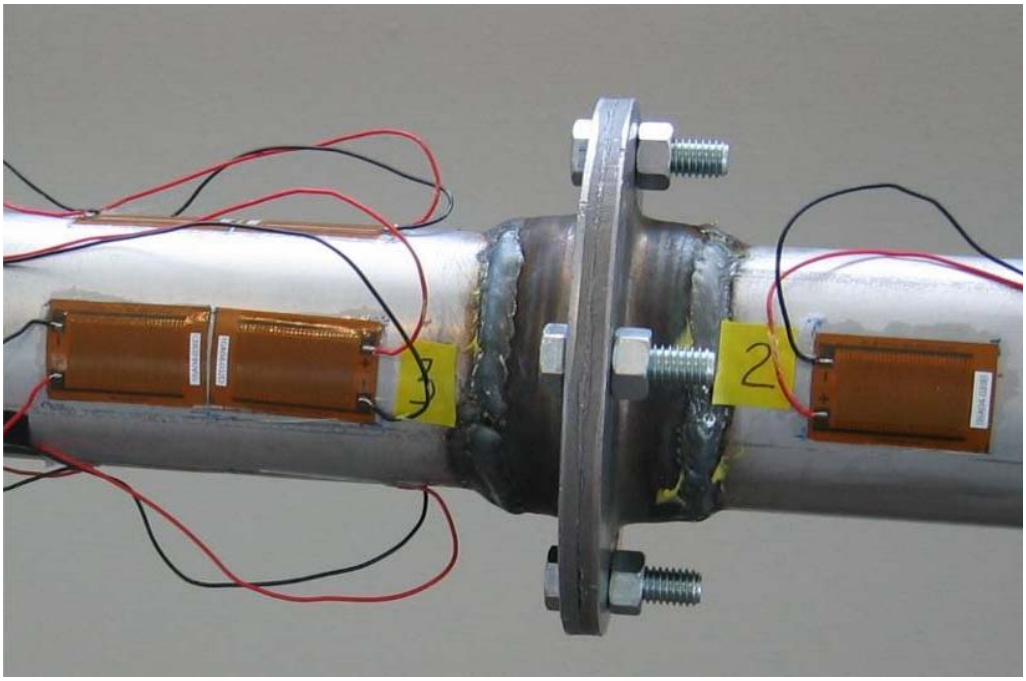

Figure 1.7: Example of a flexible MFC patch bonded to the curved surface of a pipe

1.4 Objectives and contributions

1.4.1 Thesis objective

The objective of this thesis is to demonstrate the benefits and feasibility of a structural health monitoring (SHM) system for pipeline systems. The proposed SHM system relies upon the deployment of macro-fiber composite (MFC) patches for the entirety of the sensor array. Two damage detection techniques, guided wave and impedance methods, are implemented using the MFC patches, avoiding the necessity for two separate sensor arrays. With the guided wave methods, the objective is to use Lamb wave techniques to correctly identify and locate the presence of damage in the main body of the pipeline system. With impedance methods, the objective is to use active-sensing techniques to correctly identify and locate the presence of damage in the flanged joints of the pipeline system. These two techniques are combined to assess the structural integrity of the entire pipeline system. Finally, suggestions are made regarding future research issues which require attention before any commercial applications can be realized.

1.4.2 Thesis contribution

The primary contribution of this thesis is a demonstration of a SHM system for pipeline structures. Two damage detection techniques, guided wave and impedance methods, were implemented in the proposed system. Although previous research has developed and demonstrated the capabilities of these techniques for nondestructive evaluation (NDE), these techniques have not been successfully adapted to SHM applications involving pipeline systems. While future issues still remain, the research of this thesis demonstrates the feasibility of commercially implementing a SHM system for pipeline structures.

Another contribution of this thesis is the use of MFC patches for a SHM system, particularly involving pipeline applications. The flexible nature of the MFC patch enables it to be mounted directly to the curved surface of the pipeline's main body. This transducer location allows the proposed system to exploit the dual purpose of the MFC patches for both guided wave and impedance methods. This dual use of MFC patches has not been substantially investigated. Therefore, the proposed SHM system can be used to monitor the structural integrity of the pipeline's main body and flanged joints.

1.5 Thesis Outline

This chapter presented the motivation for developing a SHM system for pipeline systems. The means for developing such a system and the objectives of this thesis are also presented. The following chapter, Chapter 2, presents a general background of Lamb wave and impedance methods. The background includes an explanation of the theory behind each method and covers previous research related to each method.

Chapter 3 through Chapter 5 present the implementation of Lamb wave methods to detect and locate damage in the main body of the pipeline system. Chapter 3 presents a detailed description of the exact Lamb wave methods implemented in the research of this thesis, including an overview of the apparatus used for the experimental procedures. Chapter 4 presents the procedures used for developing the damage detection algorithm. In this chapter, only reversible types of simulated damage are implemented. Chapter 5 then presents the results of Lamb wave methods used for detecting and locating permanent types of simulated damage. Various types of permanent damage are implemented in an effort to simulate crack, corrosion, and excavation damage. The results from these damage cases are used to assess the performance of the damage detection algorithm developed in Chapter 4.

A new test apparatus is used in Chapter 6 to present the capability of impedance methods to detect and locate damage to the flanged joints of a pipeline system. In addition, a simple Lamb wave measurement is presented to demonstrate the ability of MFC patches to perform both impedance and Lamb wave methods.

Chapter 7 presents the capability of Lamb wave and impedance methods to detect the presence of deposits on the interior surface of pipes. Unlike crack or corrosion damage, deposits inside pipelines do not directly affect the pipe material itself. However, deposits create serious hazards of their own.

Finally, concluding remarks are made in Chapter 8, including an outline of remaining issues which still need to be addressed in future research.

Chapter 2 Background of Lamb wave and impedance methods

2.1 Overview

This chapter presents a general overview of the background for Lamb wave and impedance methods. A brief explanation of the general theory behind each method is given. In addition, some of the research involving these methods is presented. In particular, applications involving pipeline systems and structural health monitoring (SHM) are the primary focus. Finally, comments are given which help relate previous research to the research of this thesis.

2.2 General background of Lamb waves

2.2.1 Definition of Lamb waves

Research in the field of Lamb wave propagations originates with early research in wave mechanics. Wave mechanics involves the propagation of mechanical waves in elastic solids. Historical work in this area dates back to the nineteenth century, as summarized in Graff (1991). Several textbooks on the topic of guided wave propagation exist, a few of which include Achenbach (1984), Miklowitz (1978), Graff (1991), and Rose (1999).

Lamb waves are a specific type of guided wave and occur in an infinite number of discrete modes. Unlike bulk wave propagations, guided wave propagations are associated with a bounded media. The actual boundary conditions determine the type or class of guided wave that propagates. Lamb waves, therefore, are associated with guided, elastic waves that propagate in a traction-free, homogeneous, isotropic plate. The thickness of the plate is generally considered to be of the same order of magnitude as the wavelength of the guided waves. The original theory of

elastic waves in an infinite plate was presented in Lamb (1917), and the author discusses the characteristics of symmetric and asymmetric modes. Since then, the term Lamb wave has been used in reference to the propagation of waves in an elastic plate. The term has also been expanded to include wave propagations in a variety of plate-like structures, such as heterogeneous plates and thin-walled tubes.

Lamb waves in a plate propagate by the means of a theoretically infinite number of discrete modes. The modes in a plate consist of two fundamental mode shapes, symmetric and asymmetric, each of which has an infinite number of orders associated with it. The first fundamental mode shape is symmetric through the thickness of the plate. Symmetric modes, termed compression waves, are often labeled as S_n, where "S" stands for symmetric and "n" is an integer of zero or higher that corresponds to the mode order. For example, S_2 is the second order, symmetric mode and has a unique shape associated with it. The second fundamental mode shape is asymmetric through the thickness of the plate. Asymmetric modes, termed transverse waves, are often labeled as A_n, where "A" stands for asymmetric. Examples of the particle displacements at the surface of the plate for the lowest order symmetric and asymmetric modes (S_0 and A_0, respectively) are shown in Figure 2.1. The Lamb wave modes are a combination of longitudinal and transverse waves. Longitudinal waves are pressure waves in which particle displacements are parallel to the direction of the propagation of the wave front. Transverse waves are vertical shear waves in which particle displacements are normal to the propagation direction of the wave front and normal to the plate surfaces. Because the actual propagation is a combination of longitudinal and transverse waves, the particle motion actually follows an elliptical path. The various modes in a plate occur as a result of the constructive interference patterns from the reflections of the longitudinal and shear waves from the plate

boundaries. This constructive interference allows the energy of the Lamb waves to propagate. (Silk, et al. 1979)

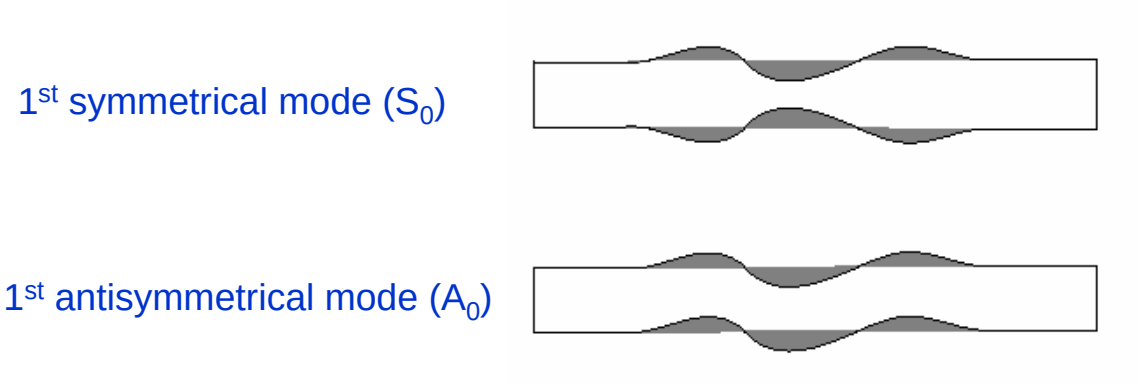

Figure 2.1: Example of S_0 and A_0 modes

2.2.2 Dispersive nature of Lamb waves

An important characteristic of Lamb waves is that they are dispersive, meaning that different frequency components propagate at different speeds. Dispersion curves are a common and useful method of displaying the relationship of frequency to the group speed and to the phase speed of the various modes. In a dispersion curve diagram, either the phase or group speed of each mode in a particular plate is plotted against frequency. An example of a dispersion curve diagram is shown in Figure 2.2. Note that, at any given frequency, numerous different modes exist and that, more importantly, each mode propagates at a different speed. To generalize dispersion curves for a specific material, the independent variable is sometimes changed to the product of frequency and plate thickness (*f*-*d*). This conversion allows the same diagram to be used for plates of various thicknesses, given that the plate material remains constant. When designing a Lamb wave experiment, one must be sure to take the dispersion curves into consideration. The dispersion curves give the experimenter knowledge of the relative speeds of the various modes at a given frequency, which provides information regarding the expected

arrival times of waves and the potential for dispersion if a narrow band of frequencies is excited. In general, the analysis of experimental results can be simplified during experimentation by generating only a limited number of modes and by selecting a frequency range at which dispersion is relatively low.

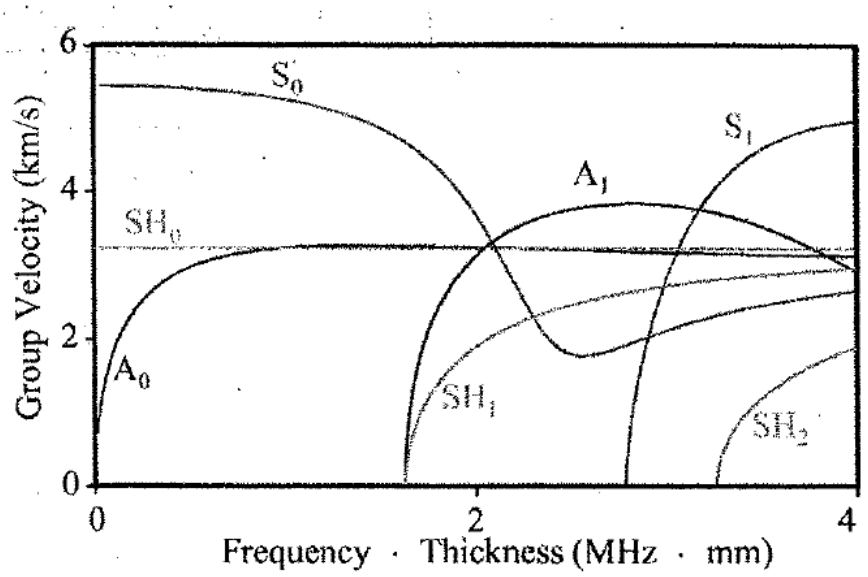

Figure 2.2: Group velocity dispersion curves for a steel plate (Cawley, et al. 2003)

Formulation of the dispersion curves comes from the solution of the period equation, as presented in Achenbach (1999), for symmetric and asymmetric waves, respectively:

$$\frac{\tan(qh)}{\tan(ph)} = -\frac{4k^2pq}{\left(q^2-k^2\right)^2} \quad \text{(Symmetric)} \tag{1}$$

$$\frac{\tan(qh)}{\tan(ph)} = -\frac{\left(q^2-k^2\right)^2}{4k^2pq} \quad \text{(Asymmetric)} \tag{2}$$

The terms in the above equations are defined as follows:

$$p^2 = \frac{\omega^2}{c_L^2} - k^2, \quad q^2 = \frac{\omega^2}{c_T^2} - k^2 \tag{3a, b}$$

$$c_L = \sqrt{\frac{\lambda + 2\mu}{\rho}}, \quad c_T = \sqrt{\frac{\mu}{\rho}} \tag{4a, b}$$

$$\mu = \frac{E}{2(1+\nu)}, \quad \lambda = \frac{E\nu}{(1-2\nu)(1+\nu)} \tag{5a, b}$$

where E is Young's modulus, ν is Poisson's ratio, ω is the circular frequency, k is the wave number, c_L is the longitudinal wave speed, c_T is the transverse wave speed, and μ and λ are Lamé constants. Using the above definitions, the period equation for symmetric and asymmetric waves can be numerically solved using an iterative process to yield the group and phase velocity curves. Details of this procedure are outlined in Rose (1999).

Another important characteristic associated with Lamb waves is the concept of attenuation. Attenuation is the continuous reduction in the amplitude of a propagating wave as it travels a given distance. Therefore, as the distance that a Lamb wave travels becomes greater, the resulting attenuation increases accordingly. The primary cause of attenuation is damping in the wave media, which causes the kinetic energy of the wave to be dissipated as heat, sound, or other forms of energy. Other potential causes include the dominant frequency leaking into sideband frequencies, changes in the geometry of the medium, or the wave spreading into other propagation paths. (Kessler, 2002)

2.2.3 Typical testing methods with Lamb waves

Numerous methods exist for exciting Lamb waves in structures. One technique is to use an angled beam transducer. A piezoelectric actuator on a wedge is placed against the test structure. The wave front propagates through the wedge, across the interface with the test

structure, and into the material of the test structure. This method excites a broad band of frequencies at a single phase velocity. By varying the angle of incidence between the wedge and the interface with the test structure, a variety of wave speeds can be excited as needed. A second technique is to use a comb transducer, which uses several actuators at an equal spacing on the surface of the structure. This method excites modes with a constant wavelength, which is determined by the spacing of the transducers. The spacing and frequency is then adjusted to excite various Lamb wave modes in the test structure. (Rose, 2002) Another method is to bond a piezoelectric actuator, usually in the form of a thin patch, directly to the surface of the test structure. The actuator is excited with a burst waveform, such as a windowed sinusoid, at a specific frequency. Therefore, all modes present at the input frequency are excited, regardless of phase velocity.

There are two primary experimental methods used with Lamb waves. The first method is termed the "pulse-echo" method. With this method, a piezoelectric actuator is used to excite Lamb waves in the test structure and also to measure the responses in the structure. The responses measured are the reflections of the Lamb waves from the various boundary conditions or geometry variations present in the test structure. Because the same piezoelectric element is used to excite and sense Lamb waves in the structure, this method is sometimes termed an "active sensing" technique. A second experimental method is termed the "pitch-catch" method. With this method, two piezoelectric elements are used. The two elements are placed at different locations on the test structure. One element is used to actuate Lamb waves in the structure, and the other is used to measure the responses as the Lamb waves propagate through the structure from the actuator element to the sensor element. Because the piezoelectric elements are capable

of active sensing, the role of actuator and sensor can be reversed for an additional measurement, allowing for wave propagations in the opposite direction.

2.2.4 Applications involving flat plates

Although Horace Lamb (Lamb, 1917) was the first person to describe the propagation of waves in a plate, he did not actually excite them experimentally. Conceivably the first, documented time that Lamb waves were used as a potential method of nondestructive evaluation (NDE) was by Worlton. (1961) Worlton noted the insufficiency of experimental data available for validation of the extensive theoretical research in the area of Lamb wave propagations. In response, he developed and implemented methods to experimentally excite Lamb waves in aluminum and zirconium plates. Worlton was able to experimentally verify the analytical dispersion curves developed by previous researchers, and he also investigated the effects of thickness variations. Over the course of the thirty or so years following Worlton's work, much research was done involving the application of guided, ultrasonic waves to NDE. A detailed review of all such work is beyond the scope of this document. For a more in depth review of Lamb wave techniques involving plate-like structures, see Kessler (2002).

2.3 Specific theory of Lamb waves in hollow cylinders

2.3.1 Lamb wave modes in hollow cylinders

Guided waves in hollow cylinders and thin walled tubes are very similar to those in flat plates. The similarity arises from hollow tubes having a thin cross section with two free surfaces, just as in a plate. Although Lamb waves, by definition, occur only in flat plates, waves that propagate in tubes are commonly termed Lamb waves. In tubes, however, the propagation of Lamb waves becomes much more complicated than in flat plates. Typical Lamb wave theory

assumes that the medium is an infinite plate, but in a hollow cylinder, the circumferential curvature results in changing the boundary condition of the plate's edge from infinite to continuous. Therefore, Lamb waves in a plate propagate infinitely far from the actuator location, but Lamb waves in a tube can repeatedly propagate around the tube's continuous circumference. Because of the different boundary conditions, the Lamb wave modes in tubes are more complex and exist in more numerous modes than in flat plates.

In tubes, there exist three fundamental classes of modes, which are longitudinal, torsional, and flexural modes. Nomenclature for describing each of the three classes is outlined in Silk and Bainton (1979). The nomenclature was slightly modified by Demma, et al. (2003) for use in their dispersion curve software. The longitudinal, torsional, and flexural modes are labeled using the following nomenclature: $L(0, n)$, $T(0, n)$, and $F(m, n)$, respectively. In the nomenclature the first index, m, is the "harmonic number of circumferential variation," and the second index, n, is a "counter variable." (Demma, et al. 2003) The longitudinal and torsional modes are symmetric with respect to the tube's axis, but the flexural modes are not. Axial symmetry, as discussed here, should not be confused with symmetry across the thickness of the medium, as discussed with a flat plate above. In fact, as the radius of the tube tends to infinity, the longitudinal modes in the tube correspond to all Lamb wave modes in the flat plate. In addition, the torsional modes correspond to horizontal shear waves in the flat plate.

2.3.2 Excitation of Lamb waves in hollow cylinders

With most measurements involving Lamb waves, one desires to excite just a single, dominant mode. In general, many more Lamb wave modes exist in a hollow cylinder over a given frequency range than in a flat plate. The presence of additional modes makes it more difficult to excite a single mode in a tube than in a flat plate. An example of a dispersion curve

for a thin walled tube can be seen in Figure 2.3. Note that at any given frequency there is a much greater number of modes present in the tube than in the flat plate from Figure 2.1 above. The additional modes present in a tube, therefore, make the measurement design and data analysis with a tube significantly more complicated than with a flat plate.

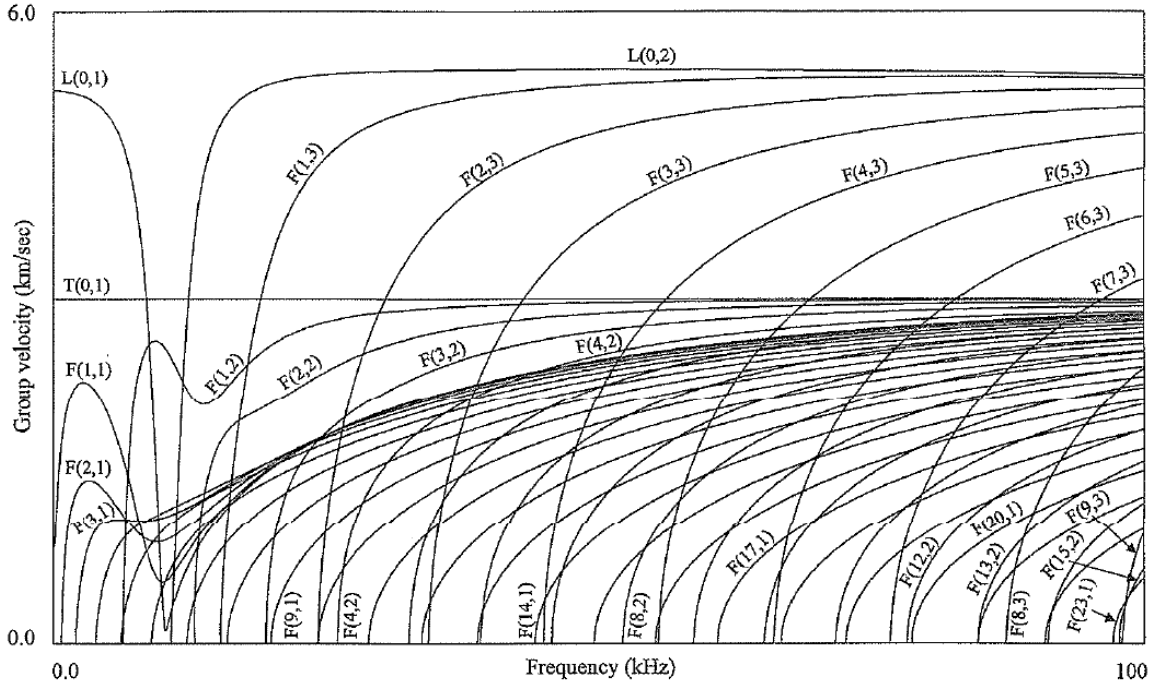

Figure 2.3: Group velocity dispersion curve for a nominal 6-in, schedule 40 (152-mm bore diameter, 7-mm wall thickness) steel pipe (Alleyne, et al. 1998)

Because of the presence of additional modes in tubes, extra considerations must be made when designing a method of exciting Lamb waves in the structure. First, an ideal excitation signal would contain only a single frequency. For this reason, narrow banded signals are generally used, such as several cycles of a sine wave to which a Hanning window is applied. The choice of frequency is based upon the selected mode one wishes to use in the particular experiment. When possible, the frequency should be chosen such that the selected mode has low dispersion over the narrow frequency band and such that the velocity of the selected mode is significantly greater than the next fastest mode. By using an area of low dispersion, all

frequencies in the narrow band of excitation will travel at nearly the same velocity, minimizing the error introduced into the measurement from dispersion. Therefore, the signal's shape and amplitude will remain consistent as it travels long distances. By using an area where the selected mode is significantly faster than the other modes, the measurement of the response of the first arrival will not have as much interference with the response from other modes.

The same excitation methods used for flat plates, such as an angled beam transducer and a phased array transducer, can be used for pipes. However, a single transducer excites all modes present at a given phase or frequency, depending on the specific type of transducer being used, such as an angled beam or phased array. Using a single transducer will include numerous flexural modes in the excitation, all of which can potentially make analysis of the responses incredibly difficult. Therefore, a ring of transducers around the circumference of the tube is used. If a sufficient number of transducers are present in the transducer ring, only axially symmetric modes will be excited, which effectively cancels the propagation of any flexural modes. In general, the number of transducers in the ring should be greater than the highest order of the flexural modes present at the chosen frequency. (Lowe, et al. 1998) In addition to the flexural modes, excitation of the torsional modes can be avoided as well. The torsional modes can only be excited by motion in the circumferential direction. By using transducers that only provide axial motion, the excitation of any torsional modes is effectively cancelled. (Alleyne, et al. 1996)

2.3.3 Previous research involving Lamb waves in hollow cylinders

In the application of Lamb wave techniques to pipes, the research group led by Cawley has produced some of the most promising results. Cawley's group performed a series of studies involving the fundamentals of Lamb wave propagations in pipes. In Lowe, et al. (1998),

Cawley's group presents a thorough summary of these fundamentals. In particular, their research addressed the reflection of the $L(0,2)$ mode from corrosion and through-thickness cracks in pipes. Using validation from finite element analysis, they established a direct relationship between the $L(0,2)$ reflection and the circumferential extent and through-thickness depth of cracks in the pipe wall. In addition, they found the mode conversion of $F(1,3)$ useful for defect detection involving welded joints. In Lowe, et al. (1998), Cawley's group further researched the mode conversion of the $L(0,2)$ mode from circumferential notches in pipes. They were able to correlate the $F(1,3)$ and $F(2,3)$ mode conversions with the circumferential extent of the notch. In fact, the $F(1,3)$ reflection was found to be as strong as the $L(0,2)$ reflection.

In Aristégui, et al. (2001), experiments were done to study the effects of viscous fluids on the interior and exterior of the pipes. Fluid on the inside or outside of the pipe leads to the presence of an additional mode, termed by the authors the "α mode." In general, an increase in viscosity correlated to an increase in the attenuation, with a few anomalies.

In Alleyne, et al. (2001), Cawley's group describes the results of field trials using a commercially available system, Guided Ultrasonics Limited's Wavemaker Pipe Screening System, used for the long-range inspection of defects in pipes using Lamb waves. This system uses the $T(0,1)$ mode instead of $L(0,2)$ because the torsional mode is not dispersive over the entire frequency range and because the torsional mode's characteristics are not affected by the presence of viscous fluids in the pipe. Torsional excitation was achieved by rotating the piezoelectric elements for the $L(0,2)$ excitation ring by 90°. There are also some disadvantages associated with the use of torsional modes, such as higher sensitivity to axial features, including welded brackets. A further study of the use of the torsional mode was done in Demma, et al. (2003). The depth and circumferential extent of defects were found to have the primary

influence on the reflection of Lamb waves from cracks in pipes. The authors developed a "wave-number-defect size product" (*ka*) to explain low and high frequency scattering characteristics. The sensitivity of the torsional mode to defects increases with frequency. However, the propagation distance decreases as frequency increases, which requires a compromise between propagation range and defect sensitivity.

In a more recent study, Cawley's group investigated the effects of corrosion patches on the reflection of the torsional mode. (Demma, et al. 2004) The authors presented a "map of the reflection coefficient" based upon the size of the defect, including the circumferential extent and the depth. The map is then used to estimate the depth of the defect from experimental data.

Additional methods for pipe inspection have been presented by a research group led by Rose. Rose's group has developed a resonance tuning technique that has produced very powerful capabilities in this field. The resonance tuning method involves exciting several Lamb wave modes in such a manner that they focus on a specific area of the structure. (Barshinger, et al. 2002) As in Cawley's research, a ring of dry-mounted piezoelectric transducers is used to excite Lamb waves in the structure. By changing the excitation signal, the focal point of the resonance tuning is then used to scan the entire surface of the pipe. The results showed that great potential exists for this method, including the inspection of pipes over long distances, even when tar coatings are present. The resonance tuning approach makes possible the ability to improve penetration power over fixed phase or fixed frequency methods.

2.4 General comments on Lamb wave methods

As a final remark, it is important to note that the experimental research discussed above was performed with a ring of dry-mounted piezoelectric transducers. While the methods have all produced very successful means of detecting defects in pipes, they are all forms of

nondestructive evaluation (NDE). Therefore, before any of the proposed tests can be performed, access must be available to at least a small section of the pipe structure such that the transducer ring can be attached. This setup requires the removal of any insulation or coatings that could potentially be present at the chosen location. In some instances, multiple test locations for the transducer ring would be needed, such as in a pipe network whose length exceeds the penetration capabilities of the equipment. In any case, the methods discussed above do not involve sensing systems that are permanently mounted to the structure.

Conversely, the methods presented in this research all involve piezoelectric patches that are permanently mounted to the host structure. The sensors can be integrated into a structural health monitoring (SHM) system, which would be in service full time. A SHM system would enable the user to continuously monitor the pipe structure for defects, such as cracks or corrosion. The information would always be available, rather than at scheduled maintenance intervals.

2.5 General background of impedance methods

2.5.1 Definition of impedance methods

Impedance methods involve monitoring the mechanical impedance of a structure. The mechanical impedance of a structure, by definition, is related to the dynamic behavior of the structure. In particular, the mechanical impedance is sensitive to changes in the structure's mass, stiffness, and damping characteristics. Because damage to a structure affects these characteristics, the mechanical impedance of a structure can indicate the presence of damage in the system. Therefore, the integrity of a structure can be monitored by monitoring the structure's mechanical impedance.

Instruments are available which can directly measure the mechanical impedance of a structure. Like the transducer rings used for NDE techniques with Lamb waves, these instruments are typically expensive and cumbersome to employ. A simpler transducer which can be used to measure a structure's mechanical impedance in a piezoelectric patch, such as a MFC patch. This method is much more appealing for the proposed pipeline SHM system because MFC patches can also be used for the Lamb wave methods described in the preceding sections of this chapter.

When mounted to the surface of a structure, such as a pipeline, the mechanical impedance of a MFC patch is directly coupled to the mechanical impedance of the structure. The piezoelectric properties of the MFC patch, in turn, couple its electrical impedance to its mechanical impedance. Therefore, the electrical impedance of a MFC patch, when it's mounted to a pipeline system, is coupled to the system's mechanical impedance. The relative size and weight of a MFC patch is negligible compared to that of it host structure, which in this case is a pipeline system. Accordingly, a MFC patch introduces negligible impact on the dynamic characteristics of the host structure. This low impact allows the use of a MFC patch to accurately measure the mechanical impedance of a structure.

An electromechanical model of a piezoelectric patch mounted to a host structure is shown in Figure 2.4. In the model, a piezoelectric patch (PZT) is shown directly bonded to a single degree of freedom system, as represented by a mass (m), spring (k), and damper (c). Liang, et al. 1994 show that the electrical admittance, $Y(\omega)$, of the piezoelectric patch is a combined function of the mechanical impedance of the piezoelectric patch, $Z_a(\omega)$, and the mechanical impedance of the host structure, $Z(\omega)$. The equation for the electrical admittance, which is simply the inverse of the electrical impedance, is as follows:

$$Y(\omega) = \frac{I}{V} = i\,\omega\,a\left(\bar{\varepsilon}_{33}^{T} - \frac{Z(\omega)}{Z(\omega) + Z_a(\omega)} d_{3x}^{2}\,\hat{Y}_{xx}^{E}\right) \tag{6}$$

where V is the input voltage, and I is the output current from the piezoelectric patch. In addition, a, d_{3x}, $\hat{Y}_{xx}^{E}$, and $\bar{\varepsilon}_{33}^{T}$ are the geometry constant, the piezoelectric coupling constant, Young's modulus, and the complex dielectric constant of the piezoelectric patch at zero stress, respectively. (Park, et al. 2003)

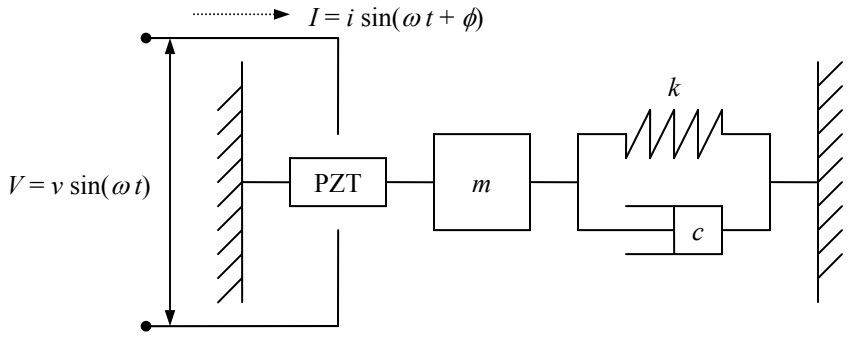

Figure 2.4: Electromechanical model of a piezoelectric patch mounted to a host structure (adapted from Park, et al. 2003)

2.5.2 Testing parameters involved with impedance methods

Assuming that the properties of the MFC patch and its bonding conditions remain constant over the course of the structure's monitoring period, Equation 6 shows that the electrical impedance of the MFC patch is directly related to the mechanical impedance of the structure. Therefore, the measured electrical impedance of the MFC patch can be used to monitor the structure's mechanical impedance. Because the electrical admittance is primarily capacitive, the imaginary part of the electrical impedance is dominant. However, only the imaginary part of the electrical impedance is affected by changes in the dielectric constant, which is temperature sensitive. Accordingly, the imaginary part of the electrical impedance is more sensitive to

temperature variations than the real part. Therefore, the real part of the electrical impedance is commonly used for SHM applications. (Sun, et al. 1995)

For SHM applications, impedance methods are similar to traditional vibrations techniques in that both methods aim to monitor the structural integrity of a structure by observing changes in its characteristic vibrations over time. An extensive review of SHM techniques based upon traditional vibrations is given in Doebling, et al. (1998). The primary difference between the two methods, however, is the frequency ranges used for the measurements. Relative to the frequency ranges used for traditional vibrations techniques, impedance methods implement a much higher frequency range. The frequency range used for impedance measurements is typically greater than 30-kHz and up to 400-kHz.

The sensitivity to incipient damage of a particular vibration based approach to damage detection, whether traditional vibrations or impedance methods, is dependent upon the frequency of the excitation used. For a given method to be sensitive to incipient damage, the wavelength of the excitation must be smaller than the characteristic length of the damage to be detected (Stokes and Cloud, 1993). Because the impedance method implements such high frequency ranges when compared to traditional vibrations, the electrical impedance of an MFC is much more sensitive to incipient damage. At such high frequency ranges, the wavelength of the excitation is relatively small, depending on the wave speed of the structure's material, and sensitive enough to detect minor changes in the structure's integrity.

Impedance measurements typically involve using a stepped sine wave across a predetermined frequency range. At each frequency step of the sine wave, the corresponding voltage and current are recorded and used to estimate the electrical impedance of the MFC patch at the particular frequency. In the area of impedance methods, there is a lack of analytical work

available which addresses the modes of vibration of complex structures over ultrasonic frequency ranges. Therefore, the frequency range used for impedance measurements with a given structure is typically determined by trial and error. A frequency range with a high mode density, as observed as the number of peaks present, is generally favorable because it contains more information regarding the condition of the structure than a frequency range with lower mode density contains. For this reason, a few frequency ranges are normally chosen, and ideally each frequency range contains 20 to 30 peaks. (Sun, et al. 1995)

Because of the relatively high frequencies involved, impedance methods are generally more sensitive to local changes in a structure, and traditional vibrations techniques are generally more sensitive to global changes in the structure. With impedance measurements, "a frequency range higher than 200-kHz is found to be favorable in localizing the sensing, while a frequency range lower than 70-khz covers a larger sensing area." (Park, et al. 2003) With pipeline structures, therefore, the impedance methods can be used to detect local damage if a sufficiently high frequency range is chosen.

2.6 Previous research involving impedance methods

Impedance methods have been successfully incorporated into SHM systems involving numerous complex structures. Several research efforts demonstrate the ability to detect cracks, loosening of joints, delaminating of composite structures, and corrosion of metallic structures. Perhaps the first successful attempt to implement impedance methods with a SHM system was performed by Sun, et al. (1995) In this research, impedance methods were used to monitor damage in a simple truss structure. A damage metric based upon the root-mean-square deviation was used to assess the structural integrity of the truss system. The research also investigated the effects of the chosen frequency range and excitation level for the measurements.

Research performed by Chaudhry et al. (1995) demonstrated the localized sensitivity of impedance measurements. In this work, impedance measurements were taken near the tail section of an airplane. Two types of damage were investigated, one which was local and a second which was distant. The local damage involved loosening the main mounting brackets of the tail section. Because this damage was close to the measurement location, the damage was easily identified. The distant damage involved alterations to the airplane's structure at other locations, such as a bracket for a wing, and was not as easily identified. The impedance measurements were shown to be relatively insensitive to the far-field damage compared to the near-field damage.

The effects of high temperature environments on impedance methods was investigated by Park, et al. (1999) High temperature piezoelectric patches were used to monitor damage in a bolted joint structure subjected to a temperature range of 482 to 593°C. The high temperature environment caused much greater variation in baseline measurements than previously had been observed at room temperature. However, the variation caused by damage, which is simulated by slightly loosening one of the bolts, was still much greater than the baseline variation.

Finally, one application related to pipeline systems was addressed by Park, et al. (2001) In this research, impedance methods were used to monitor damage in the flanged joints of a simple pipeline system, as seen in Figure 2.5. Piezo-ceramic patches were mounted to the surface of the flanges and used locally to monitor damage in each flange. The impedance method was implemented to perform a rapid assessment of the structural integrity of the flanged joints. Such an application would be useful after an event of short duration, such as an earthquake or nearby excavation. In addition, the impedance methods were shown to be capable of making measurements while the structure is in service. Therefore, the methods developed in

this research can easily be integrated into a SHM system. Because the piezoelectric patches were mounted to the flanges of the pipeline system, however, these methods can not efficiently detect damage in the pipeline's main body.

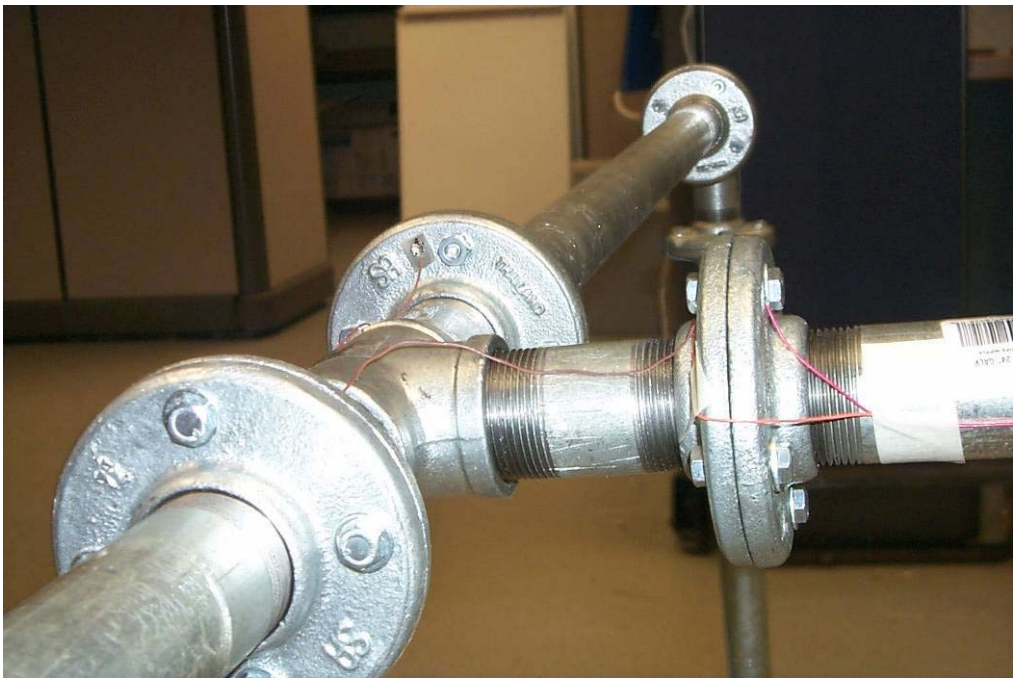

Figure 2.5: Application of impedance methods to a simple pipeline structure (Park, et al. 2001)

2.7 General comments on impedance methods

Previous research has proven that impedance methods are an effective means to detecting damage in the flanged joints of a pipeline system. This research demonstrates the potential application of impedance methods to SHM systems. The localized sensitivity of impedance methods is shown to be capable of not only detecting the presence of damage in the flanged joints but also specifying the location of the damage. However, the research methods use brittle, piezo-ceramic patches which must be mounted directly to the flat surface of the flanged joints. This sensor location prohibits the monitoring of the main body of the pipeline. In the research of this thesis, the flexible nature of MFC patches will enable the sensors to be mounted to the

curved surface of the main body of the pipeline. From this location, impedance methods will still be able to detect damage to the flanged joints of the pipeline system. In addition to the flanged joints, this new sensor location will enable the dual use of MFC patches for Lamb wave methods as well, which will provide a means for detecting damage in the main body of the pipeline system.

Chapter 3 Experimental procedure for Lamb wave methods

3.1 Apparatus for Lamb wave measurements

3.1.1 Pipe structure

Common applications for pipeline systems involve the transport of natural resources, such as natural gas and petroleum. Standard pipe sizes are used in the design of pipelines for such applications. The pipe sizes are organized according to schedules, which specify a wall thickness for a particular pipe diameter. Because it is commonly implemented in oil and natural gas pipelines, Schedule 40 pipe has been used as test articles of various research topics in the area of damage detection (Alleyne et al. 1998, Barshinger et al. 2002). Some examples of Schedule 40 pipe dimensions can be seen in Table 3.1. Because pipe sizes and schedules originate in English units, the test articles used in the research of this thesis are referenced directly using these units. To assist the reader, metric units are listed parenthetically.

nominal pipe size [in (cm)]	outside diameter [in (cm)]	wall thickness [in (mm)]	inside diameter [in (cm)]	weight (mass) [lb/ft (kg/m)]
3 (8)	3.500 (8.890)	0.216 (5.49)	3.068 (7.793)	7.58 (54.7)
6 (15)	6.625 (16.83)	0.280 (7.11)	6.065 (15.41)	18.97 (136.9)
12 (30)	12.75 (32.39)	0.406 (10.3)	11.94 (30.33)	53.52 (386.2)

Table 3.1: Dimensions for common sizes of Schedule 40 pipe

In the research of this thesis, a pipe with a 6.0-in (15-cm) outside diameter of the longest length possible was the desired test article. However, the available testing facility could not accommodate the use of Schedule 40 pipe. The size of the pipe was limited to 10-ft (3-m). A 10-ft (3-m) section of Schedule 40 pipe with a nominal 6-in (16.83-cm outside diameter) size weighs close to 190-lb (86.2-kg), which would be quite difficult to manage in the available space. In addition, purchasing small quantities of Schedule 40 pipe for non-commercial use is

difficult and extremely expensive. Therefore, a lighter and cheaper pipe was chosen as an alternative for the test article.

The pipe used in the research of this thesis was a thin-walled, carbon steel tube. This pipe was obtained from a local supplier. The dimensions of the pipe are given in Table 3.2. A photograph of the test apparatus can be seen in Figure 3.1. The pipe was suspended in the air with a metal wire which ran through the inside of the pipe, as shown in Figure 3.2. Each end of the wire was connected to a test stand using elastic cords, and a rubber space was used at the mouth of the pipe to prevent the wire from rattling against the interior surface of the pipe.

length [ft (m)]	outside diameter [in (cm)]	wall thickness [in (mm)]	inside diameter [in (cm)]	weight (mass) [lb/ft (kg/m)]
10 (3.0)	6.00 (15.2)	0.063 (1.60)	5.94 (15.1)	2.00 (14.4)

Table 3.2: Dimensions of pipe used for test apparatus

Figure 3.1: Apparatus for Lamb wave measurements

Figure 3.2: Suspension method

3.1.2 Sensor locations

MFC patches were located at two axial locations along the length of the pipe. The first axial location was 1.0-in (2.5-cm) from the left end of the pipe, and the second axial location was 36.0-in (91.4-cm) from the right end of the pipe. At each of the two axial locations, eight MFC patches were mounted to the pipe's exterior surface. The MFC patches were equally spaced around the circumference of the pipe. Details of the actual locations of the MFC patches are shown in Figure 3.3. The MFC patches were manufactured by Smart Material Corp. (Sarasota, Florida). The patches were d_{33}-effect sensors with an active ceramic area of 1.1 x 0.6-in (2.8 x 1.5-cm). Each MFC patch could actuate strain in a single direction, which was along the length of the patch. Additionally, each MFC patch could only sense strain in this same direction. The patches were mounted to the pipe's surface using two-part epoxy and a vacuum bagging process.

Because the desired Lamb wave modes were longitudinal, as discussed in the following section, the MFC patches were all aligned to actuate and sense strain in the pipe's axial direction. A photograph of the MFC patches at axial location #1 can be seen in Figure 3.4.

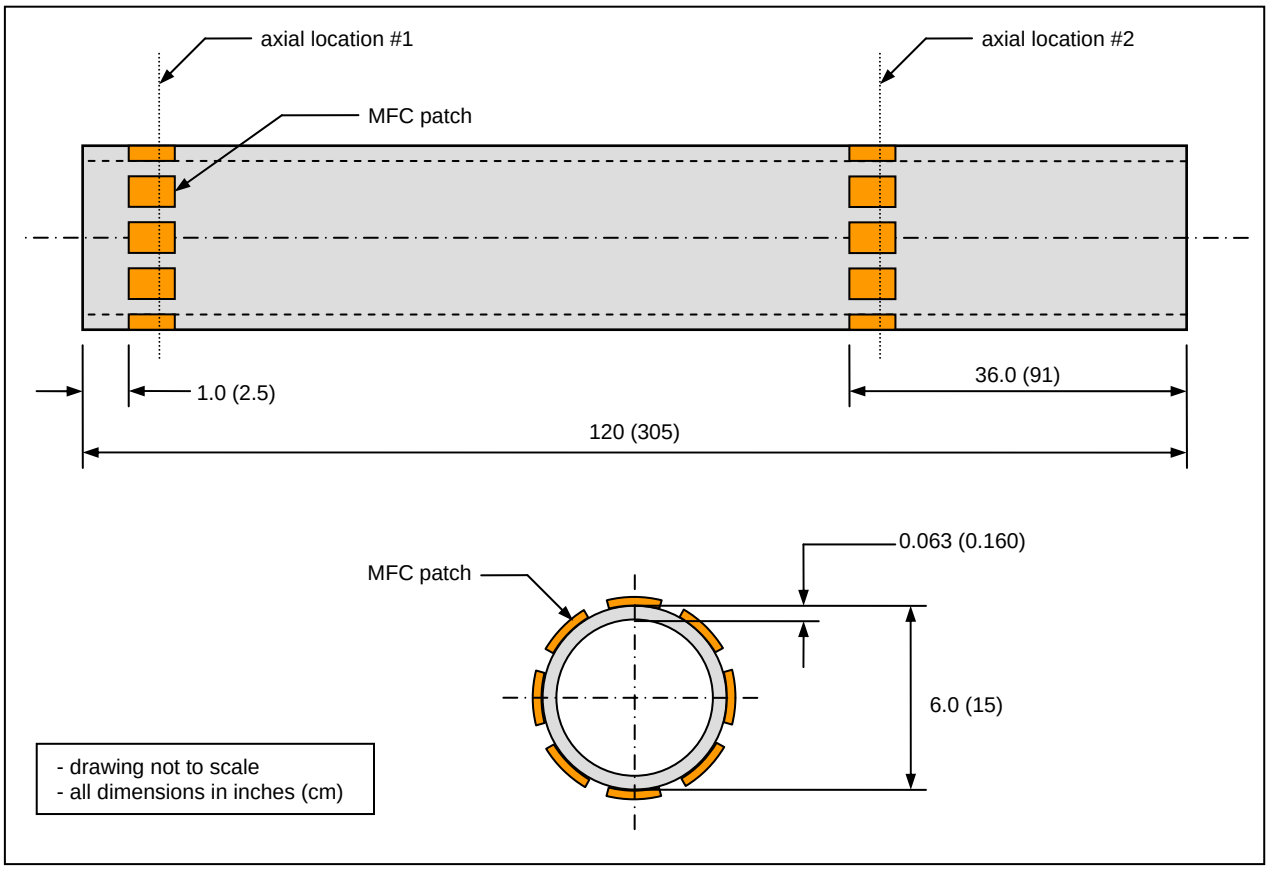

Figure 3.3: Dimensioned drawing of 6-in steel pipe

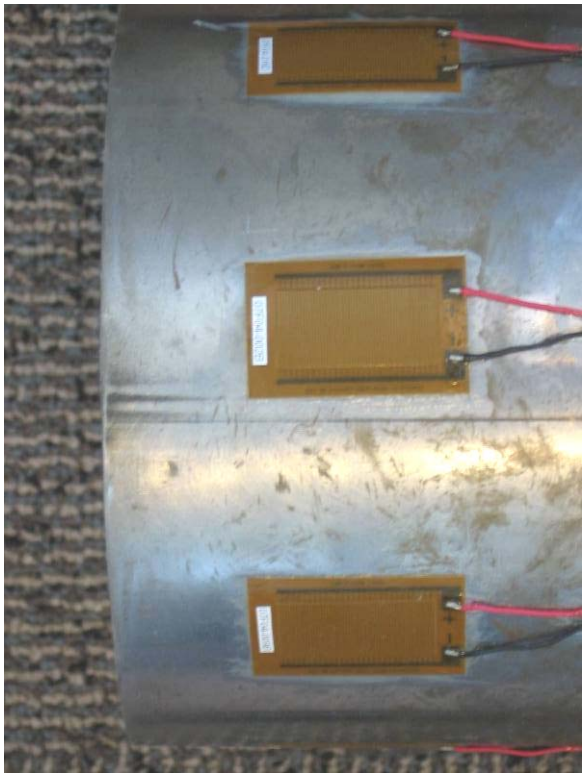

Figure 3.4: Alignment of MFC patches at axial location #1

1.5.1 Analytical dispersion curves

Various Lamb wave methods were implemented throughout the testing procedures of this research. Because Lamb waves are dispersive, their properties in a structure are commonly represented with dispersion curves. In order to help characterize the test apparatus used, the analytical dispersion curves for the 6-in (15-cm) steel pipe were formulated. A MATLAB based program, PCDISP, was used to calculate the dispersion curves. The PCDISP software was developed at the Instituto de Automática Industrial (CSIC) and could be used to calculate the dispersion curves for the propagation of mechanical waves in cylindrical waveguides. (Seco, et al. 2002)

The dispersion curves for the group velocity of the 6-in (15-cm) steel pipe are shown in Figure 3.5. Each of the modes has been labeled according to the nomenclature presented in

Demma et al. (2003) Note that the Figure only includes the dispersion curves for the longitudinal (*L*), torsional (*T*), and first three flexural (*F*) modes. Modes higher in order than the third flexural mode have been omitted for clarity. In addition, only frequencies up to 100-kHz were used so that the details at low frequencies could be seen. In this research, frequencies up to 300-kHz were considered. The dispersion curves over this frequency range are shown in Figure 3.6. In this figure, the flexural modes up to the tenth order have been included.

As seen in the dispersion curves, the group velocity of the *L*(0,2) mode had a slope near to zero over the frequency range of 25 to 300-kHz, which meant that the velocity of the *L*(0,2) mode was almost constant over this frequency range. Therefore, the *L*(0,2) mode propagated as if it was non-dispersive over this frequency range. Another observation made was that there was little separation in speed between the *L*(0,2) mode and the first few flexural modes. If excited, all of these modes would propagate at approximately the same speed, causing unwanted interference between them. Therefore, measures were taken during experimentation to ensure that minimal excitation was provided for the flexural modes. These measures would allow the *L*(0,2) mode to propagate with little interference.

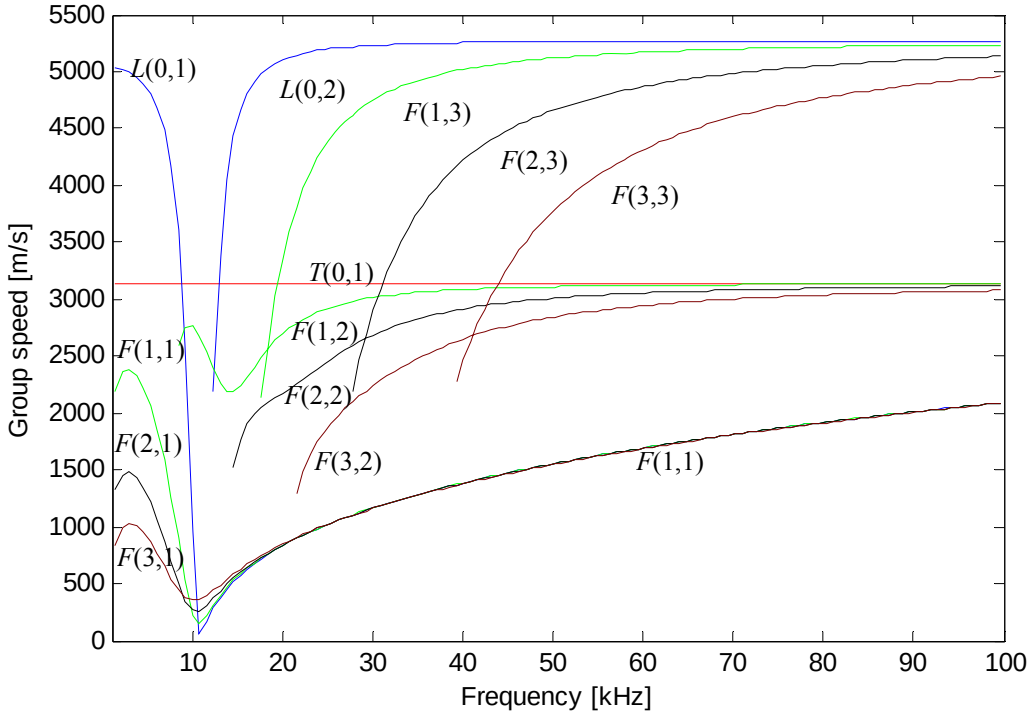

Figure 3.5: Dispersion curves for group velocity of 6-in (15-cm) steel pipe (100-kHz)

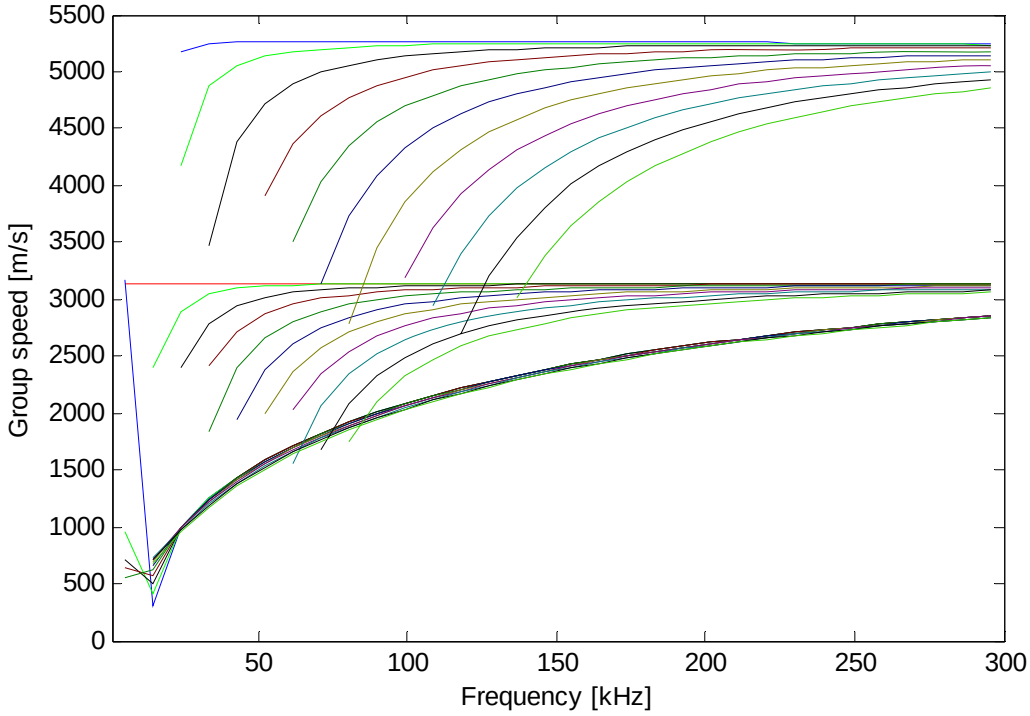

Figure 3.6: Dispersion curves for group velocity of 6-in (15-cm) steel pipe (300-kHz)

3.2 Experimental procedure for Lamb wave measurements

3.2.1 Overview

When using guided waves in experimental procedures, the first step is to excite mechanical waves in a structure of interest. Using the structure as a waveguide, properties of the wave propagation can be observed through measurements. These observations allow one to characterize the structure's condition. In the case of damage detection, as presented in this research, the goal is to be able to infer whether or not damage is present in the structure, which in this case was a steel pipe.

The type of guided waves that propagate in a structure depends upon the structure's material properties, geometry, and boundary conditions. In the case of a thin plate with free surfaces, the guided waves are termed Lamb waves. Because a pipe has a thin wall thickness and free surfaces, it is considered to be a plate-like structure. Therefore, the guided waves in a pipe are commonly termed Lamb waves as well. Various methods exist for exciting Lamb waves in a pipe, as discussed in Chapter 2. In the experimental procedures of this research, MFC patches were used as the propagation source. An AC voltage signal was applied across the terminals of an MFC patch which was mounted to the surface of the pipe. The electro-mechanical coupling of the piezoelectric material transferred the voltage signal to a strain, which is referred to as the "inverse effect," at the pipe's surface. The varying strains resulted in the excitation of Lamb waves, which then propagated down the length of the pipe. Once the Lamb waves propagated across a second MFC patch, the "direct effect" of the piezoelectric material caused the strain experienced by the patch to generate an output voltage signal. This signal could then be acquired and used for analysis.

3.2.2 Pitch-catch measurements

Experimental procedures with Lamb waves typically involve exciting Lamb waves at one location on a structure and measuring at a second location the corresponding responses to wave propagations. With pitch-catch measurements, the actuator and sensor locations are separated by a given distance on the structure. Depending upon the relative speeds of the particular modes excited, faster traveling modes will arrive at the sensor location sooner than slower modes. If the first and second arrivals are sufficiently separated in time when they arrive at the sensor location, they can be easily distinguished in a time-history plot of the response. If, however, they are not sufficiently separated, then the two modes may constructively or destructively interfere. The interference may make the analysis of the measurement difficult because the two modes cannot be distinguished from each other. For this reason, designing the measurement such that the mode or modes of interest are free of interference is important.

An important aspect of using MFC patches for Lamb wave methods is that each MFC patch is capable of actuating and sensing, which is termed active sensing. For example, one measurement may be made by sending Lamb waves from an MFC patch at the left end of a pipe to an MFC patch at the right end of a pipe. In this case, the MFC patch at the left end serves as the actuator, and the MFC patch at the right end serves as the sensor. Using the exact same MFC patches, a second measurement can be made in the opposite direction, which would be from the right end to the left end. Therefore, the MFC patch at the right end serves as the actuator, and the MFC patch at the left end serves as the sensor. Because the MFC patches are capable of active sensing, the two measurements require only changes in the hardware setup, such as the excitation source and data acquisition equipment. No change in the actuators and sensors is

required. This characteristic helps reduce the cost required for a permanently installed monitoring system.

For the steel pipe used in this research, pitch-catch measurements were made using one ring of MFC patches as an actuator. The eight MFC patches were wired together in parallel so that the same voltage input signal was applied to every MFC patch in the ring simultaneously. The second ring of MFC patches then served as the sensor. Again, the eight MFC patches were wired together in parallel. The response measured at the sensor ring was, therefore, the sum of the signals from each individual MFC patch.

In this research, the input voltage signal to the actuator was a high frequency (ultrasonic) burst waveform. The burst waveform was simply a windowed sine wave, as shown in Figure 3.7. In this case, the windowing function was a Hanning window, the width of which was set according to the number of peaks desired by the user. For a given signal amplitude, increasing the number of peaks increases the amount of energy excited in the structure. Because damping in the system causes attenuation, the increase in energy leads to an increase in the distance which the Lamb waves can propagate. However, increasing the number of peaks also increases the width of the pulse. If there is insufficient separation in the arrival times of two modes, then a wider pulse will increase the amount of interference between the two modes.

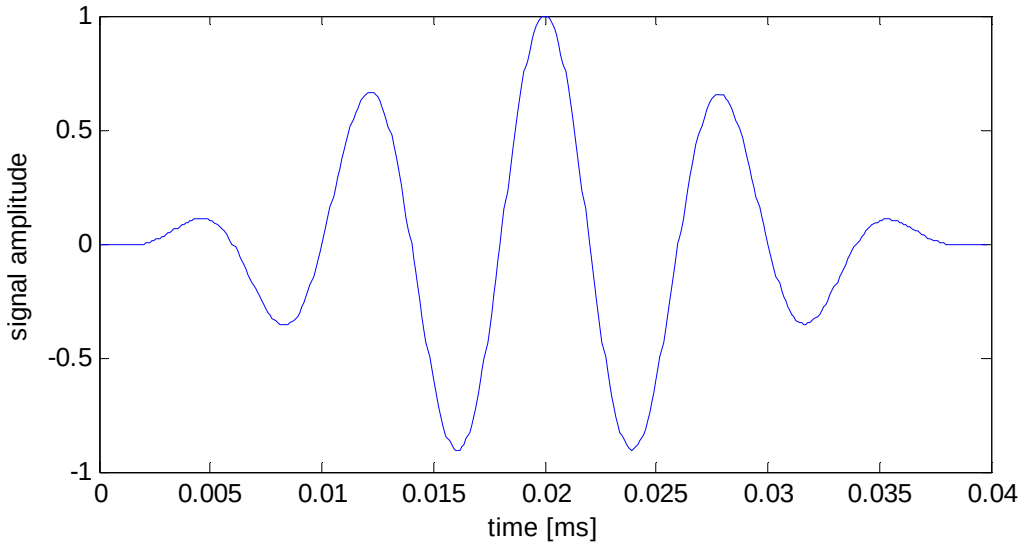

Figure 3.7: Normalized input signal for actuator

An example of the response from a pitch-catch measurement from the pipe can be seen in Figure 3.8. In this measurement, the MFC patches at axial location #1 (see Figure 3.3) were used as the actuator, and the MFC patches at axial location #2 were used as the sensor. The signal shown in Figure 3.7, which is discussed above, was the excitation signal. The signal had five peaks and an excitation frequency of 100-kHz. The signal's amplitude was normalized because the voltage amplitude was controlled by the settings of the system's amplifier. The diagram in Figure 3.8-a shows the propagation paths for the arrivals of the first four modes. This diagram shows where reflections occurred, which are depicted using vertical arrows. The corresponding signal for each of these arrivals is labeled in Figure 3.8-b. Because there was only a slight difference between the distance traveled by the first arrival and the distance traveled by the second arrival, the two arrivals were not sufficiently separated. Therefore, interference between the responses of the first two arrivals caused their signals to overlap. For this same reason, the third and fourth arrivals overlapped as well. Note that the signal before 0.1-ms was associated with electro-magnetic interference (EMI). For better resolution, a close-up view of

the first and second arrivals is shown in Figure 3.8-c. Although the original excitation signal contained only five peaks, the interference between the first and second arrivals caused the response shown here to have six peaks. This observation could be made for the third and fourth arrivals as well. A more detailed discussion of experimental results is in the following chapters.

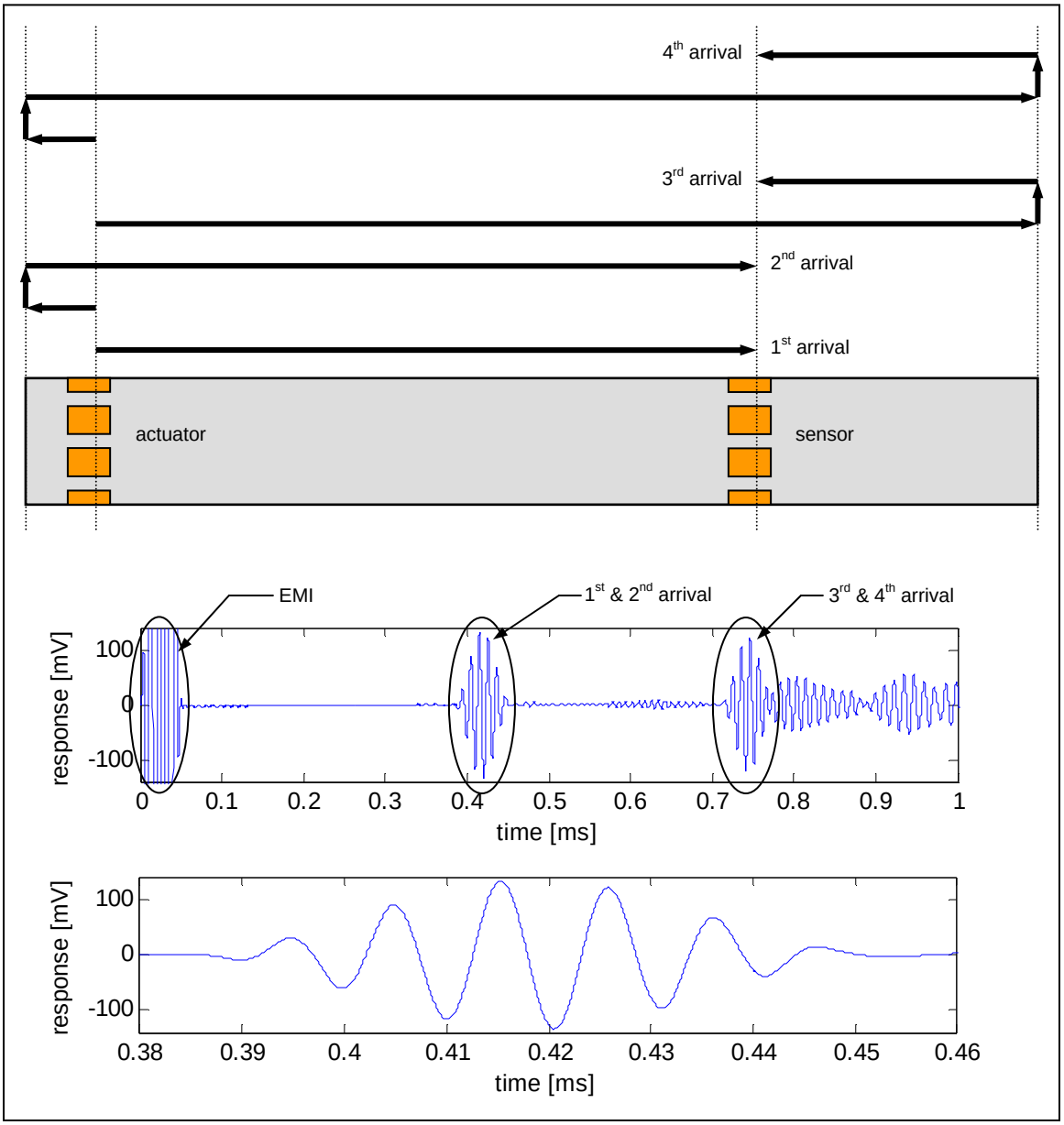

Figure 3.8: Example of a pitch-catch measurement – (a) Diagram of paths traveled by the first four arrivals, including reflections, (b) Full time history for 0 to 1.0-ms with first four arrivals labeled, (c) Close-up view of 1st and 2nd arrivals

There are some advantages and disadvantages of pitch-catch measurements compared to pulse-echo measurements, which are discussed in the next section. The main advantage is that a longer length of pipe is covered with a single pitch-catch measurement than with a single pulse-echo measurement. Conversely, the main disadvantage of pitch-catch measurements is that two arrays of MFC patches are required, one for the actuator and one for the sensor, but pulse-echo measurements only require one array. In addition, there are no reflection features with pitch-catch measurements that can be used for locating damage. These topics are further discussed in the next section.

3.2.3 Pulse-echo measurements

The methods used for making pulse-echo measurements are almost identical to pitch-catch measurements. The significant difference between the pitch-catch measurements and pulse-echo measurements is the locations of the senor and actuator. In pitch-catch measurements, the sensor and actuator are located at two different places on the structure, as discussed in the previous section. In pulse-echo measurements, however, the sensor and actuator are located at the same place on the structure. In fact, the same MFC patch is simultaneously used as an actuator and a sensor. Therefore, there is no direct path from the actuator to the sensor. Once the actuator initiates the propagation of Lamb waves in the structure, only reflections of Lamb waves from discontinuities in the structure will return to the sensor. Such discontinuities range from changes in boundary conditions to changes in geometry, including the edges of a plate, the end of a pipe, or structural damage, such as surface corrosion, cracks, and joint deterioration.

In the case of the steel pipe used in this research, pulse-echo measurements were made using one ring of MFC patches. Because of equipment limitations, however, the same MFC

patch could not be used simultaneously as an actuator and sensor. Instead, four of the eight MFC patches in a ring were wired together in parallel to serve as the actuator, and the remaining four were wired similarly to serve as the sensor. The wiring was arranged such that the MFC patches alternated along the circumference between an actuator MFC patch and a sensor MFC patch. Therefore, the array of sensor MFC patches and the array of actuator MFC patches were both axially symmetric.

An example of the response from a pulse-echo measurement from the pipe can be seen in Figure 3.9. In this measurement, the MFC patches at axial location #1 were used as the actuator and sensor. The same excitation signal for the pitch-catch measurement discussed above was used here. The diagram in Figure 3.9-a shows the propagation paths for the first three arrivals. This diagram shows where reflections occurred, which are depicted using vertical arrows. All three arrivals were the $L(0,2)$ mode, but the different arrival times resulted from the various propagation paths. Note that the first arrival traveled the shortest distance, and note that the second and third arrivals traveled equal distances even though the paths were different. The corresponding signal for the response to these arrivals is labeled in Figure 3.8-b. Because there was only a slight difference between the distance traveled by the first arrival and the distance traveled by the second and third arrivals, the three arrivals were not sufficiently separated. Therefore, interference between the responses of the first three arrivals caused their signals to overlap. The signals after the first through third arrivals were from higher order modes. For this reason, the actual propagation paths could not be easily identified. Note that the signal before 0.1-ms was associated with electro-magnetic interference (EMI) and numerous concurrent reflections from the left end of the pipe, which will be ignored here. For better resolution, a close-up view of the first and second arrivals is shown in Figure 3.8-c. Although the original

excitation signal contained only five peaks, the interference between the first three arrivals caused the response shown here to have seven peaks. A more detailed discussion of experimental results is in the following chapters.

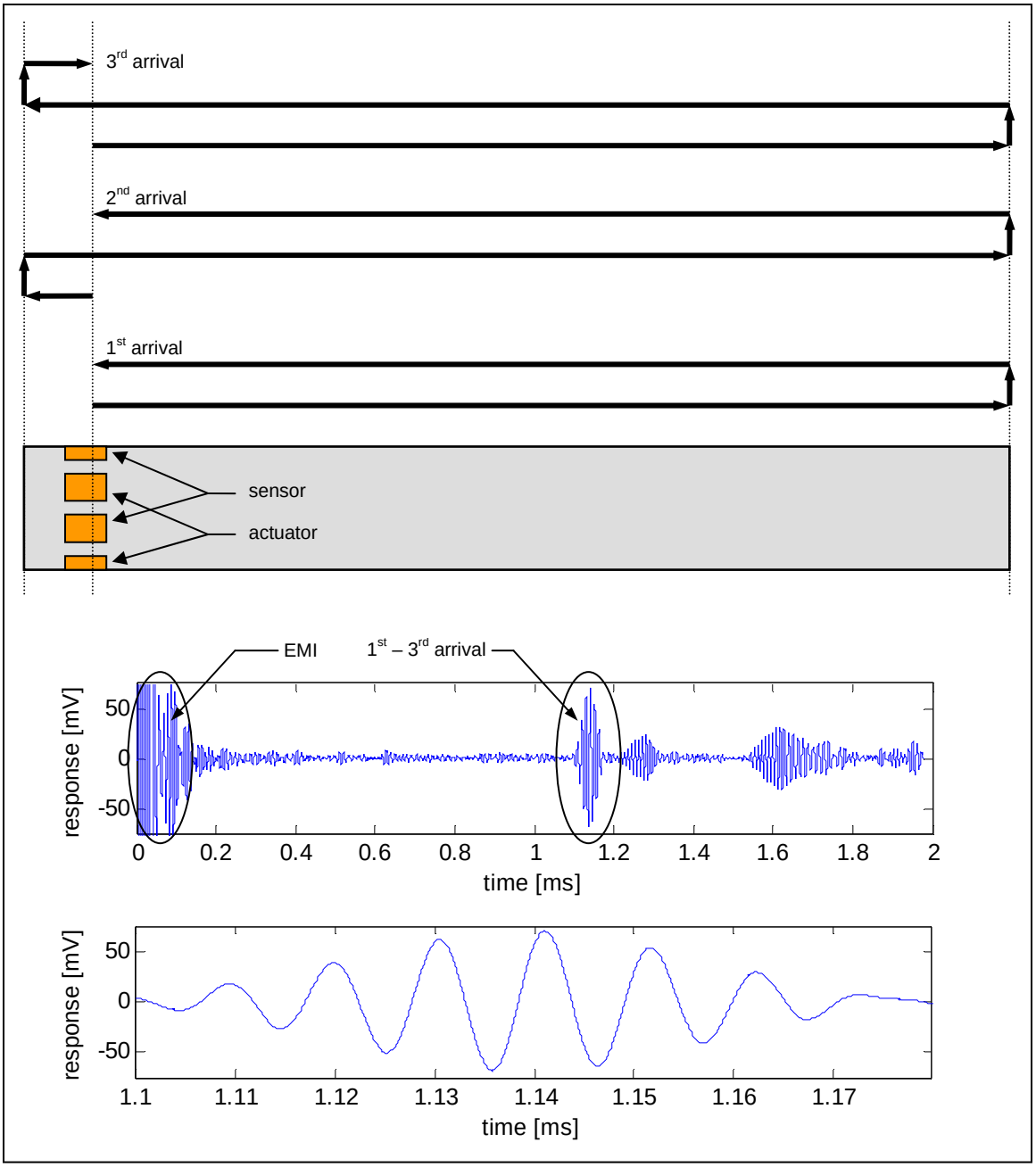

Figure 3.9: Example of a pulse-echo measurement – (a) Diagram of paths traveled by the first three arrivals, including reflections, (b) Full time history for 0 to 2.0-ms with first two arrivals labeled, (c) Close-up view of 1st and 2nd arrivals

As mentioned in the previous section, there are some advantages and disadvantages of pitch-catch measurements and of pulse-echo measurements. The main advantage of pitch-catch measurements is that a longer length of pipe can be covered with a single pitch-catch measurement than with a single pulse-echo measurement. For a given length of pipe, the Lamb waves in a pitch-catch measurement need to travel only once through any section of the pipe, which is on the way from the actuator to the sensor. The Lamb waves in a pulse-echo measurement, however, must travel at least twice through any section of the pipe. The first is on the way from the actuator to a reflection point, and the second time is on the way back to the sensor after reflection. On the other hand, an advantage of pulse-echo measurements is that only one array of MFC patches is required because each MFC is simultaneously used as an actuator and a sensor. The main advantage of pulse-echo measurements is the ability to use reflection features to locate damage. When a reflection from damage is observed in a response signal, the time of flight required for the particular mode to travel to the damage location and back to the sensor can be extracted. Assuming that minimal dispersion occurs, the velocity of the mode, which is given in the dispersion curve, can be used with the time of flight to estimate the distance between the sensor and the damage. Pitch-catch measurements can also be used to locate damage. However, reflection features cannot be used as in pulse-echo measurements. If a given pitch-catch measurement detects damage, then the location of the damage is between the actuator and sensor. For high fidelity in the location of the damage, a dense array of sensors along the length of the pipe would be required, which is not as convenient as using reflection features with sensors at a single axial location.

3.2.4 Controlling coherent noise

With Lamb wave methods, precautions to control the coherent noise in measurements must be taken while designing an experiment. The most significant source of coherent noise in a Lamb wave measurement with a pipe is the interaction of the various modes. As seen in the dispersion curve, shown again in Figure 3.11, numerous modes existed in the pipe, even below 100-kHz (over 50 modes, if all orders are included). When excited, each of these modes traveled at a different speed, resulting in a different arrival time of each mode in a given measurement. In addition, dispersion caused each individual mode to vary in speed with frequency. When excited over a broad band of frequencies, a single mode itself would travel at various speeds, which further complicated matters. The effects of dispersion in a measurement were seen as the broadening of the pulse from the arrival of a specific mode. A wider pulse from the arrival reduced the spatial fidelity of the measurement and may have resulted in the mode interfering with a neighboring arrival.

One method for reducing the coherent noise in a measurement is to control the Lamb wave modes that are excited. In general, the ideal case is to excite just a single mode. If just one mode is excited, then there are no other modes present to cause interference. For damage detection in pipe, the mode of choice is desired to have a uniform stress distribution in its mode shape across the thickness of the waveguide, which in this case was the wall of the pipe. (Cawley et al. 2003) Such a stress distribution would help the wave propagation be equally sensitive to a defect at any location across the wall of the pipe, whether it would be surface corrosion or an internal crack.

One mode which has the desirable stress distribution of its mode shape is the $L(0,2)$ mode. This property makes the use of the $L(0,2)$ mode attractive for damage detection methods

in pipes. In addition, there are other characteristics of this mode that make it attractive. The $L(0,2)$ mode has a mode shape which does not vary circumferentially around the surface of the pipe, making this mode simple to excite with surface mounted transducers. Therefore, this mode lends itself well to excitation using surface bonded MFC patches. Another advantage of the $L(0,2)$ mode for this pipe thickness is that it is nearly non-dispersive over a large range of frequencies. This non-dispersive nature reduces the adverse effects of dispersion.

In order to prevent coherent noise, measures must be taken to ensure that only the $L(0,2)$ mode is excited. While a single MFC patch which is mounted to the surface of the pipe will excite the $L(0,2)$ mode, it may also excite any flexural mode present at the given excitation frequency. Because the $L(0,2)$ is axially symmetric and the flexural modes are not, the $L(0,2)$ mode can be excited without exciting flexural modes if the actuator is a continuous, monolithic transducer which covers the entire circumference of the pipe. If such an actuator is not available, as is the case when using individual MFC patches, at least some of the flexural modes can be avoided by mounting actuators in an equally spaced ring around the circumference of the pipe. The highest order of flexural modes that can be cancelled by the actuator ring is equal to the number of transducers in the ring. (Lowe, et al. 1998) For example, the four MFC patches used as the actuator in the pulse-echo measurements described above could cancel all the flexural modes, $F(m, n)$, for which $m \leq 4$. Therefore, mounting the MFC patches edge to edge around the circumference would maximize the cancellation of flexural modes. Because of space limitations for the vacuum-bagging process used in this research, only eight patches were mounted in each actuator ring. Implementing more advanced processes from industry could enable the installation of additional patches, but additional patches would also require more power, further complicating the proposed system.

Although using a circumferential array of transducers helps to eliminate the coherent noise caused by exciting multiple modes at once, it does not address the issue of dispersion. Even if all of the flexural modes are effectively cancelled, dispersion of the $L(0,2)$ mode can still be a source of coherent noise. Therefore, an important decision when designing a measurement with Lamb waves is the choice of excitation frequency. An excitation signal with narrow banded frequency content is used to minimize the potential for dispersion to occur. To further ensure that dispersion within the narrow band of excitation is avoided, the excitation frequency is chosen such that the dispersion curve for the $L(0,2)$ has the lowest slope. If the slope is equal to zero for a given frequency, then the mode is non-dispersive at that particular frequency. (Kessler, 2002) In general, modes become less dispersive as frequency increases. Using an extremely high excitation frequency, however, is not practical. Equipment limitations of the data acquisition system may limit the sampling frequency available. Also, as the excitation frequency increases, higher order modes tend to the same velocity as the lower order modes and the $L(0,2)$ mode. Because the actuator ring employed in this research had a discrete number of MFC patches around the circumference, some of the higher order flexural modes were excited. Therefore, the excitation frequency must be chosen such that a compromise is reached between limiting the dispersion and maximizing the separation of the velocities of the higher order modes that may be excited.

To help with the selection of the excitation frequency used in this research, a series of preliminary measurements were taken at various frequencies. Pulse-echo measurements using the MFC patches at the first axial location were made with the excitation frequency varied from 50 to 300-kHz in 25-kHz intervals. The responses from a few of these measurements are shown in Figure 3.10. From these measurements, 100-kHz was chosen as the optimal excitation

frequency for the Lamb wave methods in this research. The 100-kHz measurement demonstrated the best separation in time between the arrival of the $L(0,2)$ mode and the arrivals of the higher order modes. As discussed above, the first four flexural modes were cancelled in the pulse-echo measurements because four MFC patches were used in the actuator array. Therefore, the fifth order and higher flexural modes were potentially excited in these measurements. From the dispersion curves, shown again in Figure 3.11, the speeds of these modes were well separated from the speed of the $L(0,2)$ mode at 100-kHz. Finally, the 100-kHz excitation frequency gave the best signal to noise ratio of those examined. This feature was primarily attributed to tuning the length of the MFC patch to the wavelength of the Lamb wave mode for the most efficient excitation. (Cawley et al. 2003)

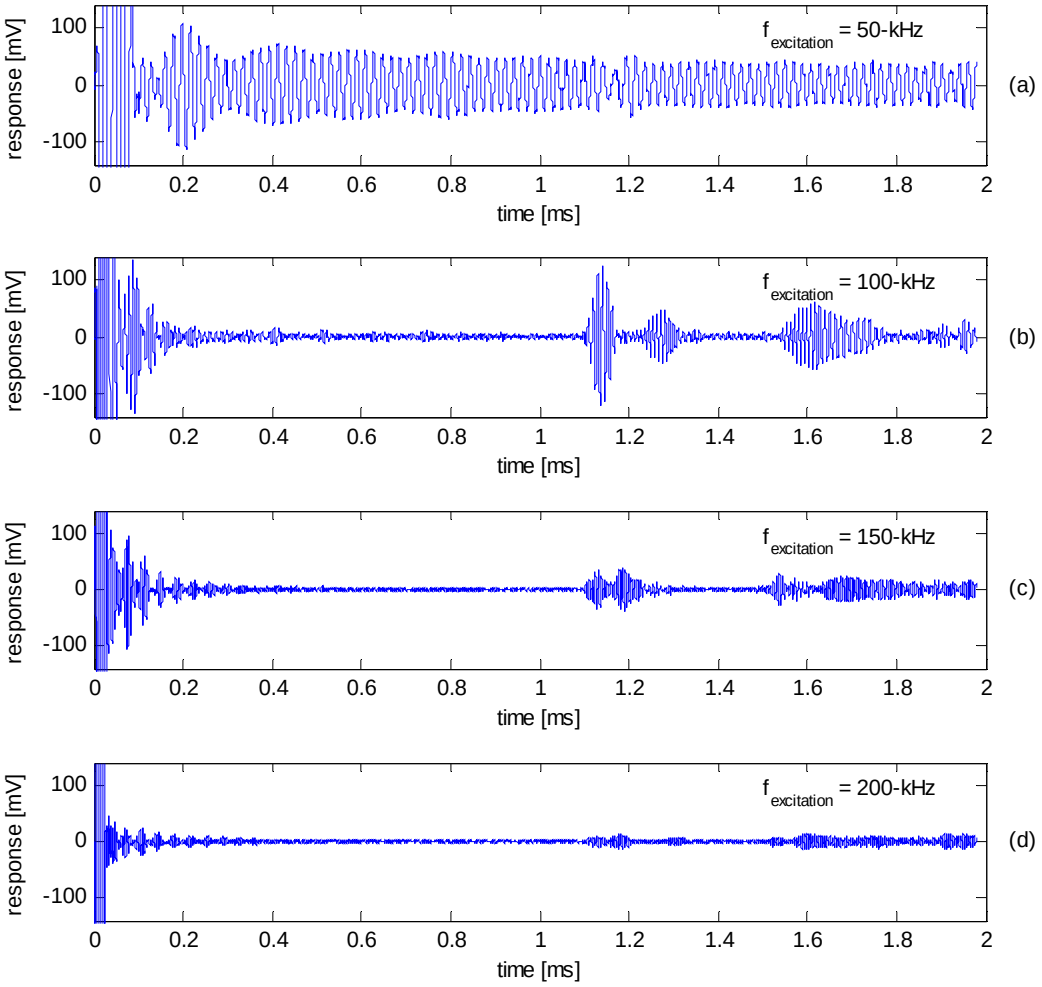

Figure 3.10: Variation of excitation frequency – (a) 50-kHz, (b) 100-kHz, (c) 150-kHz, (d) 200-kHz

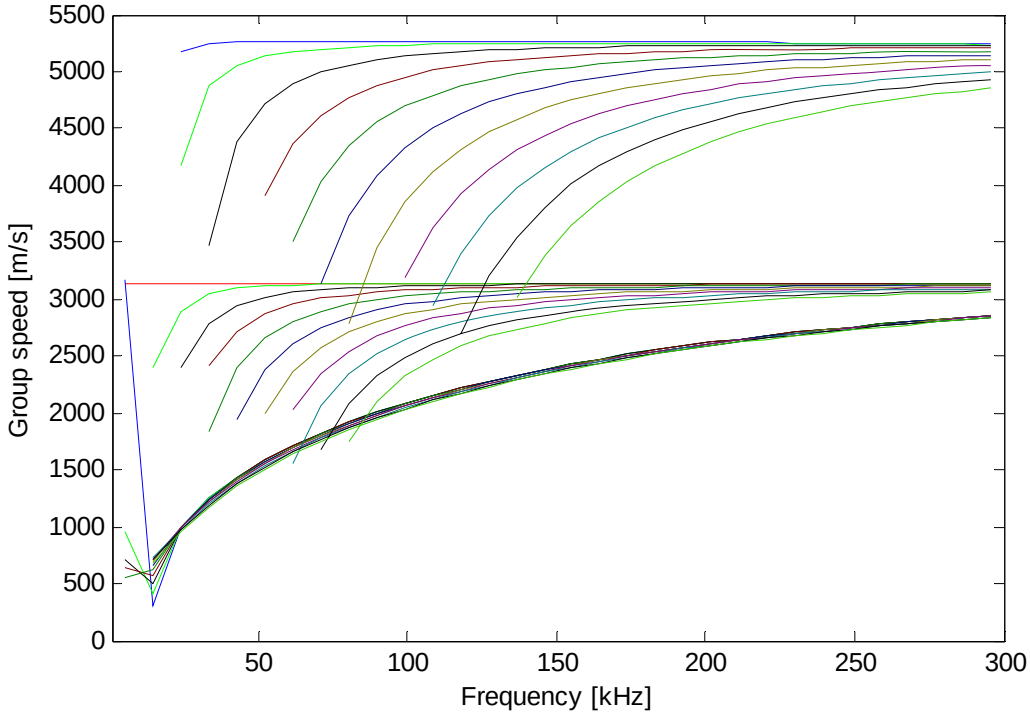

Figure 3.11: Dispersion curves for group velocity of 6-in steel pipe (300-kHz)

Chapter 4 Development of Lamb wave methods

4.1 Overview

When using pulse-echo measurements, a reflection feature can be used to detect and locate damage in a structure. Damage in a pipe, such as cracks and corrosion, causes a local change in the pipe's mass, stiffness, and damping. As Lamb waves propagate through a damaged section of the pipe, the local changes from the damage can cause a portion of the Lamb waves to reflect. If the reflection is strong enough to propagate back to the transducer ring, the reflection feature can be detected. However, the damping in the pipe causes Lamb waves to attenuate exponentially as they propagate. In some cases, such as when the damage is located a large distance from the sensor ring, the reflection can completely attenuate to the level of the sensor's noise floor. If complete attenuation occurs before the reflection returns to the sensor, the reflection feature is left undetectable. Therefore, the sensitivity of pulse-echo measurements to a reflection feature decreases as the distance between the damage and transducer ring increases.

The presence of damage at a given point in time is detected by comparing a current measurement with a baseline measurement which was taken under damage-free conditions. The comparison of the two signals can be used to identify reflections in a current measurement that are not present in the baseline measurement. New reflections can indicate that damage is currently present in the pipe which was not present at the time when the baseline measurement was taken. If no new reflections are detected, then no new damage is present in the structure since the baseline measurement.

Once the presence of damage is identified, an effort can then be made to identify the location of the damage. Using the time history of the response signal from the damage case measurement, the approximate time of arrival of the reflection from the damage can be estimated. Given that the group velocity of the reflected mode is known from the analytical dispersion curves or from a previous experiment, the distance traveled by the mode can be estimated from the time that elapsed between the pulse excitation and the arrival of the reflection. Once the traveled distance is known, the location of the damage is then identified relative to the location of the transducer ring. In this case, the location of the damage is half the distance traveled by the reflected mode because the mode must travel the distance twice, first on the way to the damage location from the actuator and then returning to the sensor after reflecting from the damage. If the transducer ring is close to an end of the pipe, such as axial location #1in Figure 4.1, then the direction of the damage is straightforward. If the transducer ring is near the center of the pipe, such as axial location #2, then the damage could be located at the estimated distance from the transducer ring in either direction down the pipe. Therefore, directional excitation methods are required when the transducer ring is located near the center of the pipe. (Cawley et al. 2003) Because of equipment limitations, however, directional excitation was not used in the research of this thesis. For this reason, this thesis concentrated on pulse-echo measurements made from axial location #1.

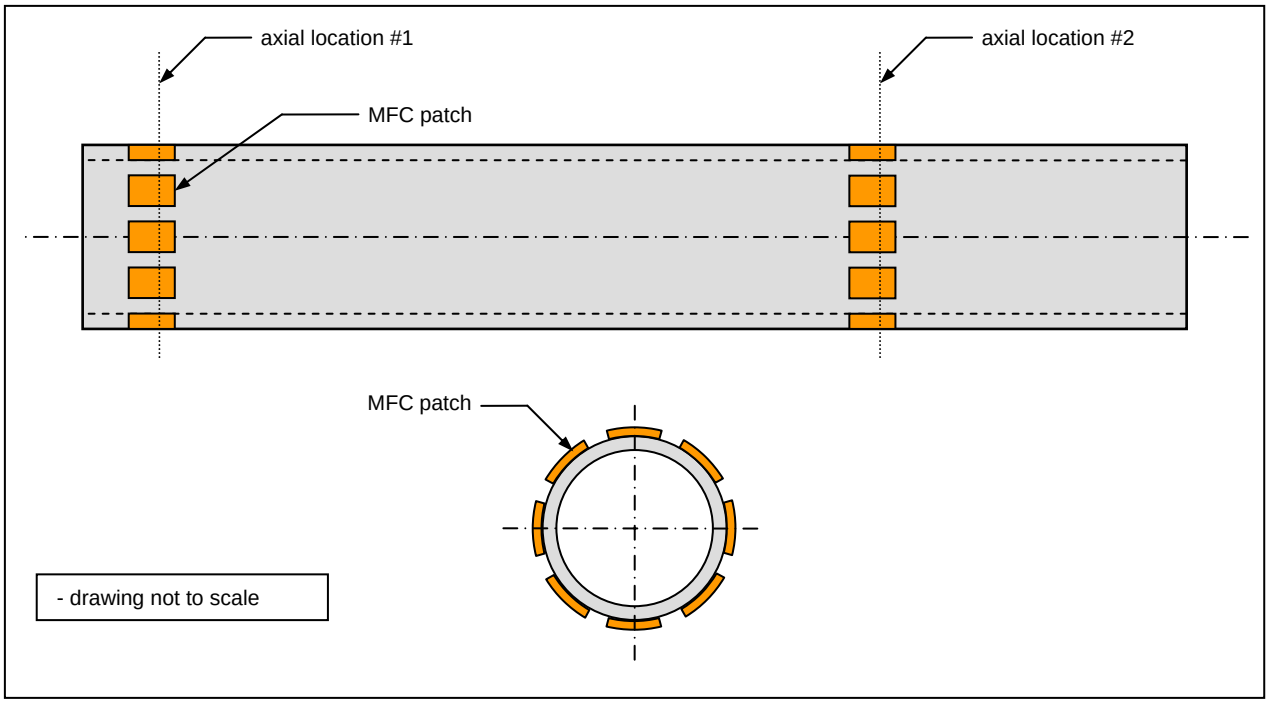

Figure 4.1: Drawing of 6-in steel pipe

Before making permanent damage to the pipe, reversible types of simulated damage were used to develop the signal processing algorithms required to detect and locate the damage. In the research of this thesis, various approaches were implemented to simulate damage in the pipe. Each type of simulated damage created a local change in the stiffness or damping of the system in an effort to simulate the local effects of cracks or corrosion damage. Different types and locations of simulated damage were used to prove the feasibility of the proposed methods and the efficiency of the proposed signal processing techniques. To allow for the comparison of each damage case to the same baseline state and to test the signal processing algorithms, only reversible types of damage were first implemented. The following sections of this chapter present the proposed damage detection algorithm and the results of a few of the reversible damage cases used to develop the algorithm. Once the algorithm was developed from measurements with reversible damage, the algorithm was tested with permanent damage in the following chapter.

4.2 Damage detection algorithm

The exact time of arrival of a given reflection is generally difficult to determine. Typically, the reflection of a given mode from damage is on the same order of magnitude as the coherent noise present in the baseline signal. In addition, the relatively low voltage level of the response signals means that there is a less than desirable signal to noise ratio (random noise). An example of two measurements can be seen in Figure 4.2-a. The reflected signal from the damage in this particular measurement, which happened to be a hose clamp, was an order of magnitude less than the reflection from the end of the pipe. In Figure 4.2-b, a better view of the reflection from the damage is shown. Even with 100 averages in a given ensemble, the random noise present in the signal was approximately 2-mV. Between the baseline and damage-case measurements, the largest difference caused by the reflection from the damage was approximately 3-mV. Therefore, the magnitude of the reflection feature was only 50% greater than the random noise in the baseline measurement. In addition, the coherent noise present in the baseline measurement made the exact time of arrival of the reflection difficult to identify. Therefore, advanced signal processing techniques were used to extract these differences so that the damage could be correctly identified.

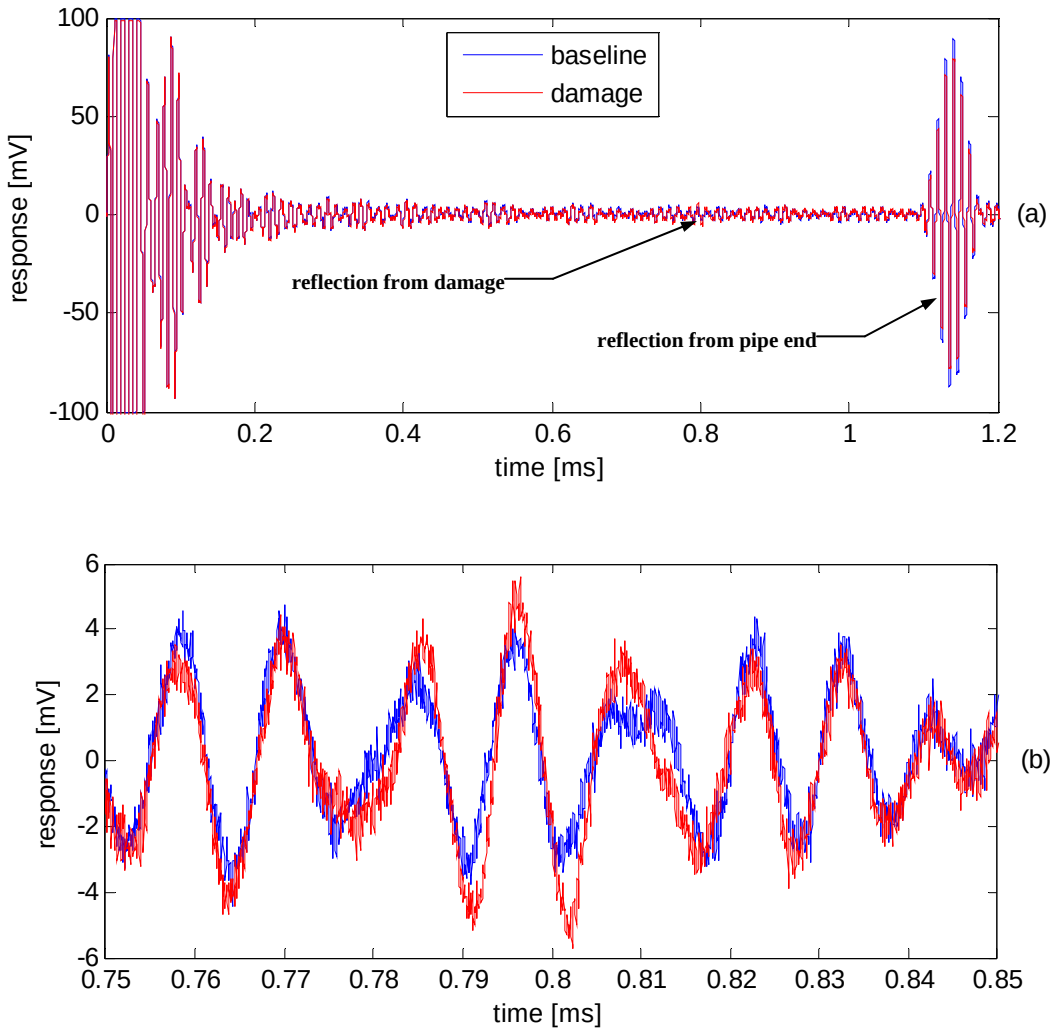

Figure 4.2: (a) Response time histories of a baseline and a damage-case measurement (b) Close-up view of reflection feature from same measurements

The technique used in the research of this thesis involved the continuous wavelet transform and the Hilbert transform. First, the continuous wavelet transform was used to de-noise the response signals from the baseline and damage case measurements. (Spanos et al. 2005; Lu and Hsu, 2000; Staszewski, 1998) Because it was similar in shape to the excitation signal, the Morlet wavelet was used as the mother wavelet for the wavelet transform. A range of scales was used to perform the wavelet transformation, and then the wavelet coefficients

corresponding to the excitation frequency were extracted, discarding all other frequency content. In this case, the range of scales was 135 to 406, which corresponded to a frequency range of 50 to 150-kHz. The coefficients over the full time and frequency range for a single baseline measurement were shown in Figure 4.3. The arrival of the reflection from the opposite end of the pipe was seen around 1.1-ms. With this reflection the effects of dispersion were seen. Although a narrow-band signal of 100-kHz was used for the excitation, the reflection from the opposite end of the pipe had energy which had dispersed to neighboring frequencies. For this reason, the coefficients corresponding to 100-kHz were extracted and used for further signal processing to compare a damage-case measurement to a baseline measurement.

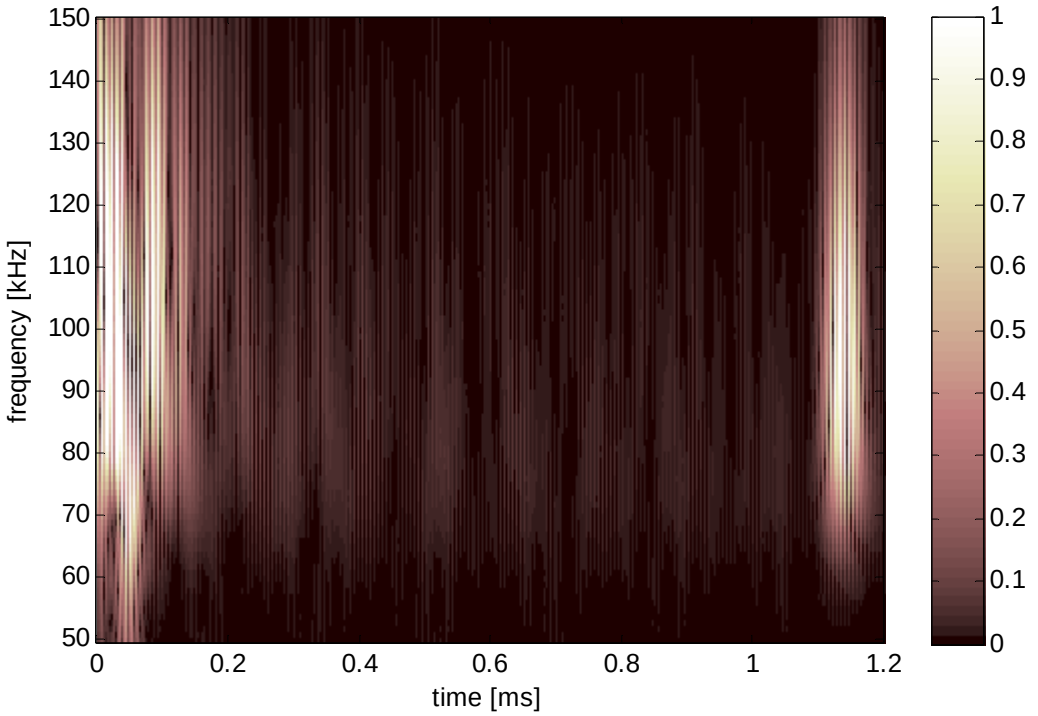

Figure 4.3: Wavelet coefficients for a baseline measurement

An example of the extracted wavelet coefficients corresponding to 100-kHz is shown in Figure 4.4. As seen in this figure, the use of the continuous wavelet transform significantly reduced the random noise present in a given response signal. Because environmental changes,

such as temperature variation, can create slight phase differences between the baseline and damage case measurements, the direct difference between the wavelet coefficients of each measurement did not lend itself well for comparison. Often, the signal differences attributed to the phase variations were much more significant than the actual amplitude differences present because of a reflection feature. To avoid this issue, the Hilbert transform of the wavelet coefficients was first used to find the envelope of each signal's wavelet coefficients, as shown in Figure 4.4. The wavelet coefficients and signal envelopes for a damage-case and a baseline measurement were plotted together for comparison in Figure 4.5. This plot was created from the same two signals shown in Figure 4.2, and the plotting ranges were set to a close-up view of the reflection feature. Because the wavelet transform had effectively de-noised the signal, the difference between the two signals was much easier to identify.

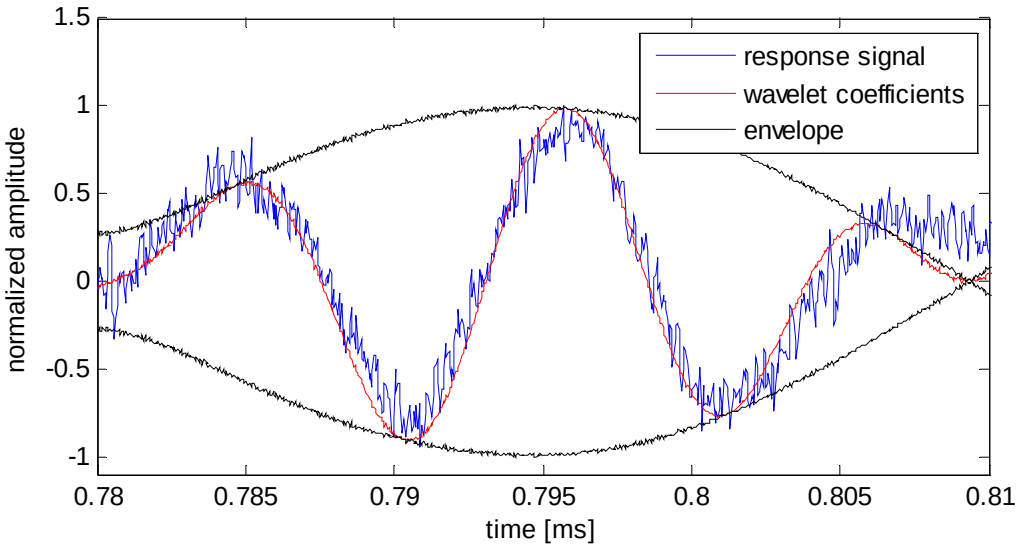

Figure 4.4: Close-up view of a baseline measurement, including the original response signal, the wavelet coefficients of the signal, and the signal envelope from the Hilbert transform

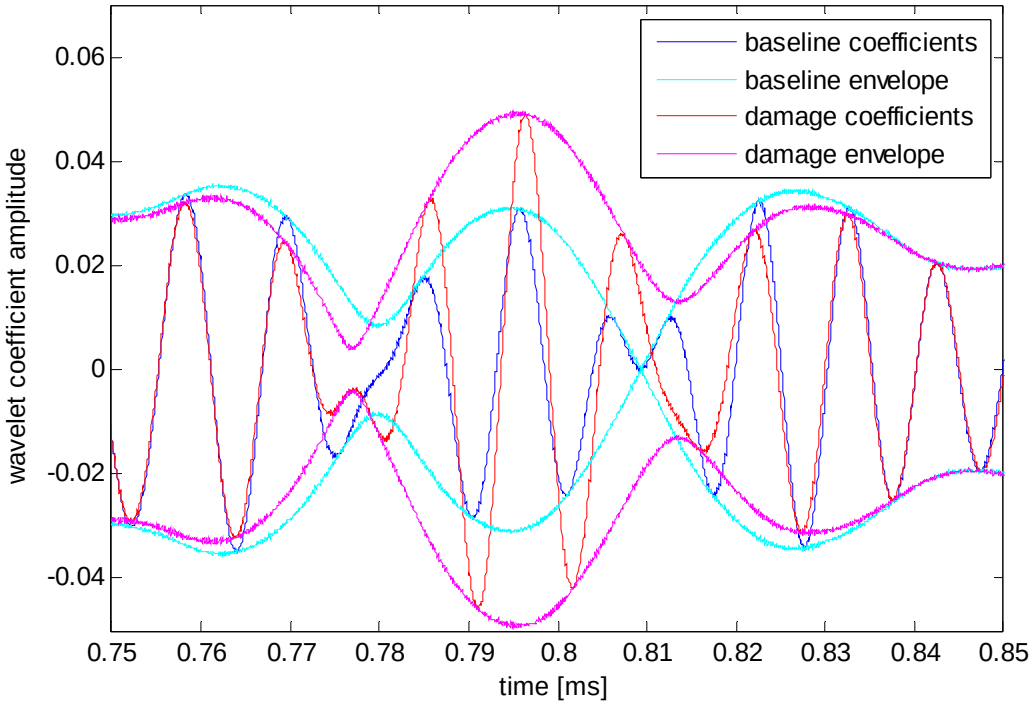

Figure 4.5: Comparison of wavelet coefficients and signal envelopes for a damage-case and a baseline measurement

The direct difference between the two signal envelopes was then used for the actual comparison of the baseline and damage case measurements, as shown in Figure 4.6-b (Figure 4.6-a is shown for reference purposes only). In this figure, the signal difference at 0.8-ms clearly shows the arrival of the reflection from the damage. However, the signal difference corresponding to the reflection from the opposite end of the pipe, which had a magnitude of 0.11 (left out of range of the plotting limits for clarity), was much larger than that corresponding to the reflection from the damage, which had a magnitude of 0.02. The reason for this dissimilarity was that the change in the signal was sensitive to the magnitude of the signal at that particular point in the measurement. Because the reflection from the end of the pipe was at least ten times greater than the coherent noise present at the arrival of the reflection from the damage, the absolute difference was also greater for the end reflection than for the damage

reflection. Therefore, the use of the percent difference between the envelopes of the damage-case and baseline measurements provided additional insight for detecting the damage reflection. The advantage of using the percent difference was that it gave a relative difference between the two measurements, helping to account for the magnitude variations. The percent difference for these two particular measurements is shown in Figure 4.6-c. The reflection from the damage was correctly identified with the large spike at 0.8-ms. In addition, the percent difference showed no spike at the corresponding arrival time of the end reflection. Because the percent difference tended to infinite amplitude as the amplitude of the baseline envelope tended to zero, there was a possibility of a spike in the percent difference occurring where no reflection feature was present. Therefore, the percent difference alone could not reliably be used to identify the presence of damage, but it could supplement the information in the plot of the absolute difference, as demonstrated with the example of the reflection from the end of the pipe. More details regarding the damage detection algorithm are given in Appendix A.

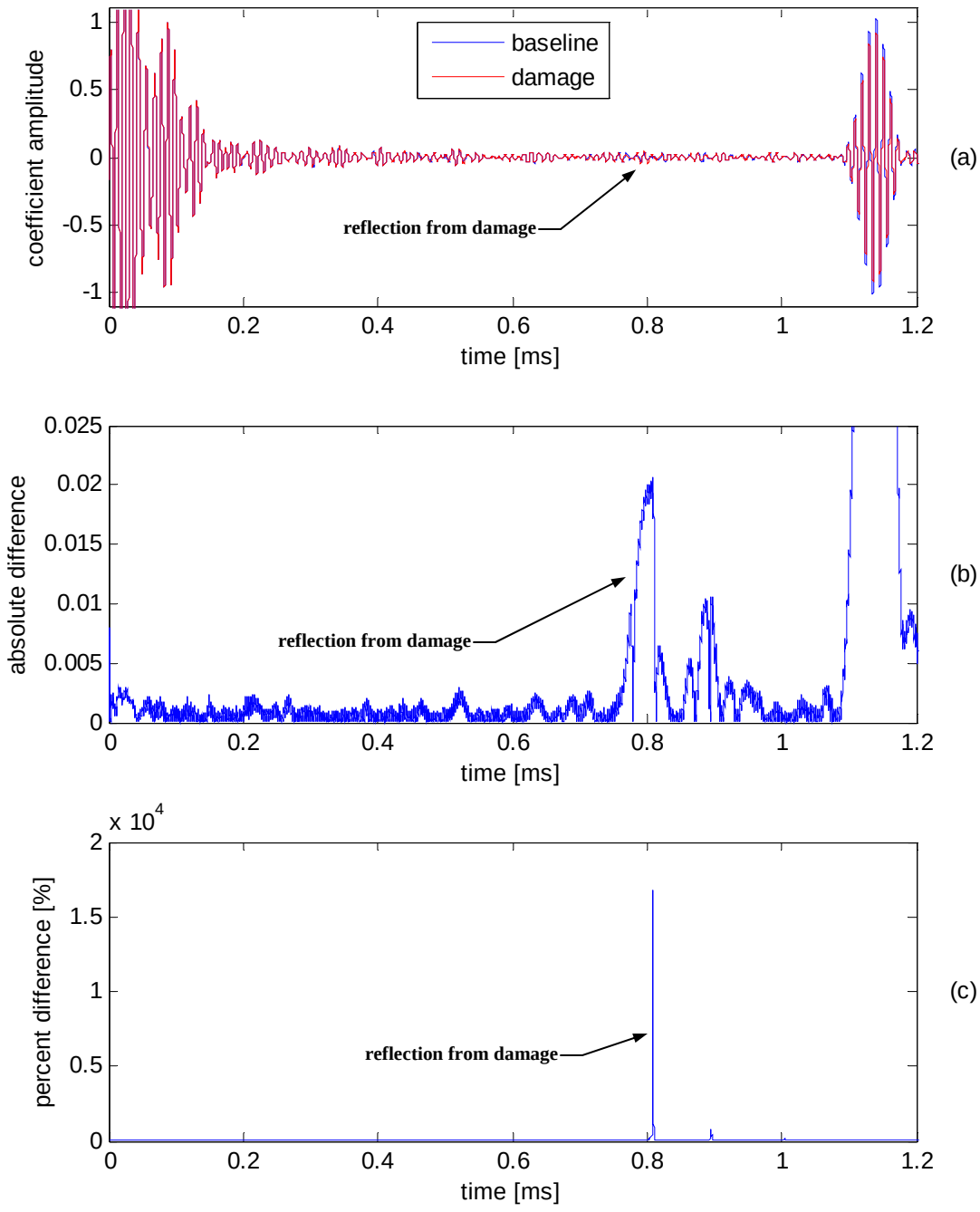

Figure 4.6: (a) Wavelet coefficients for a damage-case and a baseline measurement (b) difference between the signal envelopes (c) percent difference between the signal envelopes

4.3 Variation in Baseline Measurements

In order to account for variation in the measurements, a threshold limit was used for identifying the presence of damage when comparing a current measurement to a baseline measurement. The signal difference at 0.8-ms in Figure 4.6-b was about six times greater than the signal difference leading up to 0.8-ms. Such a large difference clearly indicated a significant change in the condition of the pipe. However, the presence of damage may not always yield such a significant change from the baseline measurement. In fact, the variation in two measurements taken under baseline conditions may be greater than the change caused by the presence of very slight damage, such as the onset of a crack or corrosion. To prevent variation from causing a false indication of damage, the variation between baseline measurements must be characterized. Therefore, numerous baseline measurements were first taken over the span of several days.

Using the signal processing methods described in the previous section, the baseline measurements were compared to each other. The corresponding absolute difference and percent difference for the various baseline measurements are shown in Figure 4.7. The maximum absolute difference observed between these measurements was 0.013 at 1.16-ms. However, this point in time came after the arrival of the reflection from the end of the pipe, which occurred at 1.10-ms. Because a reflection from damage must arrive before the end reflection, only the signal difference occurring before the arrival of the end reflection was taken into consideration. Recall that electromagnetic interference (EMI) at the beginning of a measurement caused coherent noise with a relatively large amplitude that rang down for approximately 3-ms. As discussed in the previous section, the large amplitude of the coherent noise increased the absolute difference between measurements. The relatively low amplitude of the percent difference from 0 to 3-ms

confirmed this observation. From 3-ms to the arrival of the end reflection, however, the absolute difference remained stable at an amplitude less than 0.003. Aside from a few spikes which could be attributed to the amplitude of the signal envelopes tending to zero, the percent difference also remained below 15%, with a peak amplitude of 422%. Considering that the reflection shown in Figure 4.2 has a peak magnitude less than 6-mV and that the coherent noise is almost 4-mV, an overall variation of 15% shows that the Lamb wave measurements presented here are very repeatable.

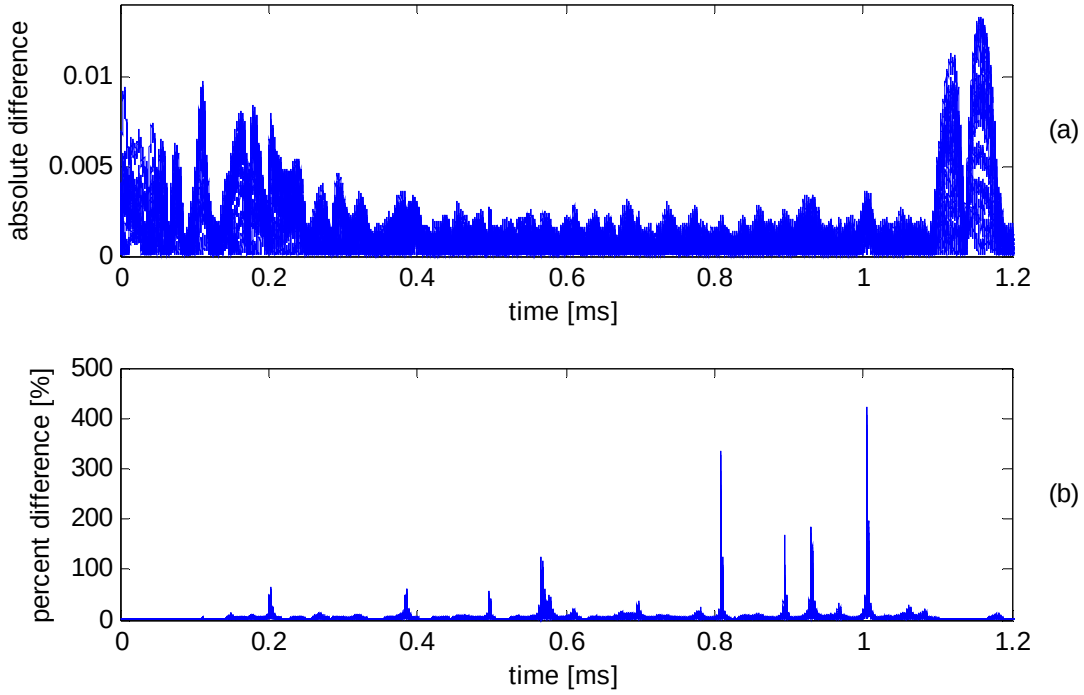

Figure 4.7: absolute difference and percent difference between baseline measurements

To avoid the chance of any false indications of damage, a threshold limit was set at twice the maximum difference seen between the two baseline measurements. Excluding the ring down of coherent noise in the first 3-ms of the measurement, the absolute difference remained below 0.003 and the percent difference remained below 500%, which included any spikes discussed above. To account for any unobserved variation and to include a factor of safety to avoid the

false identification of damage, the threshold limit was set at 200% of the largest observed variation. In this case, the threshold limit for the absolute difference was set at 0.006, the units of which were relative to the amplitude of the wavelet coefficients. Likewise, the threshold limit for the percent difference was set at 1000%. The use of these threshold limits to detect and locate damage was demonstrated in the following sections, which cover a few of the implementations of reversible damage. The reversible damage cases were used prior to implementing permanent damage to allow for the development of the damage detection algorithm discussed in the previous section. Permanent damage was then used as a means to assess the performance of the proposed methods.

4.4 Hose clamp

The first type of reversible damage was a metal hose clamp, the cross section of which was 1/2 x 1/32-in (1.27 x 0.08-cm). At various locations along the axis of the pipe, the hose clamp was tightened around the pipe's outer surface and left in place for a given damage-case measurement. To ensure that the hose clamp was tightened to approximately equal tension at all locations considered, a strain gage mounted to the hose clamp was used to monitor the strain in the clamp. The hose clamp, as mounted to the pipe, can be seen in Figure 4.8.

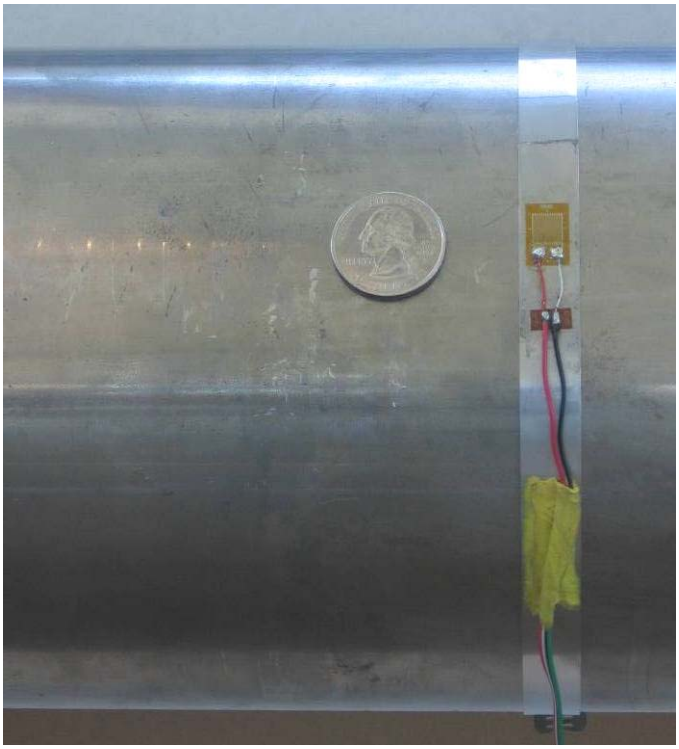

Figure 4.8: Hose clamp as mounted to pipe, including strain gage for monitoring tension in the clamp

The hose clamp was then mounted to the pipe at an axial location 5-ft from the end of the pipe near axial location #1. The corresponding damage-case measurement was taken, and the signal difference between this measurement and a previous baseline measurement was determined. The calculated absolute difference and percent difference for this damage case are shown in Figure 4.9. For this particular measurement, the signal difference surpassed the threshold limit at approximately 0.545-ms, which corresponded to a damage location of 5.043-ft (1.537-m) from the end of the pipe near axial location #1. The peak value of the absolute difference for this reflection feature was 0.085. In addition, the percent difference between the two measurements also crossed the threshold limit around 0.553-ms and reached a peak value of 4,735%, confirming that the absolute difference was correctly identifying the presence of damage. Ten damage-case measurements were taken at two different damage locations, one with the hose clamp at 5.0-ft (1.5-m) and another with the hose clamp at 7.0-ft (2.1-m). The

corresponding estimates of the damage location and the percent difference from the actual location are shown in Table 4.1. For each damage location considered here, all ten measurements correctly identified the presence of the damage and accurately identified the location of the damage within 1.0% difference, which amounts to less than 1.0-in (2.5-cm).

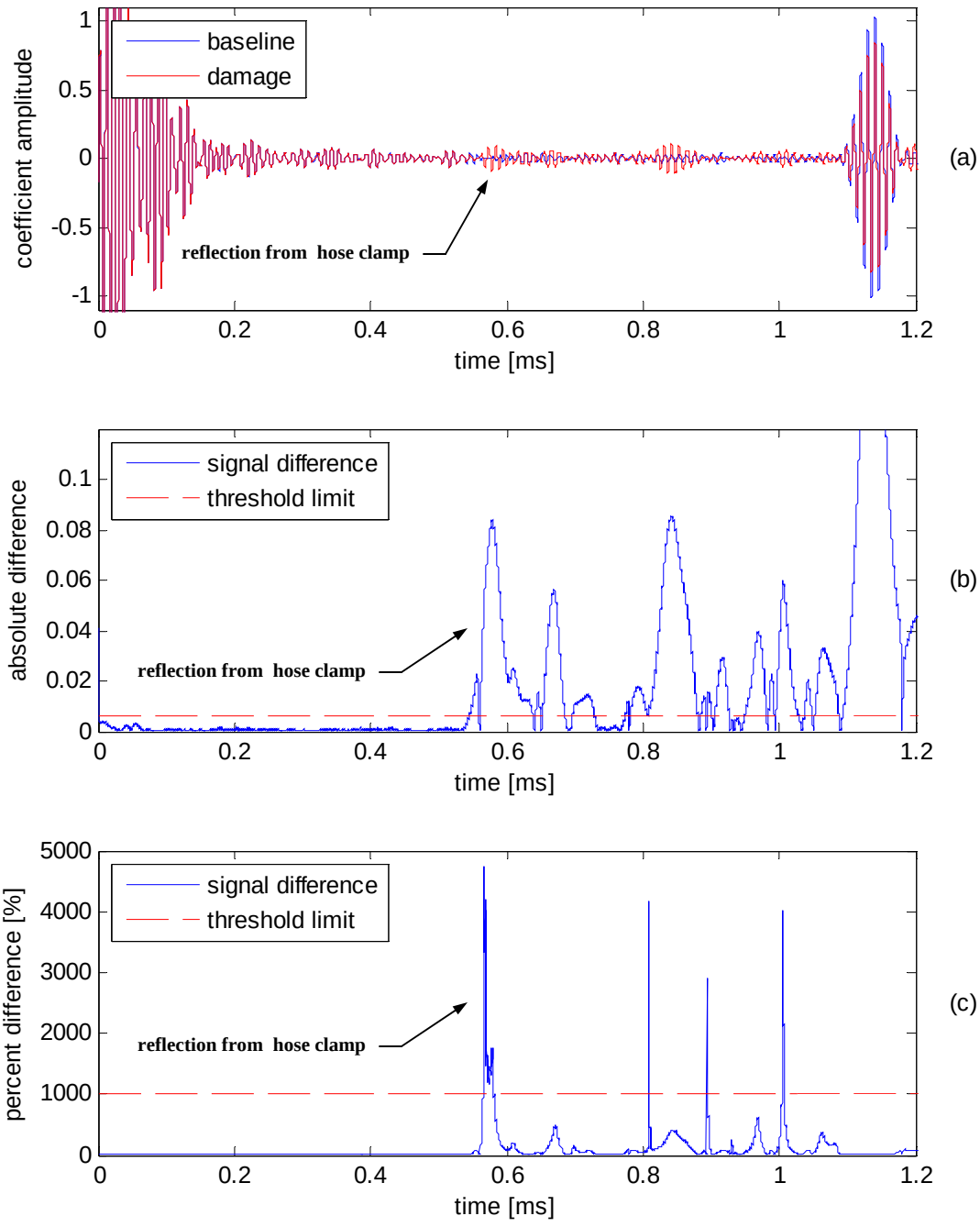

Figure 4.9: Signal difference between baseline and damage case measurements (hose clamp at 5.00-ft (1.52-m))

actual damage location [ft (m)]	estimated damage location [ft (m)]	percent difference [%]	actual damage location [ft (m)]	estimated damage location [ft (m)]	percent difference [%]
5.00 (1.52)	5.04 (1.54)	0.87	7.00 (2.13)	6.95 (2.12)	0.67
5.00 (1.52)	5.05 (1.54)	0.93	7.00 (2.13)	6.94 (2.12)	0.84
5.00 (1.52)	5.05 (1.54)	0.94	7.00 (2.13)	6.96 (2.12)	0.54
5.00 (1.52)	5.04 (1.54)	0.87	7.00 (2.13)	6.96 (2.12)	0.59
5.00 (1.52)	5.04 (1.54)	0.87	7.00 (2.13)	6.96 (2.12)	0.62
5.00 (1.52)	5.04 (1.54)	0.79	7.00 (2.13)	6.95 (2.12)	0.65
5.00 (1.52)	5.04 (1.54)	0.71	7.00 (2.13)	6.97 (2.12)	0.44
5.00 (1.52)	5.03 (1.53)	0.51	7.00 (2.13)	6.96 (2.12)	0.54
5.00 (1.52)	5.04 (1.54)	0.73	7.00 (2.13)	6.95 (2.12)	0.65
5.00 (1.52)	5.04 (1.54)	0.84	7.00 (2.13)	6.95 (2.12)	0.78

Table 4.1: Actual and estimated damage locations for hose clamp damage cases

4.5 Hose clamp with adhesive

The second type of reversible damage utilized the same metal hose clamp, but this time a strip of adhesive was added between the pipe surface and the clamp. Because the adhesive was soft and malleable, it dampened the reflection from the hose clamp, resulting in a weaker reflection feature than with the hose clamp alone. At various locations along the axis of the pipe, the hose clamp with the adhesive was tightened around the pipe's outer surface and left in place for a given damage-case measurement. To ensure that the hose clamp was tightened to approximately equal tension at all locations considered, a strain gage mounted to the hose clamp was used to monitor the strain in the clamp. The tension in the hose clamp was half the tension from the previous damage case when the hose clamp was used without the adhesive. The hose clamp with the adhesive, as mounted to the pipe, can be seen in Figure 4.10.

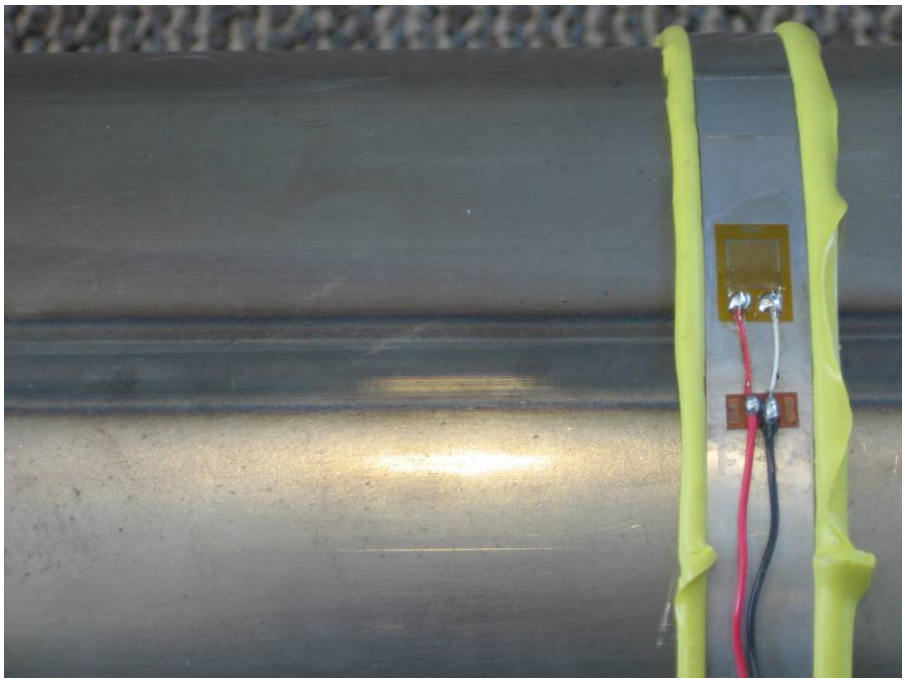

Figure 4.10: Hose clamp with adhesive as mounted to pipe

The hose clamp with the adhesive strip was then mounted to the pipe at an axial location 9-ft (2.7-m) from the end of the pipe near axial location #1. The corresponding damage-case measurement was taken, and the signal difference between this measurement and a previous baseline measurement was determined. The calculated absolute difference and percent difference for this damage case are shown in Figure 4.11. For this particular measurement, the signal difference surpassed the threshold limit at approximately 0.997-ms, which corresponded to a damage location of 8.940-ft (2.725-m) from the end of the pipe near axial location #1. The peak value of the absolute difference for this reflection feature was 0.024. In addition, the percent difference between the two measurements also crossed the threshold limit around 1.005-ms and reached a peak value of 2,623%, confirming that the absolute difference was correctly identifying the presence of damage. Because the adhesive added damping to the damage applied by the hose clamp, the reflection from this damage case was less than a quarter of the magnitude of the reflection from the hose clamp damage case. Ten damage-case

measurements were taken at three different damage locations. The corresponding estimates of the damage location and the percent difference from the actual location are shown in Table 4.2. For each damage location considered here, all ten measurements correctly identified the presence of the damage and accurately identified the location of the damage within 2.0% difference, which amounted to less than 1.2-in (3.0-cm).

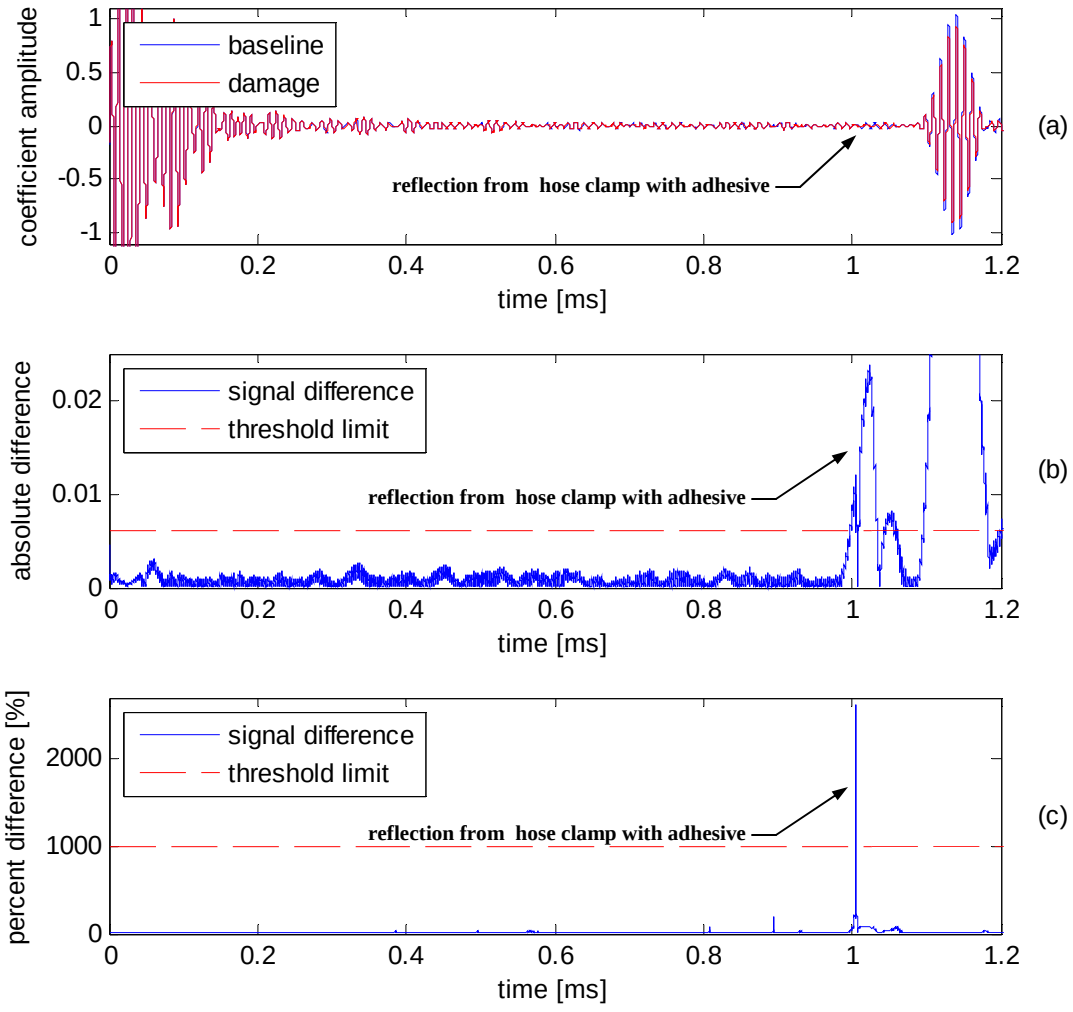

Figure 4.11: Signal difference between baseline and damage case measurements (hose clamp with adhesive at 9.00-ft (2.74-m))

actual damage location [ft (m)]	estimated damage location [ft (m)]	percent difference [%]	actual damage location [ft (m)]	estimated damage location [ft (m)]	percent difference [%]	actual damage location [ft (m)]	estimated damage location [ft (m)]	percent difference [%]
5.00 (1.52)	5.07 (1.55)	1.41	7.00 (2.13)	6.92 (2.11)	1.09	9.00 (2.74)	8.94 (2.72)	0.70
5.00 (1.52)	5.07 (1.55)	1.45	7.00 (2.13)	6.94 (2.12)	0.90	9.00 (2.74)	8.94 (2.72)	0.67
5.00 (1.52)	5.06 (1.54)	1.28	7.00 (2.13)	6.95 (2.13)	0.77	9.00 (2.74)	8.93 (2.72)	0.78
5.00 (1.52)	5.07 (1.55)	1.49	7.00 (2.13)	6.95 (2.12)	0.78	9.00 (2.74)	8.94 (2.72)	0.62
5.00 (1.52)	5.10 (1.55)	1.92	7.00 (2.13)	6.93 (2.11)	0.98	9.00 (2.74)	8.94 (2.72)	0.70
5.00 (1.52)	5.07 (1.55)	1.49	7.00 (2.13)	6.94 (2.12)	0.89	9.00 (2.74)	8.93 (2.72)	0.82
5.00 (1.52)	5.06 (1.54)	1.13	7.00 (2.13)	6.93 (2.11)	1.00	9.00 (2.74)	8.94 (2.72)	0.62
5.00 (1.52)	5.06 (1.54)	1.26	7.00 (2.13)	6.93 (2.11)	0.96	9.00 (2.74)	8.94 (2.72)	0.64
5.00 (1.52)	5.07 (1.55)	1.38	7.00 (2.13)	6.95 (2.12)	0.74	9.00 (2.74)	8.95 (2.73)	0.53
5.00 (1.52)	5.07 (1.55)	1.37	7.00 (2.13)	6.93 (2.11)	1.02	9.00 (2.74)	8.94 (2.72)	0.70

Table 4.2: Actual and estimated damage locations for hose clamp with adhesive damage cases

4.6 Clamped blocks

The next type of reversible damage was a set of three aluminum blocks clamped to the pipe with two hose clamps. The blocks were used to simulate damage that was not continuous around the circumference of the pipe, as with the hose clamp. The three blocks, each of which has dimensions 0.5 x 0.5 x 1.5-in (1.27 x 1.27 x 3.81-cm), were equally spaced around the circumference of the pipe and clamped in place using two hose clamps, as shown in Figure 4.12. At various locations along the axis of the pipe, the blocks were clamped to the pipe's outer surface and left in place for a given damage-case measurement. As with the previous damage cases, a strain gage mounted to each hose clamp was used to monitor the strain in the clamp.

Using the same threshold limit from the previous damage case, the clamped blocks were mounted to the pipe at an axial location 7-ft (2.13-m) from the end of the pipe near axial location #1. The corresponding damage-case measurement was taken, and the signal processing

technique outlined in the previous section was used to find the signal difference between this measurement and a previous baseline measurement. The calculated absolute difference and percent difference for this damage case are shown in Figure 4.13. For this particular measurement, the signal difference surpassed the threshold limit at approximately 0.759-ms, which corresponded to a damage location of 6.945-ft (2.117-m) from the end of the pipe near axial location #1. The peak value of the absolute difference for this reflection feature was 0.021. In addition, the percent difference between the two measurements also crossed the threshold limit around 0.810-ms and reached a peak value of 1,035%, which was just above the threshold of 1,000%. This value still confirmed that the absolute difference was correctly identifying the presence of damage. Because the clamped blocks did not make contact around the entire circumference of the pipe, the reflection from this damage case was less than a quarter of the magnitude of the reflection from the hose clamp damage case, which did contact the entire circumference. Ten damage-case measurements were taken for two different damage cases, one with the hose clamp at 5-ft 1-in (1.55-m) and another with the hose clamp at 7.0-ft (2.13-m). The corresponding estimates of the damage location and the percent difference from the actual location are shown in Table 4.3. For each damage location considered here, all ten measurements correctly identified the presence of the damage and accurately identified the location of the damage within 1.0% difference, which amounted to less than 1.0-in (2.5-cm).

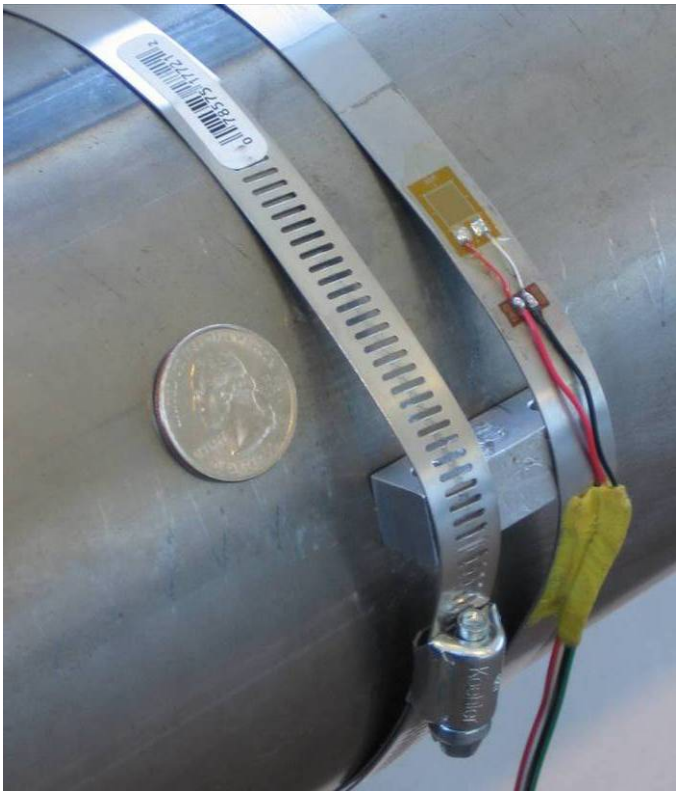

Figure 4.12: Clamped blocks as mounted to pipe

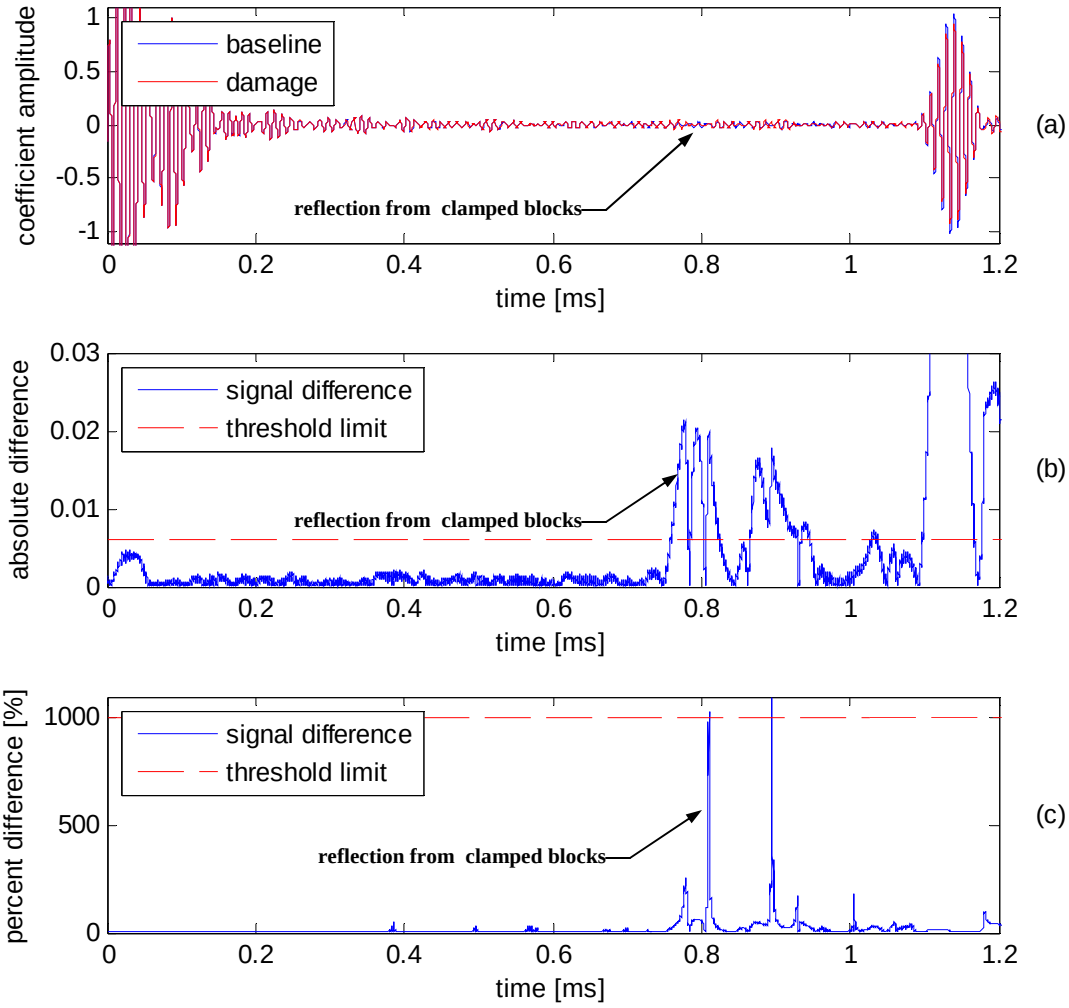

Figure 4.13: Signal difference between baseline and damage case measurements (clamped blocks at 7.00-ft (2.13-m))

actual damage location [ft (m)]	estimated damage location [ft (m)]	percent difference [%]	actual damage location [ft (m)]	estimated damage location [ft (m)]	percent difference [%]
5.08 (1.55)	5.08 (1.55)	0.08	7.00 (2.13)	6.94 (2.12)	0.79
5.08 (1.55)	5.07 (1.55)	0.21	7.00 (2.13)	6.94 (2.12)	0.87
5.08 (1.55)	5.07 (1.55)	0.14	7.00 (2.13)	6.94 (2.12)	0.79
5.08 (1.55)	5.06 (1.54)	0.30	7.00 (2.13)	6.93 (2.11)	0.95
5.08 (1.55)	5.06 (1.54)	0.30	7.00 (2.13)	6.94 (2.12)	0.82
5.08 (1.55)	5.07 (1.55)	0.21	7.00 (2.13)	6.94 (2.12)	0.89
5.08 (1.55)	5.07 (1.55)	0.19	7.00 (2.13)	6.94 (2.12)	0.82
5.08 (1.55)	5.07 (1.55)	0.23	7.00 (2.13)	6.93 (2.11)	0.99
5.08 (1.55)	5.06 (1.54)	0.33	7.00 (2.13)	6.94 (2.12)	0.83
5.08 (1.55)	5.07 (1.55)	0.16	7.00 (2.13)	6.94 (2.12)	0.86

Table 4.3: Actual and estimated damage locations for clamped blocks damage cases

4.7 Constrained damping layer

The third type of reversible damage considered was a constrained damping layer. For this damage case, an 18 x 9-in (45.7 x 22.9-cm) sheet of a constrained damping layer (3M Scotchdamp SJ-2052X T1005) was adhered around the pipe's circumference at an axial location 5-ft (1.5-m) from the end of the pipe near axial location #1. The damping layer extended in the axial direction from 5-ft (1.5-m) to 5-ft 9-in (1.75-m). The damage case, as applied, can be seen in the photograph in Figure 4.14.

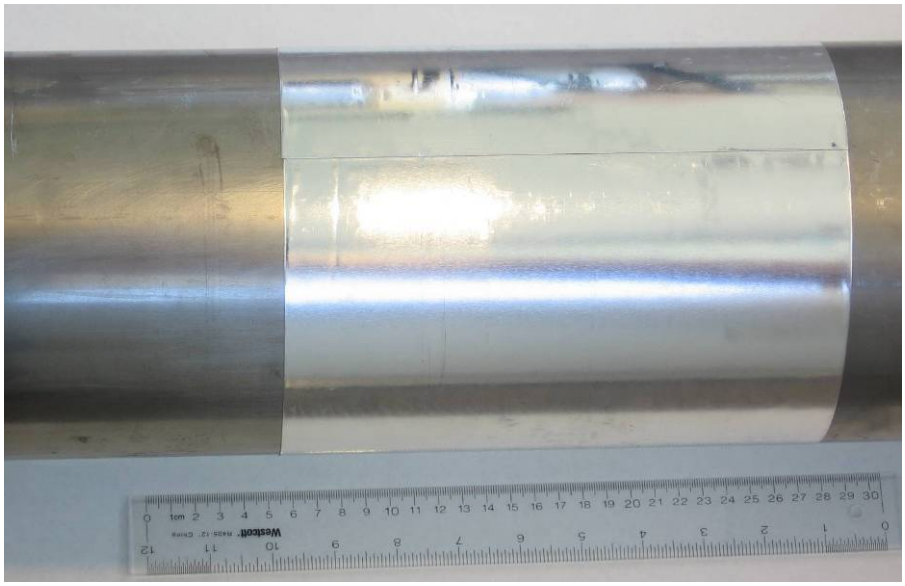

Figure 4.14: Constrained damping layer as mounted to pipe

Because the constrained damping layer ideally increases the damping of a structure without a significant stiffness or mass change, the reflection from this damage case was much less than the damage cases presented above. The reflection was so slight, in fact, that the threshold limit of 0.006 for the absolute difference, as described above, was abandoned. With such a small response from the reflected mode, the amplitude of the signal difference at the reflection was only 20 to 30% greater than 0.003 variation in the absolute difference with the baseline measurements.

Although the signal difference method can not accurately locate the damage because of the lack of a strong reflection feature, the attenuation feature of the reflection from the pipe's opposite end can at least correctly identify the presence of damage. As seen in Figure 4.15, there was significant attenuation in the reflection from the pipe's opposite end. The attenuation, which was attributed to the increased damping in the structure as a result of the addition of the constrained damping layer, is a feature that showed that damage was present in the pipe. However, the attenuation feature could not be used to locate the damage.

Because the approximate time of arrival for the reflection was known from previous measurements which were made with stronger damage at the same location, the peak which corresponded to the reflection from the constrained damping layer could still be identified. Therefore, the threshold limit could be decreased from 0.006 to 0.004 to accommodate the reduced amplitude of the reflection. Assuming that the reflection occurred at the leading edge of the constrained damping layer, the estimated locations and corresponding percent differences are shown in Table 4.4. With this assumption, the mean percent difference was 4.73%. However, the standard deviation of the estimated damage location was only 0.03-ft (0.91-cm) with a mean of 5.24-ft (1.60-m), which demonstrated that the effective reflection point of the damping layer was 0.24-ft (7.32-cm) from the leading edge of the damping layer. Using this location, the percent difference for all 20 measurements was less than 1.0%. Therefore, adjusting the threshold limit showed that all twenty measurements correctly identified the presence of the damage and accurately identified the location of the damage.

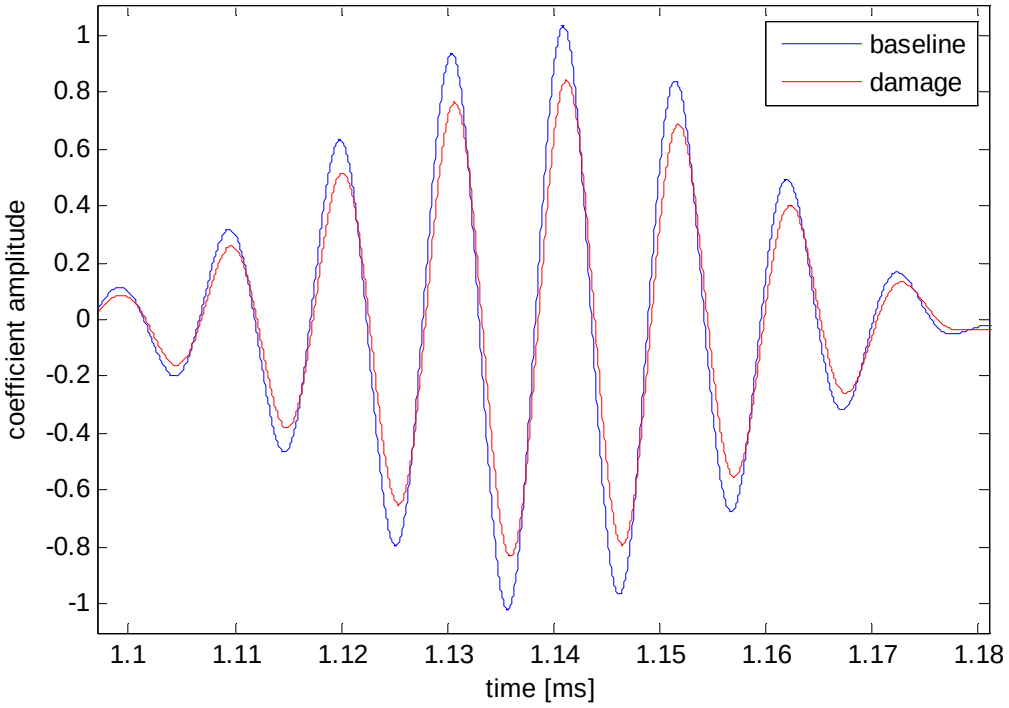

Figure 4.15: Close-up view of wavelet coefficients of pipe-end reflection for baseline and damage measurements

actual damage location [ft (m)]	estimated damage location [ft (m)]	percent difference [%]	actual damage location [ft (m)]	estimated damage location [ft (m)]	percent difference [%]
5.00 (1.52)	5.24 (1.60)	4.72	5.00 (1.52)	5.24 (1.60)	4.74
5.00 (1.52)	5.23 (1.60)	4.68	5.00 (1.52)	5.24 (1.60)	4.74
5.00 (1.52)	5.24 (1.60)	4.74	5.00 (1.52)	5.23 (1.60)	4.68
5.00 (1.52)	5.24 (1.60)	4.74	5.00 (1.52)	5.24 (1.60)	4.75
5.00 (1.52)	5.24 (1.60)	4.73	5.00 (1.52)	5.24 (1.60)	4.81
5.00 (1.52)	5.24 (1.60)	4.70	5.00 (1.52)	5.24 (1.60)	4.74
5.00 (1.52)	5.24 (1.60)	4.76	5.00 (1.52)	5.24 (1.60)	4.79
5.00 (1.52)	5.24 (1.60)	4.72	5.00 (1.52)	5.24 (1.60)	4.76
5.00 (1.52)	5.24 (1.60)	4.72	5.00 (1.52)	5.24 (1.60)	4.75
5.00 (1.52)	5.23 (1.60)	4.69	5.00 (1.52)	5.24 (1.60)	4.73

Table 4.4: Actual and estimated damage locations for constrained damping layer damage cases

4.8 Discussion

The results presented here demonstrate the ability of the proposed methods to correctly identify the presence of damage and, using reflection features, the ability to accurately identify the location of the damage. For the few types of simulated damage presented here, the reflection features were used to correctly identify that damage was present. Likewise, the comparison of multiple baseline measurements shows that the methods avoided the problem of falsely giving a positive inclination of damage when there was in fact no damage present. The baseline comparison shows that Lamb wave measurements were very repeatable. Even when comparing baseline measurements from a wide range of times in a given day or even week, the variation from measurement to measurement remained well below the threshold limit. In addition to correctly identifying the presence of damage, the use of time-of-flight calculations accurately determined the location of the damage. For all damage cases described above, the location of the damage was accurately estimated within 2.0% of the actual location.

In the damage cases presented here, only reversible types of damage are implemented. The initial use of reversible cases to simulate damage allowed for the development of the damage detection algorithm. The reversible damage cases have enabled the proof of the concept that MFC patches can be used for damage detection with Lamb waves. The next chapter addresses damage cases that involve making permanent alterations to the pipe, such as cracks and corrosion.

Chapter 5 Assessment of Lamb wave methods

5.1 Overview

As presented in the previous chapter, reversible types of simulated damage are used to develop the signal processing algorithms required to detect and locate the damage. Once the algorithm is proven to successfully detect and locate reversible types of damage, permanent forms of damage are then used to test the performance of the algorithm. Only with the implementation of permanent damage can conclusions be drawn regarding the actual potential application of the proposed methods to industrial situations.

In the research of this thesis, three approaches were implemented to simulate real-world damage in the pipe. Each type of simulated damage was designed to simulate either cracks or corrosion damage that might occur in actual applications in industry. Different types and locations of simulated cracks and corrosion damage were used to prove the feasibility of the proposed methods. The final implementation of damage involves actual corrosion which has been accelerated using electrolytic processes. The following sections of this chapter present the performance of the proposed damage detection algorithm for detecting permanent damage to the main body of the pipe.

5.2 Circumferential notch, 50% through thickness

The first type of permanent damage was a circumferential notch. The width of the notch was approximately 1/16-in (1.6-mm), and the depth was approximately 1/32-in (0.8-mm), which was 50% through the thickness of the pipe's wall. Such a notch is a reasonable representation of a circumferential crack if the axial depth of the notch is significantly smaller than the wavelength

of the guided waves and significantly smaller than the circumferential length of the notch. (Alleyne, et al. 1996) From the dispersion curve for the $L(0,2)$ mode, the group velocity was 17,200-ft/s (5.24-km/s) at 100-kHz. The corresponding wavelength was 2.06-in (5.23-cm), which was over 50 times greater than the axial depth of the notch. In addition, the minimum circumferential extent of the notch used here was 1.18-in (3.00-cm), which was over 25 times greater than its axial depth. According to Alleyne, et al. (1996), the notch was, therefore, a reasonable representation of a circumferential crack.

The circumferential notch was made at an axial location 9.0-ft (2.74-m) from the end of the pipe near axial location #1. The length of the notch for the first damage case extended around the pipe's circumference from 0.0° to 22.5° (1.18-in, 3.00-cm), as seen in Figure 5.1. For the second damage case, the length of the notch was increased from 22.5° to 45.0°, as seen in Figure 5.2. For the final damage case with the 50% through thickness notch, the length was increased to 67.5°, as seen in Figure 4.8.

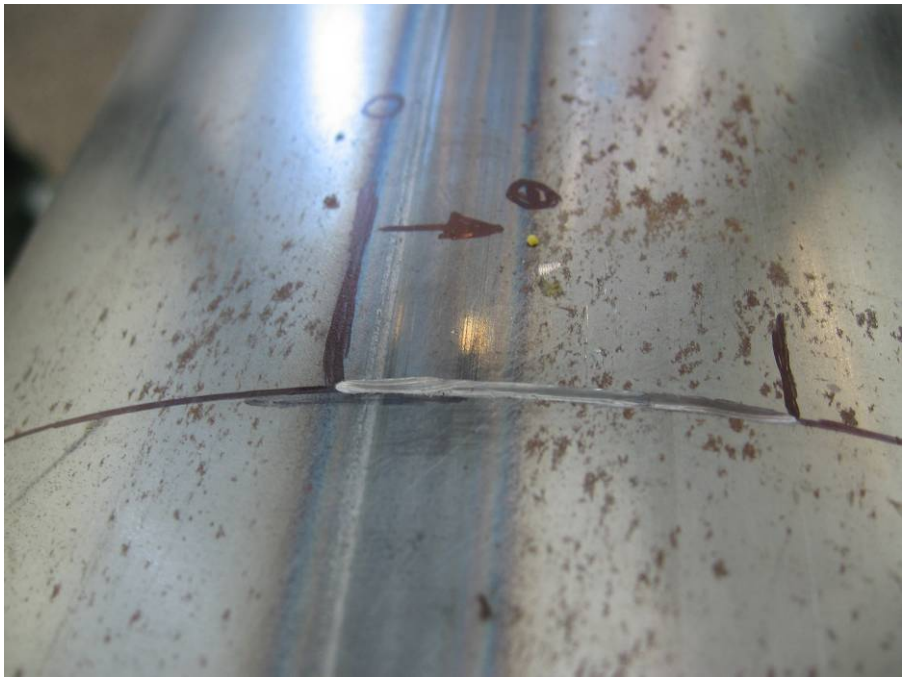

Figure 5.1: Circumferential notch, 50% through thickness, 0.0° to 22.5°

Figure 5.2: Circumferential notch, 50% through thickness, 0.0° to 45.0°

Figure 5.3: Circumferential notch, 50% through thickness, 0.0° to 67.5°

The corresponding damage-case measurements were taken for each of the three circumferential lengths described above. For each damage case, ten measurements were taken. Using the algorithm outlined in the previous section, the signal differences between these

measurements and a previous baseline measurement were determined. The calculated absolute difference and percent difference for each of the damage cases are shown in Figure 4.9.

For the circumferential extent of 0.0° to 22.5°, the notch of 50% through thickness was not detected by the proposed algorithm even though there was a slight peak in the absolute and percent difference. The peak value of the absolute difference was 0.005, which as just under the threshold limit of 0.006. Likewise, the peak value of the percent difference was 594%, which was well below the threshold limit of 1,000%. On the other hand, the circumferential notch of 50% through thickness was successfully detected for the other two damage cases. For the circumferential extent of 0.0° to 45.0°, the peak value of the absolute difference was 0.010, and the peak value of the percent difference was 1,350%. The absolute difference and percent difference were in agreement because both values were well above the corresponding threshold limit. When the circumferential notch was again extended by 22.5° to 67.5°, the absolute difference and percent difference showed increases to 0.018 and 2,266%, respectively.

For the second and third damage cases, the estimates of the damage location and the percent difference from the actual location are shown in Table 4.1. The first damage case, 0.0° to 22.5°, was omitted from the table because the presence of the damage could not be identified with the given threshold limits. For both of the damage cases where the presence of the damage was detected, all ten measurements accurately identified the location of the damage within 1.0% difference of the actual location, which amounted to less than 1.0-in (2.54-cm).

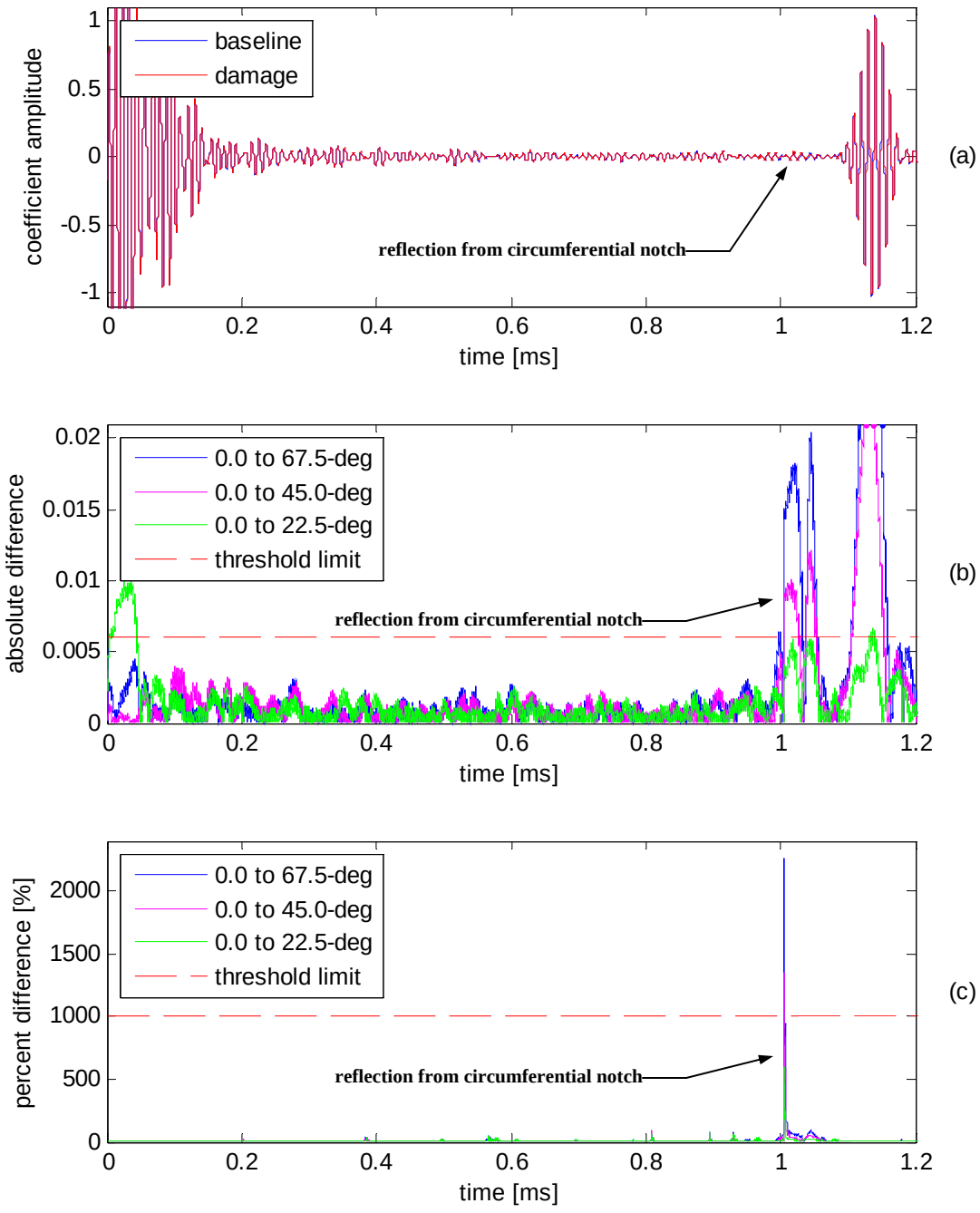

Figure 5.4: Signal difference between baseline and damage case measurements (circumferential notch, 50% through thickness)

circumferential extent [deg]	estimated damage location [ft (m)]	percent difference [%]	circumferential extent [deg]	estimated damage location [ft (m)]	percent difference [%]
0.0 to 45.0	9.07 (2.76)	0.83	0.0 to 67.5	9.01 (2.75)	0.08
0.0 to 45.0	9.07 (2.76)	0.83	0.0 to 67.5	9.02 (2.75)	0.18
0.0 to 45.0	9.08 (2.77)	0.84	0.0 to 67.5	9.00 (2.74)	0.02
0.0 to 45.0	9.07 (2.76)	0.83	0.0 to 67.5	9.02 (2.75)	0.22
0.0 to 45.0	9.08 (2.77)	0.84	0.0 to 67.5	9.02 (2.75)	0.18
0.0 to 45.0	9.08 (2.77)	0.84	0.0 to 67.5	9.00 (2.74)	0.05
0.0 to 45.0	9.07 (2.76)	0.83	0.0 to 67.5	9.00 (2.74)	0.05
0.0 to 45.0	9.08 (2.77)	0.84	0.0 to 67.5	9.00 (2.74)	0.02
0.0 to 45.0	9.07 (2.76)	0.83	0.0 to 67.5	9.01 (2.75)	0.15
0.0 to 45.0	9.08 (2.77)	0.84	0.0 to 67.5	9.02 (2.75)	0.18

Table 5.1: Estimated damage locations for circumferential notch at 9.0-ft (2.74-m), 50% through thickness

5.3 Circumferential notch, 100% through thickness

The second type of permanent damage was similar to the circumferential notch from the previous damage cases, but the depth was increased from 50% through the thickness of the pipe's wall to 100%. Rather than making a new notch at a different axial location, the middle portion of the notch from the previous damage cases was simply altered. The existing notch at 9.0-ft (2.74-m) was cut completely through the thickness of the pipe from 22.5° to 45.0°, resulting in a slit through which the contents of the pipe could potentially leak and escape, as seen in the photograph in Figure 5.5.

Figure 5.5: Circumferential notch, 100% through thickness, 22.5° to 45.0°

The corresponding damage-case measurement was taken, and the signal difference between this measurement and a previous baseline measurement was determined. The calculated absolute difference and percent difference for this damage case are shown in Figure 4.11. For this particular measurement, the signal difference surpassed the threshold limit at approximately 0.989-ms, which corresponded to a damage location of 8.993-ft (2.741-m) from the end of the pipe near axial location #1. The peak value of the absolute difference for this reflection feature was 0.076. In addition, the percent difference between the two measurements also crossed the threshold limit around 1.005-ms and reached a peak value of 6,341%, confirming that the absolute difference was correctly identifying the presence of damage. The absolute difference for the reflection from the 100% through thickness notch was nearly four times greater in magnitude than the largest reflection from the 50% through thickness notch. The corresponding estimates of the damage location and the percent difference from the actual location are shown in Table 5.2. All ten measurements correctly identified the presence of the damage and accurately

identified the location of the damage within 0.1% difference, which amounted to less than 0.1-in (2.5-cm).

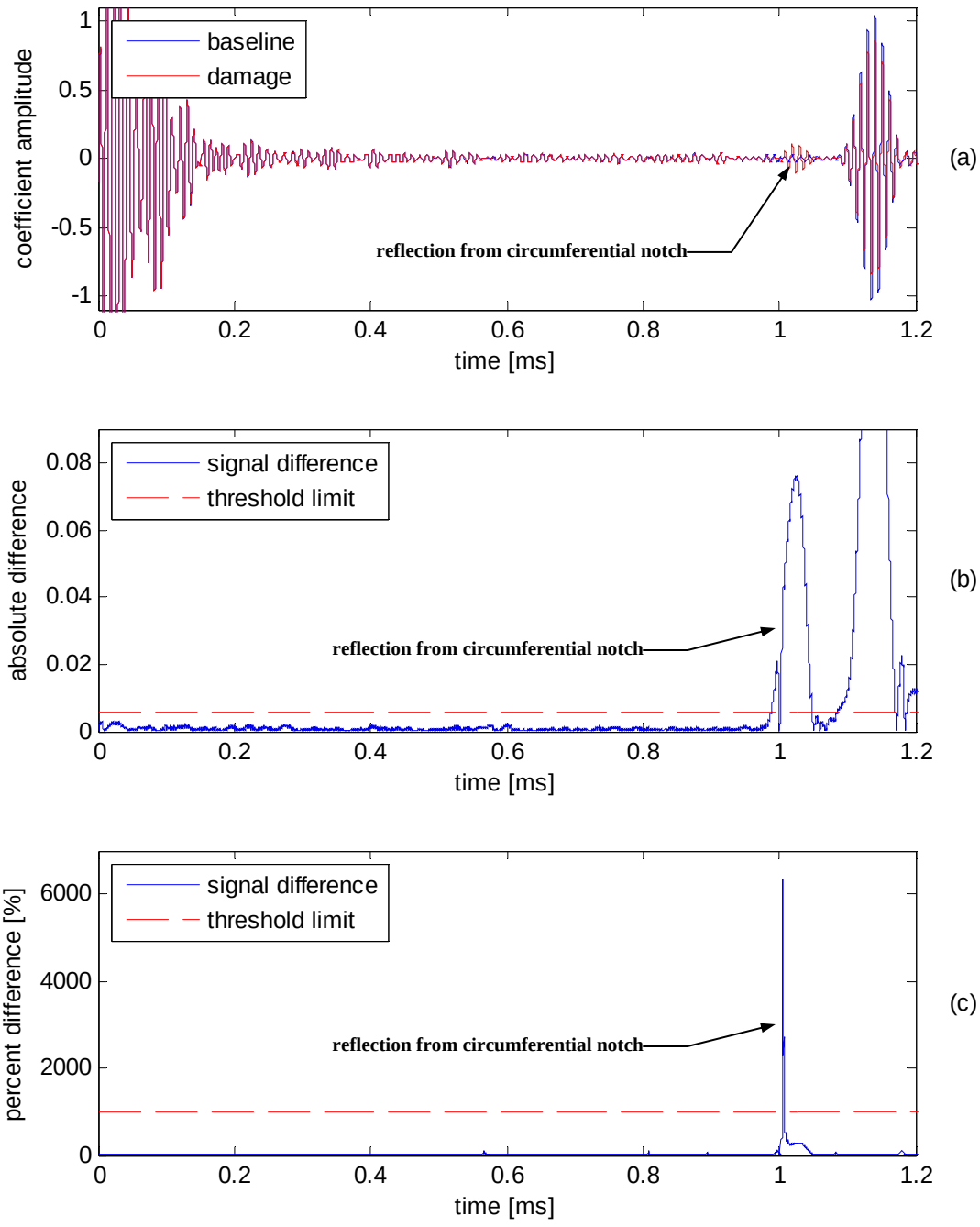

Figure 5.6: Signal difference between baseline and damage case measurements (circumferential notch, 22.5° to 45.0°, 100% through thickness)

circumferential extent [deg]	estimated damage location [ft (m)]	percent difference [%]
22.5 to 45.0	9.00 (2.74)	0.02
22.5 to 45.0	9.00 (2.74)	0.01
22.5 to 45.0	8.99 (2.74)	0.07
22.5 to 45.0	9.01 (2.75)	0.07
22.5 to 45.0	9.00 (2.74)	0.02
22.5 to 45.0	9.00 (2.74)	0.05
22.5 to 45.0	9.00 (2.74)	0.02
22.5 to 45.0	9.00 (2.74)	0.05
22.5 to 45.0	9.00 (2.74)	0.05
22.5 to 45.0	9.00 (2.74)	0.03

Table 5.2: Estimated damage locations for circumferential notch at 9.00-ft (2.74-m), 100% through thickness

5.4 Surface grinding

The next type of permanent damage was surface grinding. In three stages, varying areas of the pipe's surface were ground to an approximate 25% reduction in the thickness of the pipe's wall. In an effort to simulate corrosion damage, a round grinding wheel was used to create the damage such that there was no sharp edge facing in the axial direction. Therefore, there was not a reflection surface perpendicular to the wave propagation direction as with the circumferential notch. The gradual reduction in cross-sectional area was similar to the effects of corrosion. In addition, the surface grinding simulated the damage that could result from accidental impact during excavation with earth moving equipment. Such damage is common with a glancing blow from a piece of equipment, such as the bucket of a backhoe.

In order to avoid interference with the circumferential notch that already existed at an axial location of 9-ft (2.7-m), the surface grinding was applied at an axial location of 8-ft (2.4-m). Therefore, any potential reflection from these damage cases would arrive before the reflections observed in the previous section with the circumferential notch. For the first damage case with surface grinding, an area extending in the circumferential direction from 0.0° to 12.3°

was ground on the pipe's exterior surface. For this case, the width of the surface grinding extended 0.25-in (6.4-mm) in the axial direction, as seen in the photograph in Figure 5.7. For the second damage case, the area of the surface grinding was extended in the circumferential direction to 22.5°, as seen in the photograph in Figure 5.8. For the third and final damage case, the area of the surface grinding was extended in the axial direction to 0.50-in (12.7-mm) wide, as seen in the photograph in Figure 5.9.

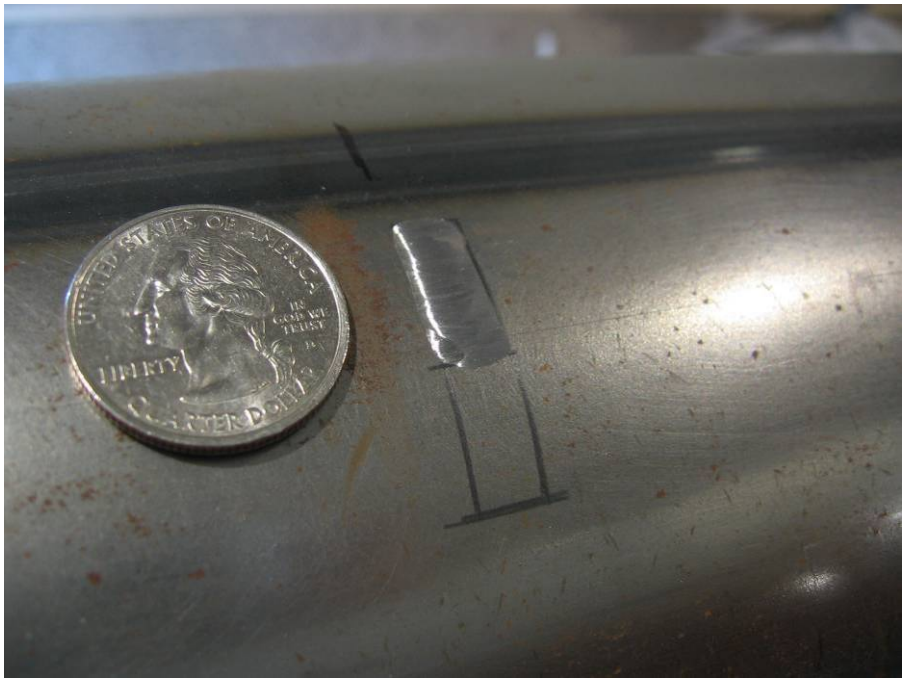

Figure 5.7: Surface grinding, 0.0° to 12.3° long, 0.25-in (6.4-mm) wide

Figure 5.8: Surface grinding, 0.0° to 22.5° long, 0.25-in (6.4-mm) wide

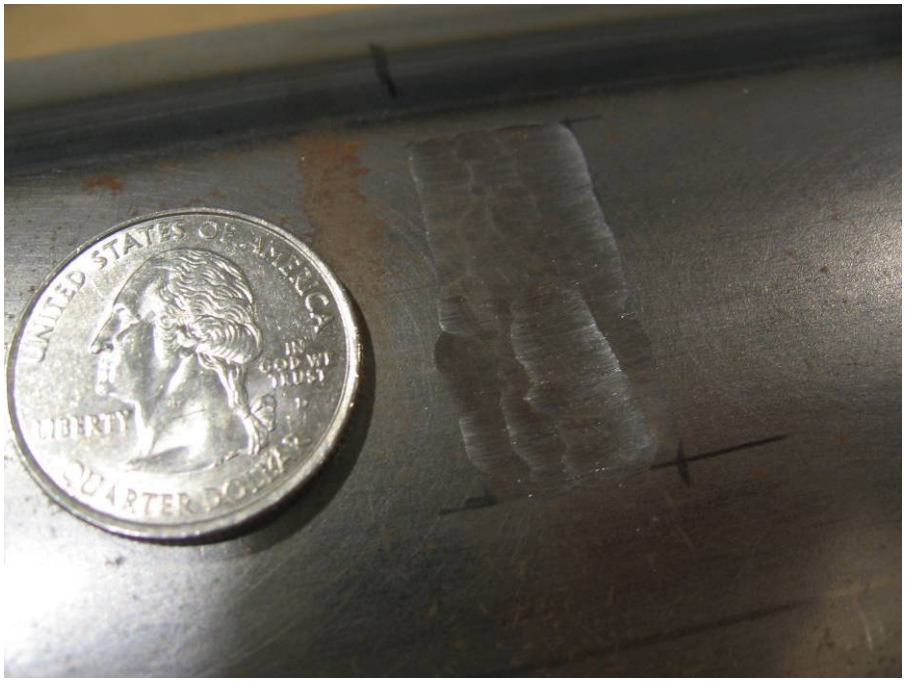

Figure 5.9: Surface grinding, 0.0° to 22.5° long, 0.50-in (12.7-mm) wide

The corresponding damage-case measurements were taken for each of the three areas of surface grinding described above. For each damage case, ten measurements were taken. Using the algorithm outlined in the previous section, the signal differences between these

measurements and a previous baseline measurement were determined. The calculated absolute difference and percent difference for each of the damage cases are shown in Figure 5.10.

For the circumferential extent of 0.0° to 12.3° and width of 0.25-in (6.4-mm), the surface grinding was not detected by the proposed algorithm. The peak value of the absolute difference was 0.005, which was just under the threshold limit of 0.006. Likewise, the peak value of the percent difference was 284%, which was well below the threshold limit of 1,000%. For the circumferential extent of 0.0° to 22.5°, the surface grinding caused a peak absolute difference of 0.010, which was above the threshold limit of 0.003. However, the peak value of the percent difference was only 584%, which was still well below the threshold limit of 1,000%. Therefore, the damage was still not detected. On the other hand, increasing the axial depth of the surface grinding to 0.50-in (12.7-mm) resulted in the proposed algorithm correctly identifying the presence of the damage from the surface grinding. The peak value of the absolute difference was 0.028, and the peak value of the percent difference was 1,329%. With this damage case, the absolute difference and percent difference were finally in agreement because both values were well above the corresponding threshold limit.

For the second and third damage cases, the estimates of the damage location and the percent difference from the actual location are shown in Figure 5.10. The first damage case was omitted from the table because the presence of the damage could not be identified with the given threshold limits. Because the absolute difference was above the threshold limit, the second damage case was included in the table even though the percent difference was not above the threshold limit. For both of the damage cases considered in the table, all ten measurements accurately identified the location of the damage within 1.0% difference of the actual location, which amounted to less than 1.0-in (2.5-cm).

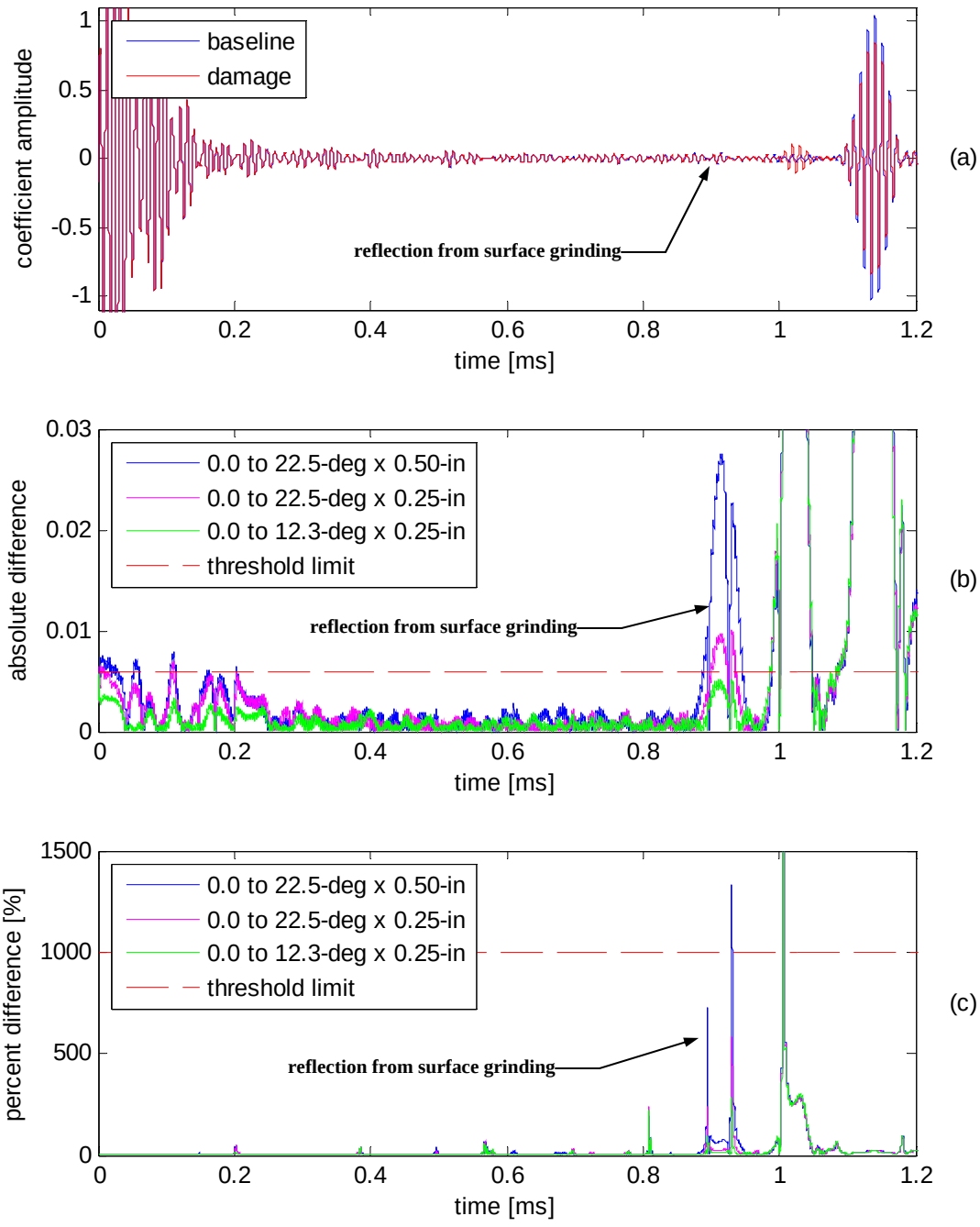

Figure 5.10: Signal difference between baseline and damage case measurements (surface grinding, 25% through thickness)

width (axial extent) [in (mm)]	estimated damage location [ft (m)]	percent difference [%]	width (axial extent) [in (mm)]	estimated damage location [ft (m)]	percent difference [%]
0.25 (6.4)	8.03 (2.45)	0.39	0.50 (12.7)	7.94 (2.42)	0.75
0.25 (6.4)	8.05 (2.45)	0.61	0.50 (12.7)	7.94 (2.42)	0.73
0.25 (6.4)	8.05 (2.45)	0.65	0.50 (12.7)	7.93 (2.42)	0.90
0.25 (6.4)	8.05 (2.45)	0.62	0.50 (12.7)	7.94 (2.42)	0.73
0.25 (6.4)	8.04 (2.45)	0.53	0.50 (12.7)	7.94 (2.42)	0.77
0.25 (6.4)	8.03 (2.45)	0.39	0.50 (12.7)	7.94 (2.42)	0.78
0.25 (6.4)	8.05 (2.45)	0.59	0.50 (12.7)	7.93 (2.42)	0.86
0.25 (6.4)	8.04 (2.45)	0.55	0.50 (12.7)	7.93 (2.42)	0.84
0.25 (6.4)	8.07 (2.46)	0.93	0.50 (12.7)	7.94 (2.42)	0.81
0.25 (6.4)	8.06 (2.46)	0.74	0.50 (12.7)	7.94 (2.42)	0.79

Table 5.3: Estimated damage locations for surface grinding at 8.00-ft (2.44-m), 0.0° to 22.5°

5.5 Accelerated corrosion

The final type of permanent damage was actual corrosion. In two stages, a 2-in (5.1-cm) diameter area of the pipe's surface was corroded to varying degrees of reduction in thickness of the pipe's wall. Electrolytic corrosion was used to accelerate the corrosion process. With electrolytic corrosion, the steel pipe was used as the anode, and a coil of copper foil was used as the cathode. The corrosion reaction was driven by applying a DC voltage across the anode and cathode, both of which were submerged in a solution of salt water (NaCl), as shown in Figure 5.11. Because the corrosion occurred in the solution of salt water, the rust from the iron ions was formed in solution rather than on the pipe's surface. (Brown, et al. 1997) Even though there was no rust present on the surface of the pipe, the resulting corrosion was the same as if the pipe had rusted over an extended period of time.

The corrosion damage was implemented at an axial location 6.0-ft (1.8-m) from the end of the pipe near axial location #1. For the first stage of corrosion damage, the accelerated corrosion process was allowed to react for three hours. After three hours, the resulting reduction in the thickness of the pipe was approximately 10%, as seen in the photographs in Figure 5.12

and Figure 5.13. For the second stage of corrosion damage, the accelerated corrosion process was allowed to react for six hours, resulting in an approximately 20% reduction, as shown in Figure 5.14 and Figure 5.15.

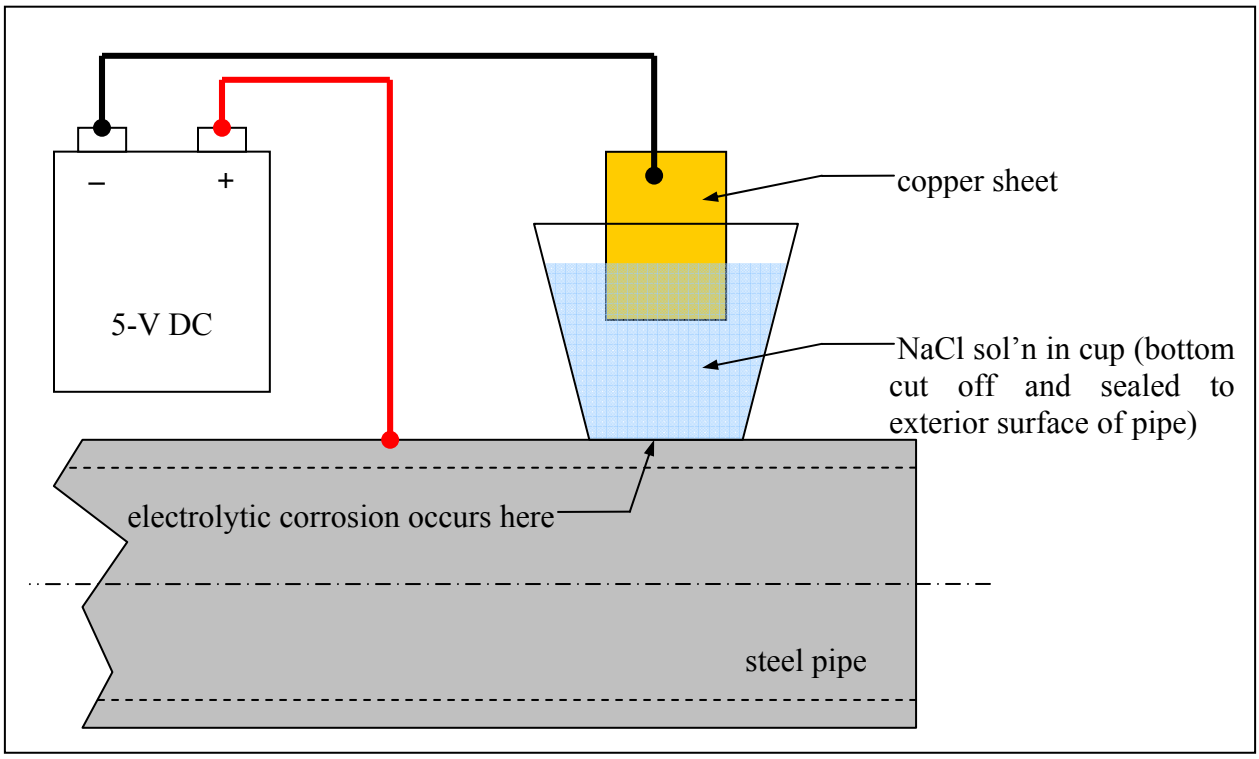

Figure 5.11: Apparatus used for accelerated corrosion

Figure 5.12: Top view of accelerated corrosion, 10% through thickness

Figure 5.13: Side view of accelerated corrosion, 10% through thickness

Figure 5.14: Top view of accelerated corrosion, 20% through thickness

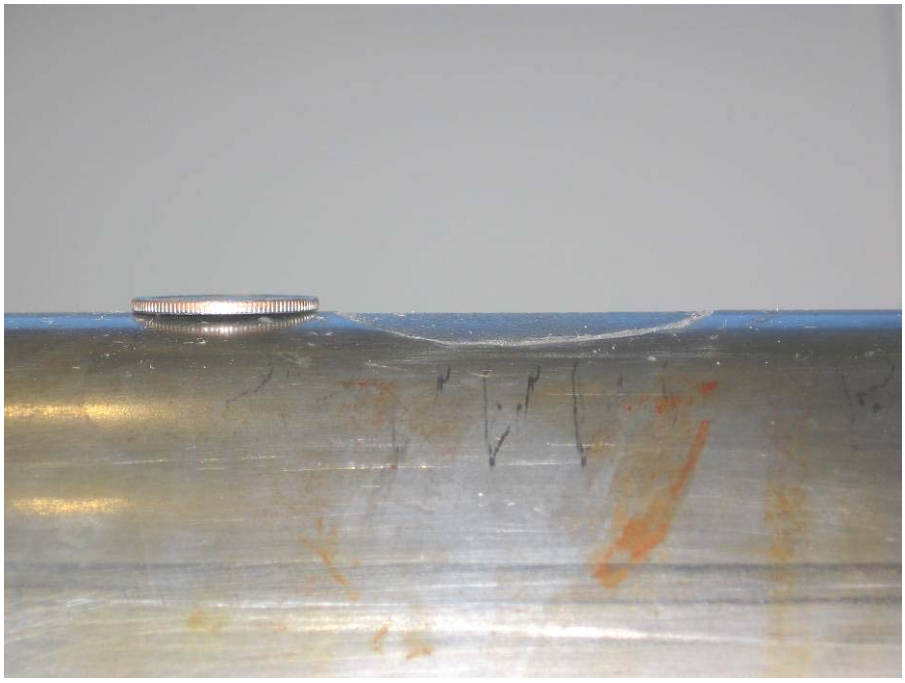

Figure 5.15: Side view of accelerated corrosion, 20% through thickness

The corresponding damage-case measurements were taken for each of the two stages of corrosion described above. For each damage case, ten measurements were taken. Using the algorithm outlined in the previous section, the signal differences between these measurements

and a previous baseline measurement were determined. The calculated absolute difference and percent difference for each of the damage cases are shown in Figure 5.16.

For the first stage of corrosion, the damage was not detected by the proposed algorithm. The peak value of the absolute difference was 0.005, which was just under the threshold limit of 0.006. Likewise, the peak value of the percent difference was 68%, which was well below the threshold limit of 1,000%. For the second stage of corrosion, the surface grinding causes a peak absolute difference of 0.011, which was above the threshold limit of 0.003. However, the peak value of the percent difference was only 154%, which was still well below the threshold limit of 1,000%. Therefore, the results from the absolute difference and the percent difference were not in agreement. Because the absolute difference successfully reached a value above the threshold limit, however, the location of the damage could still be estimated.

For the second damage case, the estimates of the damage location and the percent difference from the actual location are shown in Table 5.4. The first damage case was omitted from the table because the presence of the damage could not be identified with the given threshold limits. Because the absolute difference was above the threshold limit, the second damage case was included in the table even though the percent difference was not above the threshold limit. For the damage case considered in the table, all ten measurements accurately identified the location of the damage within 1.0% difference of the actual location, which amounted to less than 1.0-in (2.5-cm).

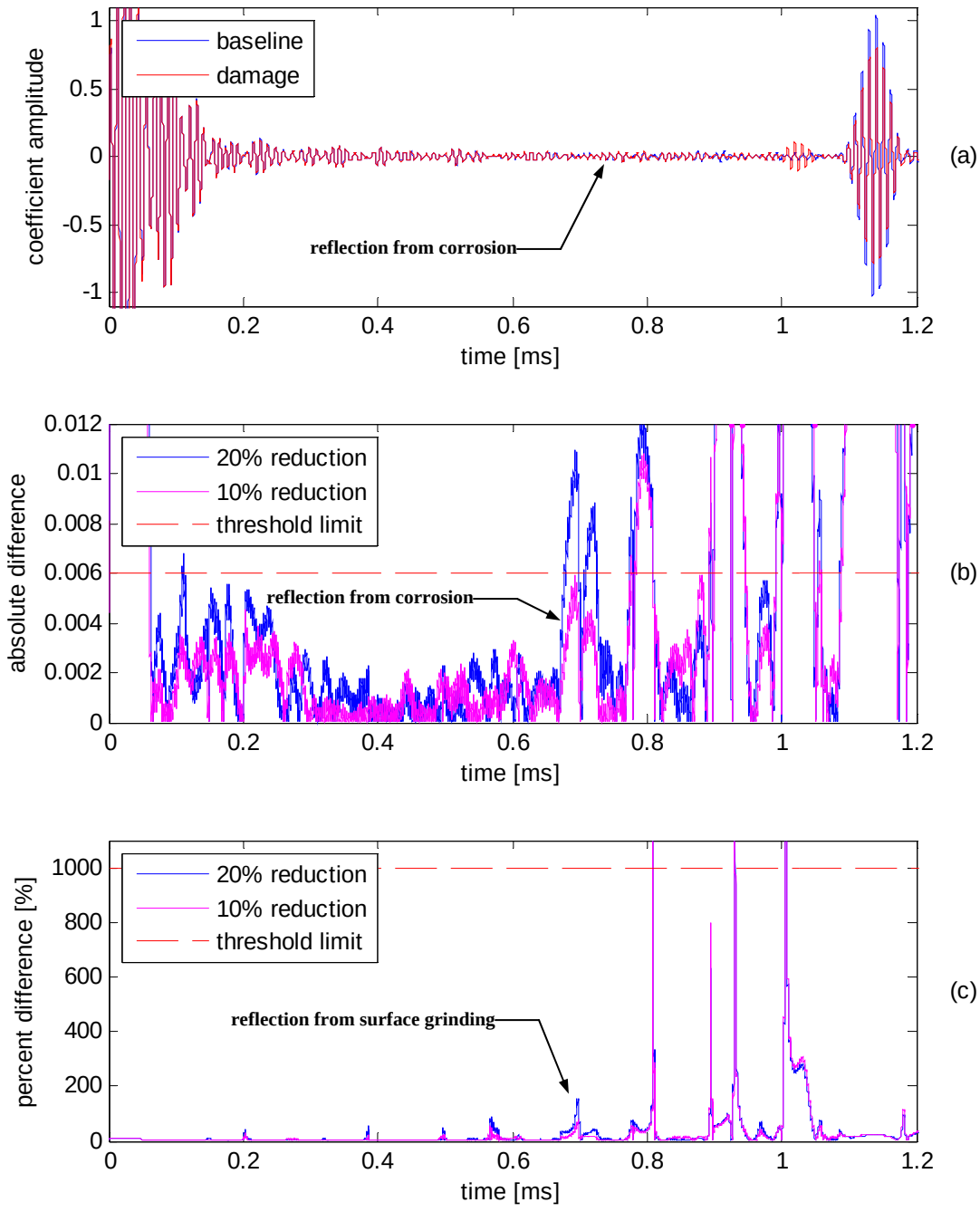

Figure 5.16: Signal difference between baseline and damage case measurements (accelerated corrosion)

corrosion depth [% of wall]	estimated damage location [ft (m)]	percent difference [%]
20	6.02 (1.83)	0.38
20	6.03 (1.84)	0.45
20	6.02 (1.83)	0.32
20	6.01 (1.83)	0.22
20	6.02 (1.83)	0.38
20	6.00 (1.83)	0.07
20	6.00 (1.83)	0.00
20	6.02 (1.83)	0.36
20	6.02 (1.83)	0.38
20	6.01 (1.83)	0.12

Table 5.4: Estimated damage locations for accelerated corrosion at 6.00-ft (1.83-m)

5.6 Discussion

The results presented here demonstrate the ability of the proposed methods to correctly identify the presence of permanent damage to the main body of the pipe, including simulated crack, excavation, and corrosion damage. Using reflection features from the damage, the results also demonstrate the ability to accurately identify the location of the damage. For the three types of permanent damage presented here, including one damage case of real corrosion, the algorithm developed in the previous chapter was used to correctly identify that damage was present. In addition to correctly identifying the presence of damage, the use of time-of-flight calculations accurately determined the location of the damage. For all damage cases described above, the location of the damage was accurately estimated within 1.0% of the actual location.

The most important aspect to remember about the proposed methods is the use of MFC patches for the actuators and sensors of all measurements. While previous research in this area has proven the ability to detect and locate damage in pipeline structures, other methods are types of non-destructive evaluation (NDE) which requires expensive equipment and direct access to the structure, which may be underground or covered with insulation. Furthermore, the sensing

systems in these approaches are temporarily mounted to the structure to take measurements over a short span of time, such as a few hours or days. However, the MFC patches used here are rugged and relatively cheap, lending themselves well to the implementation of a structural health monitoring system. The sensors can be permanently embedded with the structure, allowing for continuous monitoring over the entire life of the structure.

Although the proposed methods are not as rigorous with detecting and locating damage as the capabilities of existing NDE techniques, they can at least perform as an early indication of damage detection and location. Once a permanently mounted, MFC-based system indicates the presence of damage and gives its approximate location, the more costly NDE techniques can then be implemented to rigorously characterize the damage and its location. Therefore, the need for frequent inspections involving relatively expensive NDE techniques can be significantly reduced.

While an extensive effort is made in the research of this thesis to effectively simulate actual crack, excavation, and corrosion damage, this research is still just an effort to demonstrate the feasibility of such an SHM system to detect and locate damage in a pipeline structure. Even though permanent forms of damage are implemented here, these are all attempts to simulate actual damage that might occur in real-world applications. Future work is still required to demonstrate that the proposed methods can effectively perform these same detection tasks with real-world applications.

Chapter 6 Impedance measurements

6.1 Overview

In the previous chapters, the proposed Lamb wave methods demonstrated the ability to effectively detect and locate damage in the main body of the pipeline structure. Damage types addressed with the Lamb wave methods include crack, excavation, and corrosion damage. The complex geometry involved with a flanged joint, however, does not serve as an ideal waveguide for experiments because very little energy is actually transmitted to the perimeter of the flange. To address the damage in flanged joints, therefore, a different approach is required.

Impedance methods, rather than Lamb wave methods, are therefore implemented to monitor the structural integrity of the flanged joints in a pipeline system. There are several reasons that impedance methods are an ideal choice for this application. The most significant advantage of impedance methods as applied to the proposed structural health monitoring (SHM) system is that MFC patches can be used to perform impedance measurements. Therefore, the exact same transducer array used to perform the Lamb wave methods with the pipeline can also be used to perform the impedance methods. Accordingly, each MFC patch used in the proposed SHM system serves two purposes, one for Lamb wave measurements and one for impedance measurements. This redundant use significantly reduces the number of MFC patches deployed in the transducer array, thereby reducing the overall cost of the proposed SHM system. An additional advantage of the impedance method is that the relatively high excitation frequencies involved make it sensitive to local damage rather than global damage. Also, the impedance method is a form of active sensing which means that no external excitation is required.

6.2 Apparatus for impedance measurements

6.2.1 Pipeline assembly with flanged joints

The apparatus used for the impedance measurements was designed to model a simple pipeline network. Because the objective for the impedance measurements was to monitor the structural integrity of the flanged joints of a pipeline, the structure consisted of three separate pipe sections. The three sections were connected together using two flanged joints to form a continuous, straight pipeline, as seen in Figure 6.1. The middle pipe section was 7-ft (2.1-m) long, and each of the end pipe sections was 3-ft (0.9-m) long, making the entire apparatus 13-ft (4.0-m) long. Each flanged joint connected using four bolts (3/8-in, 9.5-mm), and each bolt was originally tightened with a torque wrench to 200-in-lb (22.6-N-m). Each of the three pipe sections was made of the same type and size of carbon steel tubing. The pipe sections had an outer diameter of 2.5-in (6.4-cm) and a wall thickness of 1/16-in (1.60-mm). The pipe was suspended using elastic cords which were looped around the pipe near each of the ends of the overall pipeline structure.

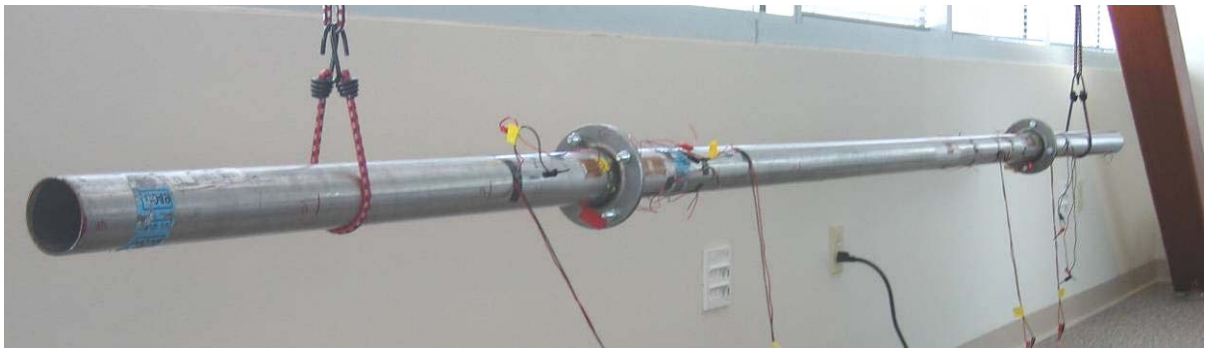

Figure 6.1: Apparatus for impedance measurements

6.2.2 Sensor Locations

Although the apparatus used for the impedance measurements was not the same apparatus used for the Lamb wave measurements, the exact same type of MFC patches were used for making both types of measurements. More importantly, the MFC patches were mounted in the exact same fashion and relative location. The active axis of each patch was aligned with the axis of the pipe, and the flexibility of the MFC patch was utilized to mount the transducer to the curved surface of the pipe.

The same MFC patches and mounting conditions were intentionally used for both apparatuses. The reason was to demonstrate the ability of the array of transducers to perform both types of measurements, Lamb wave and impedance. Therefore, the same MFC patches could monitor the structural integrity of the flanged connections in a pipeline and monitor the body of each pipe for cracks and corrosion damage. This dual use of each MFC patch greatly reduces the number of transducers required for the entire monitoring system, thereby reducing the potential cost of such a system.

MFC patches were located at four axial locations along the length of the pipeline structure. Details of the actual locations of the MFC patches are shown in Figure 6.2. The first two axial locations were 2.5-in (6.4-cm) from each side of flange A, and the second two locations were 2.5-in (6.4-cm) from each side of flange B. At each of the axial locations, a single MFC patch was mounted to the pipe's exterior surface. The MFC patches at the first three axial locations were mounted at the same circumferential location, but the MFC patch at the fourth axial location was mounted on the opposite side (180° around the circumference) from the other three.

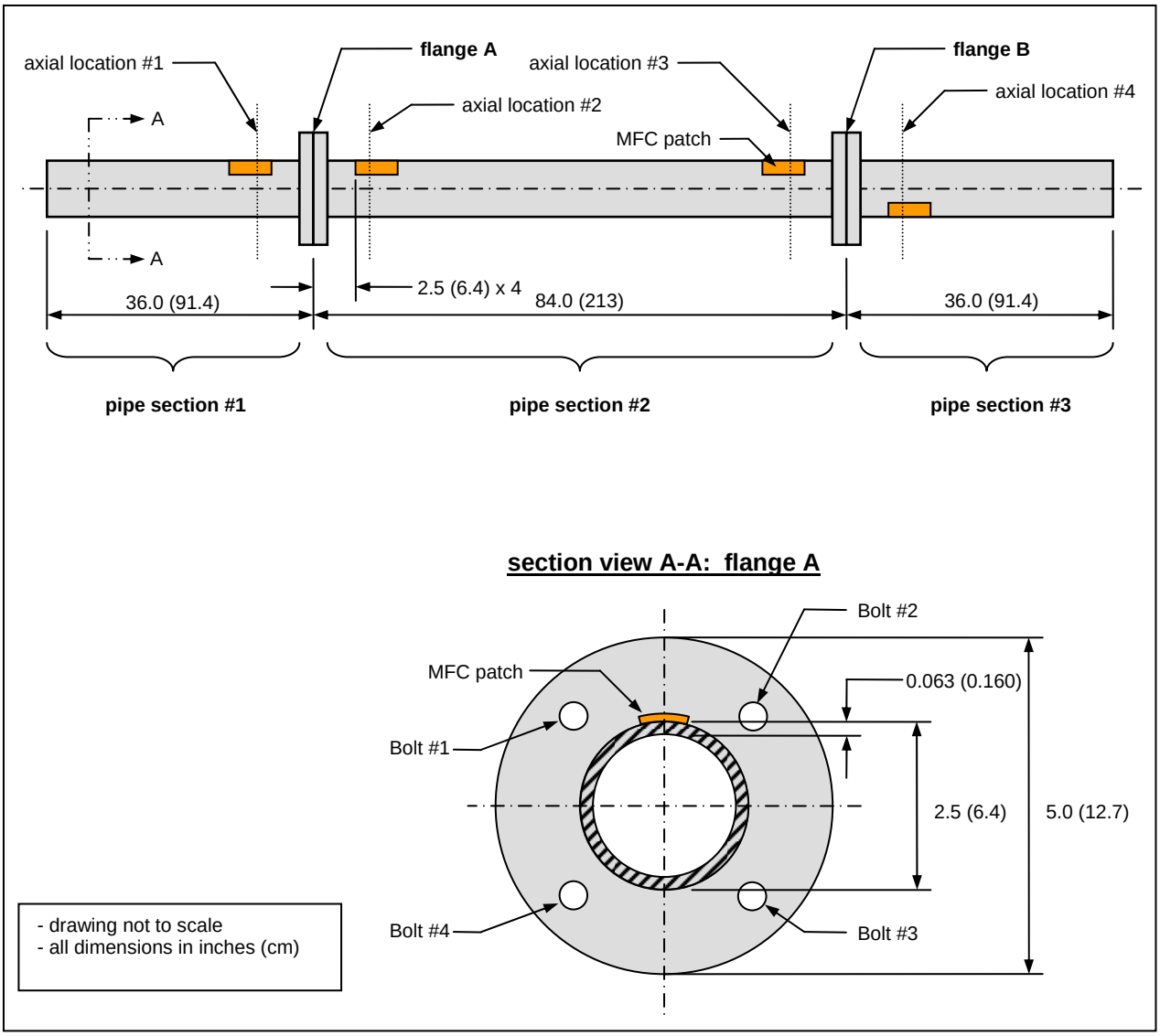

Figure 6.2: Dimensioned drawing 2.5-in (6.4-cm) pipeline structure, including flanged joints

6.3 Experimental procedure for impedance measurements

The impedance method is used to monitor variations in a structure's mechanical impedance. An impedance analyzer is used to measure the electrical impedance of an MFC patch which is mounted to the structure. The electro-mechanical coupling of an MFC patch couples the electrical impedance of the patch to the mechanical impedance of the structure. Therefore, changes in the mechanical impedance of the structure will cause changes in the

electrical impedance of an MFC patch. Because damage in a structure can affect its mass, stiffness, and/or damping characteristics, the damage also affects its mechanical impedance. Consequently, changes in the structure's mechanical impedance can also be used to identify the presence of damage in the structure. Therefore, monitoring changes in the mechanical impedance of the pipeline structure will reflect changes caused by damage, such as the loosening of a flanged joint.

For the impedance measurements, four MFC patches were used. Each patch was located 2.5-in (6.4-cm) from either side of the flanges. An impedance analyzer was used for the data acquisition. Two frequency ranges were used for the measurements. The lower frequency range was 50 to 60-kHz, and the higher frequency range was 110 to 120-kHz. For both frequency ranges, 801 data points were taken using a 1-V swept sine wave for the excitation, and four averages were made per frequency point.

All impedance data were taken in sets, and each set of data contained eight ensembles. Each of the eight ensembles involved measuring the impedance of a given MFC patch for one of the two frequency ranges. For both frequency ranges, an impedance measurement was taken from the MFC patch located at each of the four axial locations. Therefore, the use of four MFC patches and two frequency ranges corresponded to eight ensembles of data per data set.

An example of a typical impedance measurement can be seen in Figure 6.3-a. This particular measurement was from the lower frequency range, 50 to 60-kHz. The Figure shows the real part of the electrical impedance for the MFC patch located at axial location #1. Peaks in the measurement corresponded to resonant frequencies of the structure. The peak near 56-kHz can be seen more clearly in Figure 6.3-b. The changes in peaks such as this one will be addressed later for detecting the presence of damage in the bolted joints.

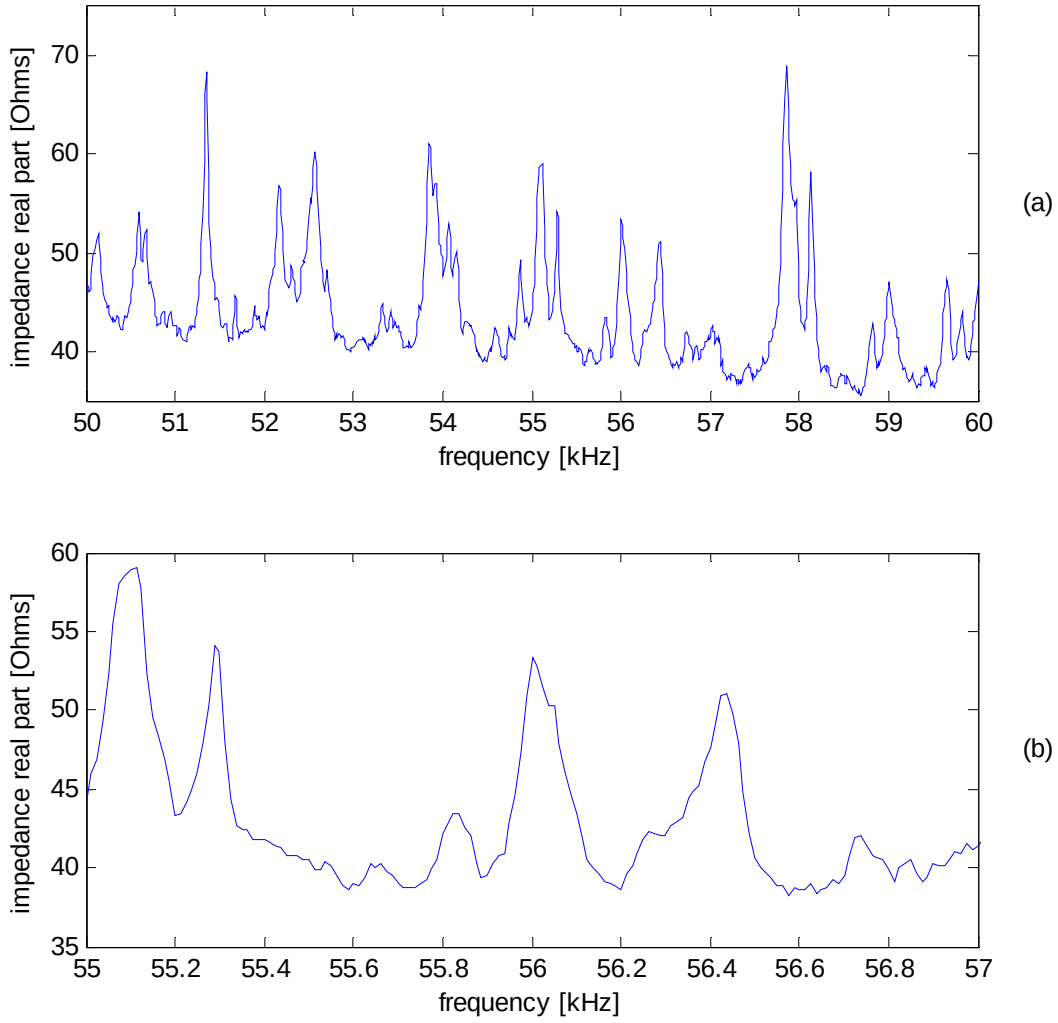

Figure 6.3: Example of an impedance measurement – (a) Impedance for MFC at axial location #1 over lower frequency range, 50 to 60-kHz, (b) Close-up view of peak at 56-kHz

6.4 Bolted joint damage and analysis

6.4.1 Overview

With the impedance method, the objective is to detect damage in the flanged joints between the sections of the pipeline. Because bolted joints are used in this apparatus, damage in

the flanged joints was simulated by loosening the bolts by a discrete amount of torque. The damage was detected by monitoring the variations in the pipeline's mechanical impedance. By measuring the electrical impedance of an MFC patch which was mounted to the pipeline structure, the mechanical impedance of the structure was indirectly measured. Therefore, various damage cases involving the loosening of the bolts in the flanged joints are presented in the following sections. Detection of the damage in the flanged joints was demonstrated through the use of the impedance method.

6.4.2 Damage detection algorithm

When using the impedance method, the differences between two measurements are generally difficult to quantify from mere observations of the frequency domain signals. As with a frequency response function, some of the peaks in an impedance measurement are affected differently by a change in the structure than other peaks are. These differences are sensitive to the frequency of a particular peak and the variation in the measurements. An example of the differences between typical baseline measurements and a given damage case can be seen in Figure 6.4. The specific damage case was irrelevant here, and each of the damage cases considered in this research are addressed in the following sections of this chapter.

The example in Figure 6.4 shows that the variation in the baseline measurements over this frequency range was relatively low compared to the changes in the impedance caused by the presence of damage. Therefore, the frequency domain signal for the impedance could be used to identify the presence of damage. However, there was no clear indication of the severity of the damage that is present. In order to better quantify level of damage present in the system, more advanced signal processing techniques were implemented.

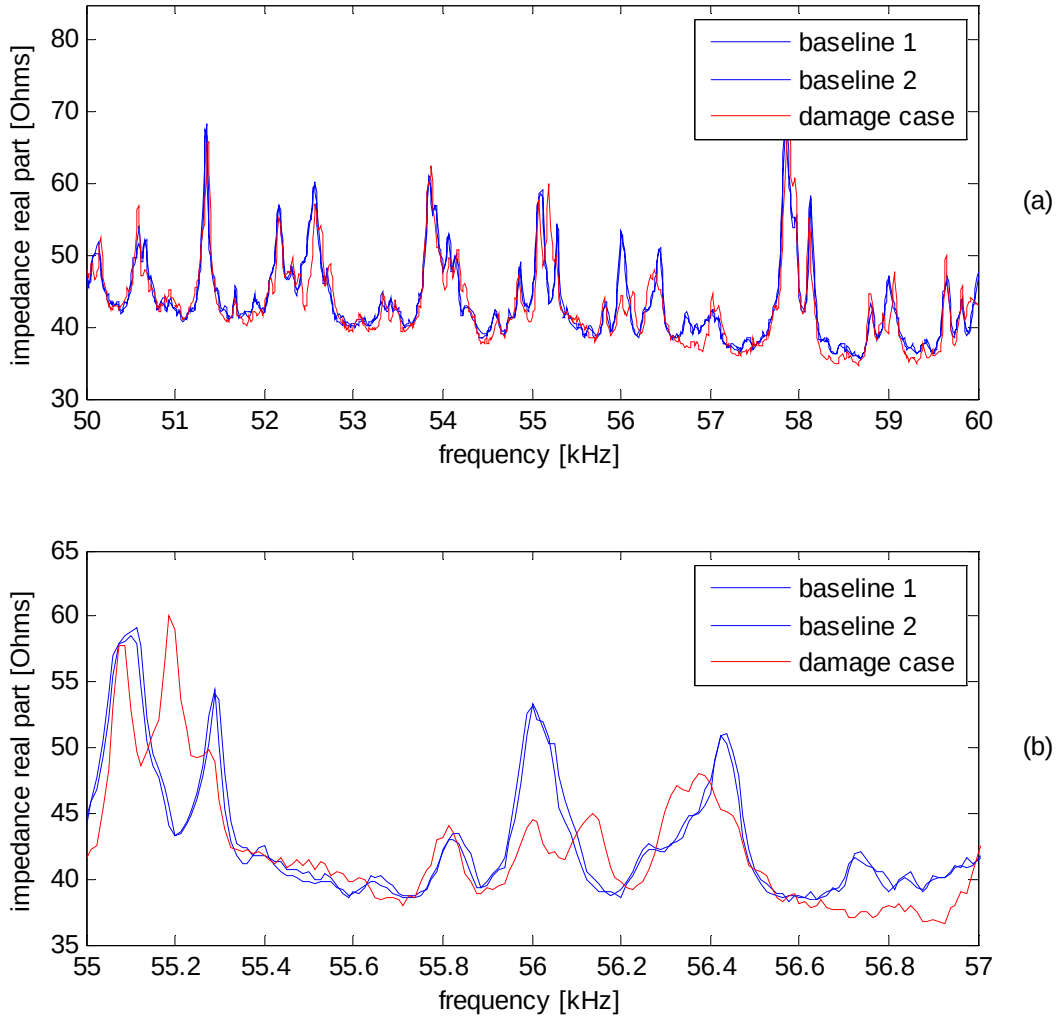

Figure 6.4: Example of the differences between typical baseline measurements and a damage case measurement

An algorithm based upon the cross correlation coefficient was used to quantify the differences between two given impedance measurements. Assuming that one of the signals was a baseline measurement, then the result of the algorithm was a damage metric which specified the degree of damage present in the other signal. The damage metric was formulated such that an increase in its value corresponded to an increase in the amount of damage present in the current measurement.

The damage metric was related inversely to the value of the cross correlation coefficient between two signals. The cross correlation coefficient was formulated as follows:

$$\rho = \frac{1}{n-1} \frac{\sum_{i=1}^{n} \left(\mathrm{Re}\left(Z_{i,1}\right) - \mathrm{Re}\left(\overline{Z}_1\right)\right)\left(\mathrm{Re}\left(Z_{i,2}\right) - \mathrm{Re}\left(\overline{Z}_2\right)\right)}{\sigma_{Z_1}\sigma_{Z_2}} \tag{7}$$

where ρ is the correlation coefficient, i is the frequency index, $Z_{i,1}$ is the impedance of the first (baseline) measurement, $Z_{i,2}$ is the impedance of the second (damage) measurement, $\overline{Z}_1$ and $\overline{Z}_2$ are the means of the respective impedances, and σ_{Z_1} and σ_{Z_2} are the standard deviations of the respective impedances. To ensure that the damage metric increases with an increase in the level of damage in the system, the damage metric was formulated as $((1-\rho)\times 100\%)$. Therefore, a damage metric value of zero corresponded to perfect correlation. Perfect correlation between a given measurement and a baseline measurement, in turn, meant that there was no damage present for that given measurement. A greater damage metric value meant that a certain degree of dissimilarity, with respect to a baseline measurement, was present in a particular measurement. In addition, an increase in the value of the damage metric corresponded to an increase in this dissimilarity.

An example of the damage metric for the measurements from Figure 6.4 are shown in Figure 6.5. In this figure, the first baseline measurement was used as the reference for calculating the damage metric. Therefore, the damage metric for the first baseline measurement was zero because it was being compared to itself. In this example the damage metric for the damage case measurement clearly had a higher value than the second baseline measurement. Because only one damage case was considered in this example, there was no indication that the damage metric could quantify the amount of damage. In the following sections, however,

various damage cases are used to demonstrate that the damage metric can be used with impedance measurements to reflect the amount of damage present in the pipeline system.

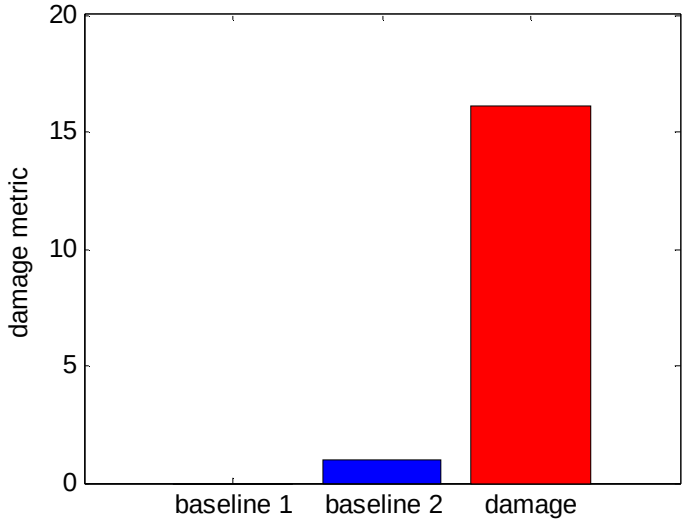

Figure 6.5: Example of the damage metric for typical baseline measurements and a damage case measurement

6.4.3 Damage to flange A

For the impedance measurements, damage cases involving damage to flange A and flange B were implemented. Primary concentration was made with the damage to flange A, the results from which are presented in this section. However, a limited number of damage cases with flange B were also implemented to verify that the proposed methods correctly identified the location of the damage.

The apparatus used for the impedance methods was designed to include bolted connections at each of the flanges. Bolted connections were chosen so that damage to the flanges could easily be implemented by loosening the bolts using a torque wrench. The loosening of bolts was also reversible so that multiple damage measurements could be made without permanently altering the apparatus. In addition, the reversible damage allowed for

repeated baseline measurements to ensure that the variation was observed. Before any damage cases were implemented, numerous baseline measurements were taken. In between each of the baseline measurements, all the bolts in each flange were completely removed and then re-tightened. In an effort to capture potential differences due to environmental changes, the baseline measurements were taken at various times over the course of three days. As will be shown below, the variation in the baseline measurements was minimal compared to the variation caused by damage.

With the damage to flange A, three different damage cases were used to demonstrate the ability of the proposed methods to detect, locate, and quantify the damage present. For the first damage case, bolt #1 was removed from flange A (see Figure 6.6). For the second damage case, bolt #2 was also removed. Because the pipeline structure was suspended by elastic cords near each of its ends, the weight of the pipeline placed the loosened part of the joint under compression. Therefore, damage case three had the same bolts removed as damage case two (bolt #1 and bolt #2 from flange A), but the pipe was rotated circumferentially by 180° so that the weight of the pipeline placed the loosened part of the joint under tension. The three damage cases for flange A are summarized in Table 6.1.

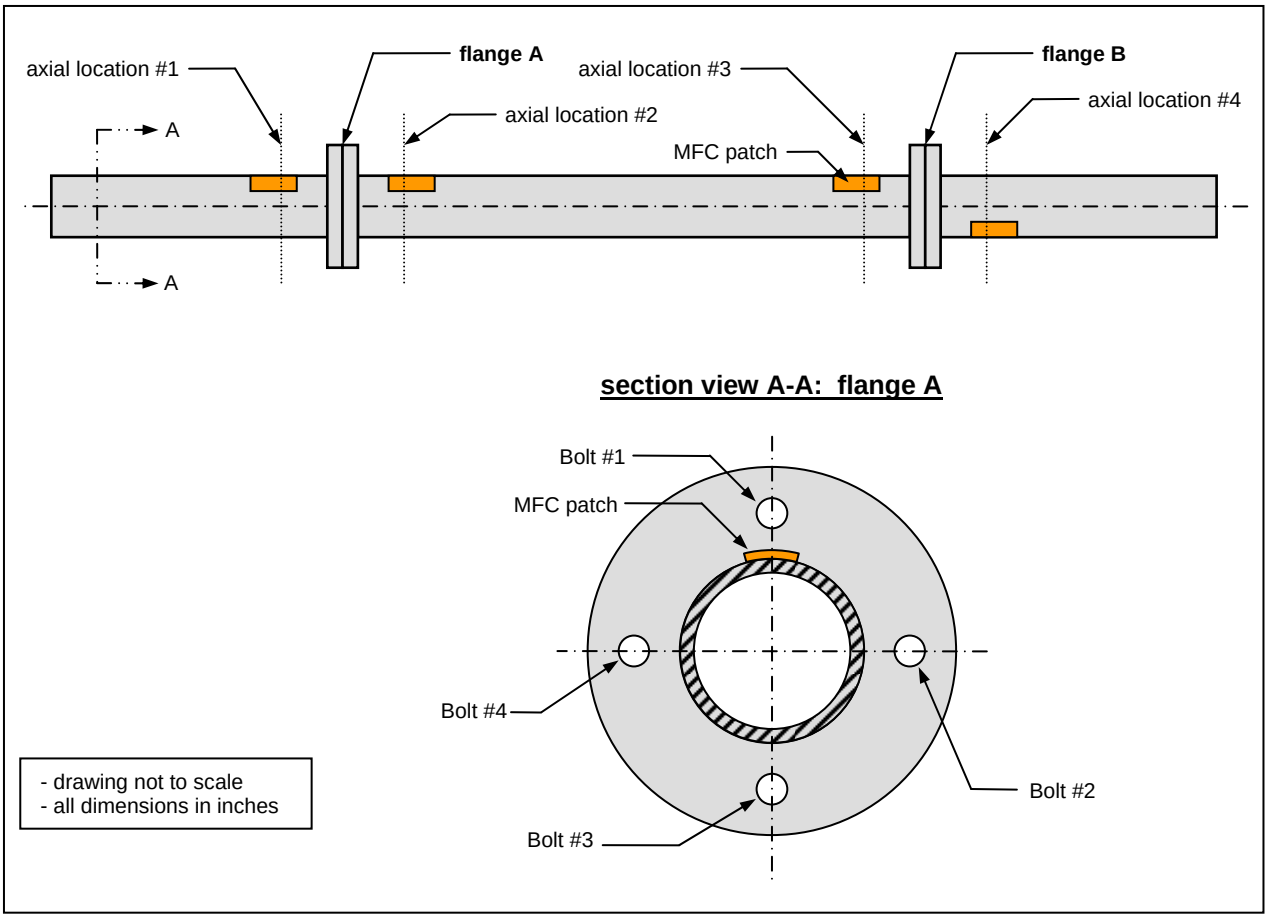

Figure 6.6: Labeled drawing of pipeline structure

Damage case	Description
Case 1	bolt #1 removed from flange A
Case 2	bolt #1 and bolt#2 removed from flange A
Case 3	same bolts removed as case 2, but pipe rotated 180°

Table 6.1: Summary of damage cases for flange A

For each of the three damage cases for flange A, two impedance measurements were taken for each frequency range, 50 to 60-kHz and 110 to 120-kHz. The damage metrics for each damage case and axial location for the lower frequency range (50 to 60-kHz) are shown in Figure 6.7. Similarly, the damage metrics for the higher frequency range (110 to 120-kHz) are shown in Figure 6.8.

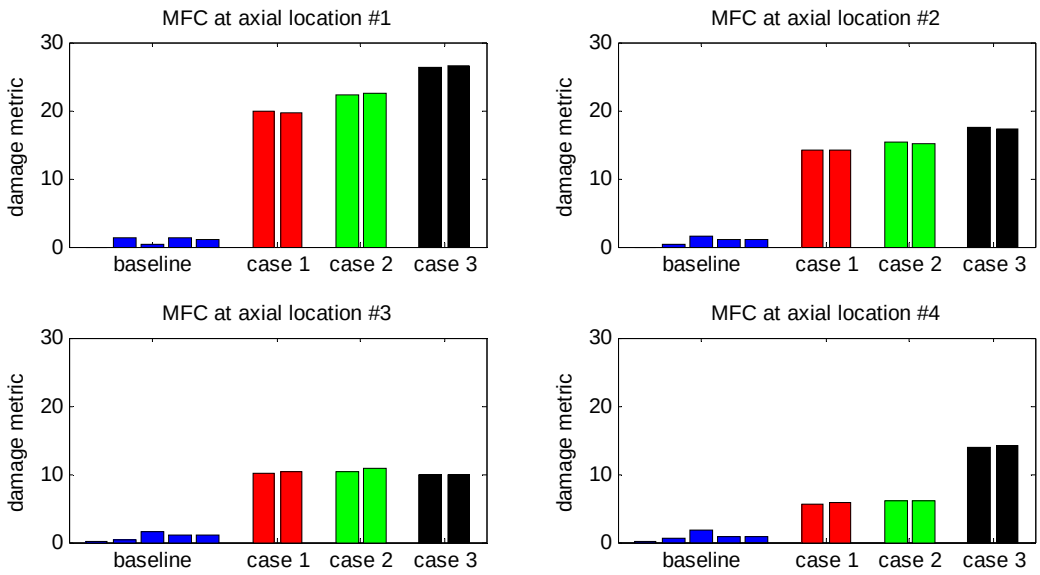

Figure 6.7: Damage metric for damage to flange A (50 to 60-kHz)

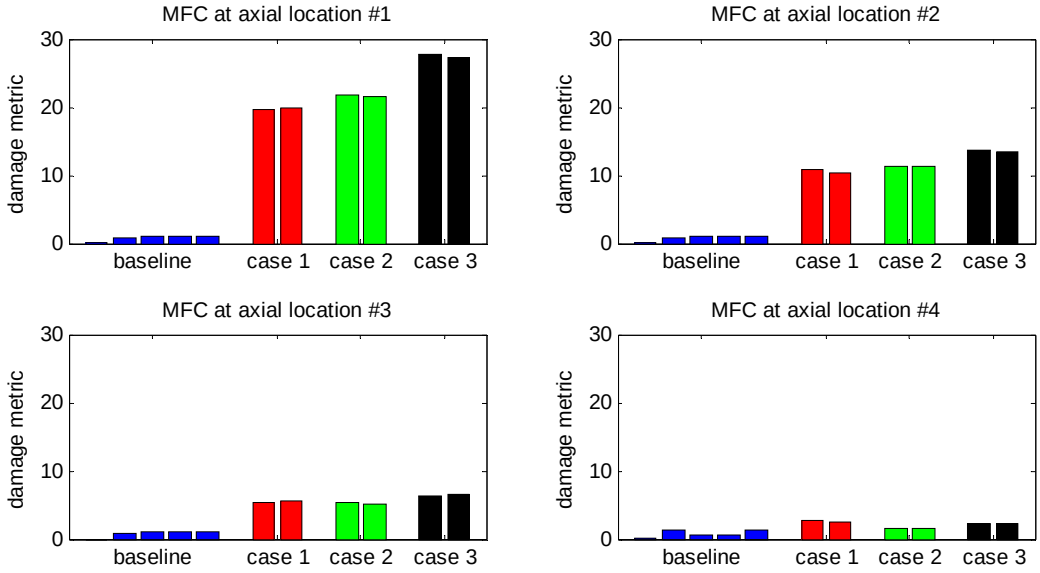

Figure 6.8: Damage metric for damage to flange A (110 to 120 kHz)

From Figure 6.7 and Figure 6.8, the damage metric is clearly seen to be effective at detecting the presence of damage in the structure. For the MFC patches closest to the damage location (axial location #1 and #2), the damage metric was at least an order of magnitude greater for all damage cases than it was for any of the baseline measurements. As mentioned above, the

variation shown in each of the five baseline measurements was insignificant compared to the variation caused by damage.

In addition, the results shown in Figure 6.7 and Figure 6.8 can be used to make a clear decision regarding the damage location and quantification. The impedance measurements for both frequency ranges were effective at locating the damage in the system. For damage case 1, the damage metrics at axial locations #1 and #2 were nearly twenty times greater than the corresponding damage metric for the baseline measurements. Note that these two axial locations were the nearest to where the damage was located (flange A) than the other two axial locations. On the other hand, the damage metrics for case 1 at axial locations #3 and #4 showed only relatively slight increases over the corresponding damage metric for the baseline. In fact, axial location #4 showed almost no relative difference between the baseline and damage measurements at 110 to 120-kHz. This lower value in the relative damage detected could be attributed to the fact that axial location #4 was on a completely different section of pipe than axial location #3. Therefore, axial location #4 showed less change from the presence of damage than axial location #4 because it was better isolated from the damage by flange B. Furthermore, the middle pipe section was 57% longer than the two end sections. The higher mass of the middle pipe section meant that it also had a much higher mechanical impedance. Therefore, the sensitivity to changes in the impedance of the flanged joint was higher for the end sections than the middle the middle section.

From the results at axial location #3 for both frequency ranges, the higher frequency range demonstrated a more localized sensitivity to damage compared to the lower frequency range. For each of the damage cases, the damage metric at axial location #3 was at least 25% lower for the higher frequency range than the lower.

The results also show that the impedance measurements for both frequency ranges were also effective at quantifying the amount of damage in the system. In each instance, the damage metric increased in value as the corresponding level of damage increased, which can be clearly observed by the results at axial location #1. Therefore, the structural damage to the bolted joints of the flanges could be detected, located, and somewhat quantified with the use of the proposed impedance methods.

6.4.4 Damage to flange B

To demonstrate that the impedance method correctly located the damage, a fourth and final damage case was implemented. This case involves damage to the opposite flange from the previous damage cases. For this damage case, the pipe was first returned to the conditions of damage case 2 by again circumferentially rotating the pipe 180° and leaving bolts #1 and #2 removed. The weight of the pipe was again placing the damage at flange A under compression. Without replacing the two bolts from flange A, the fourth damage case was then implemented by removing bolts #1 and #2 from flange B. Therefore, a total of four bolts were absent, two from flange A and two from flange B.

As with the previous damage cases, two impedance measurements were taken for each frequency range, 50 to 60-kHz and 110 to 120-kHz. The damage metrics for damage case 4 at each axial location for the lower frequency range (50 to 60-kHz) are shown in Figure 6.9. Because the two bolts were left out of flange A, the damage metric for damage case 2 was repeated in this figure. Similarly, the damage metrics for the higher frequency range (110 to 120-kHz) are shown in Figure 6.10.

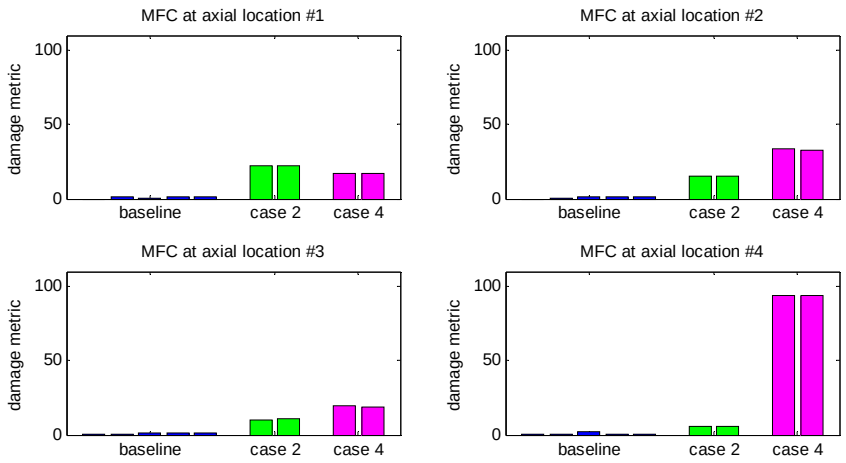

Figure 6.9: Damage metric for damage to flange B (50 to 60-kHz)

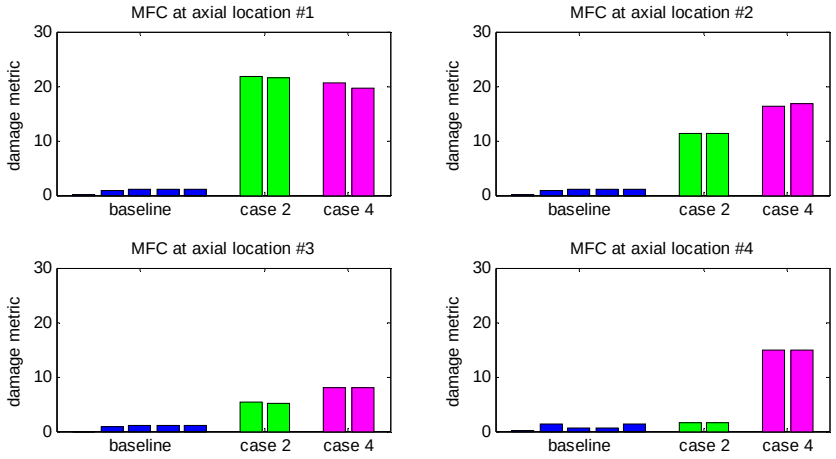

Figure 6.10: Damage metric for damage to flange B (110 to 120-kHz)

From the damage metrics in Figure 6.9 and Figure 6.10, the proposed methods correctly identified the additional damage at flange B. For both frequency ranges, the MFC at axial location #4 showed a dramatic increase in the value of the damage metric with case 4 when compared to case 2. At the same time, the MFC at axial location #1 showed no increase in the damage metric with case 4 when compared to case 2. Although the changes are not as significant as at axial location #4, the damage metrics for axial location #2 and #3 showed slight

increases as well. The fact that the increases were both less than 25% could be attributed to the larger mechanical impedance of the middle pipe section, as discussed in the previous section.

6.4.5 Discussion

The results presented here prove that the structural damage to the bolted joints of the flanges could be detected, located, and somewhat quantified with the use of the proposed impedance methods. First, the results show that the presence of damage was correctly identified. The baseline measurements were repeatable, and the presence of damage caused much greater changes in the impedance than the variation in baseline measurements caused. Even with the least severe damage case considered here, which is the removal of a single bolt from a flange, the damage metric increased by a factor of twenty.

Second, the results show that the use of the damage metric could correctly determine the location of the damage. In all cases considered here, the two axial locations nearest the damage showed greater indications of damage than the other two axial locations. As expected, the higher frequency range showed the most localized results, with the farthest axial location showing nearly zero change with the damage cases when compared to the baseline measurements. Damage was implemented in both of the flanges of the structure, and the resulting damage metrics successfully determined the flange that had been loosened.

Third, the proposed method also demonstrates the ability to quantify the level of damage present in the system. For axial location #1, the damage metric increased with each corresponding increase in the severity of damage that was implemented to flange A. Although the results were not consistent across all measurements, the results at axial location #1 showed that quantification of damage was at least feasible.

6.5 Lamb wave demonstration

6.5.1 Overview

A very important aspect of the previous section is that the same MFC patches used to make the impedance measurements can also be used to make Lamb wave measurements. Using the Lamb wave and impedance methods proposed in the research of this thesis, therefore, a single set of MFC patches mounted to a pipeline structure can serve the dual purpose of detecting damage in the flanged joints and detecting damage in the body of the pipe, such as cracks and corrosion damage. To demonstrate this principle, a simple pulse-echo measurement was made using the center section of the apparatus from the previous sections of this chapter. The pulse-echo measurement presented here was essentially the same as the pulse-echo measurements presented in Chapter 3.

6.5.2 Apparatus and experimental procedure

The MFC patch at axial location #2 of the pipeline structure used in the previous section, as seen in Figure 6.2, was now used to make a Lamb wave measurements. A pulse-echo measurement from axial location #2 was used merely as a demonstration that the same MFC patch which was used to detect joint damage in the previous section could now be used to detect corrosion damage to the main body of the pipe. Two pulse-echo measurements, one baseline and one damage case, were used to identify the presence of damage and determine its location.

In order to make a pulse-echo measurement from axial location #2, seven additional MFC patches were mounted around the circumference of the pipe at axial location #2. Because of space constraints, three of the patches were mounted in a ring with the existing patch at axial location #2, and the remaining four patches were mounted in a ring directly next to the first ring,

as seen in the photograph in Figure 6.11. Therefore, two circumferential rings of MFC patches were used to make the pulse-echo measurements. One ring was used as the actuator and the other as the sensor. Because the two rings were mounted at nearly the same axial location, the measurement was considered pulse-echo rather than pitch-catch.

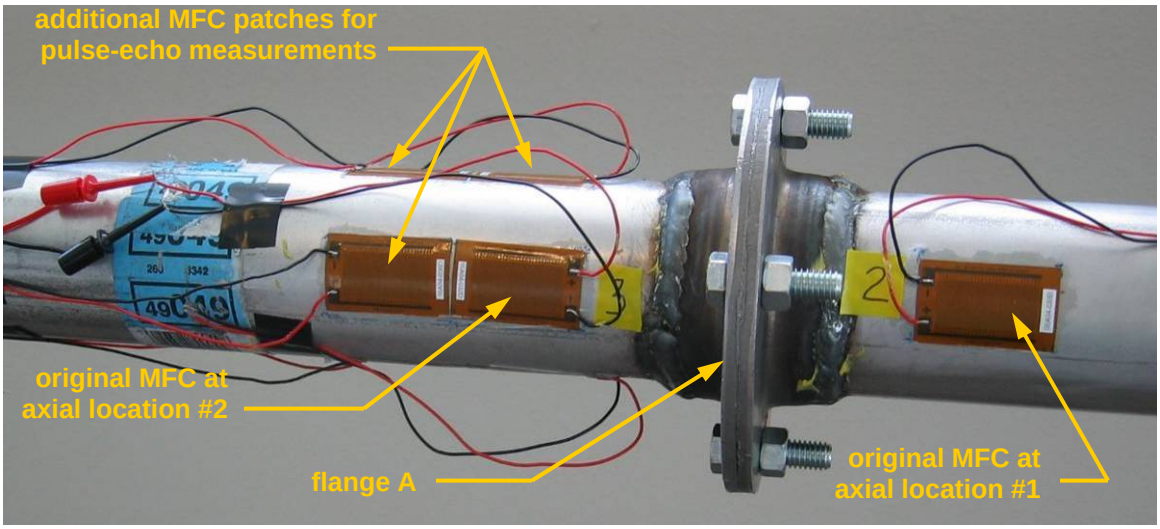

Figure 6.11: Additional MFC patches for pulse-echo measurements

6.5.3 Damage measurement and analysis

Using an excitation frequency of 70-kHz, a baseline measurement and a damage case measurement were taken. Damage was simulated by attaching two pipe clamps to the structure. The clamps were located on the middle pipe section 3.5-ft (1.1-m) from flange A. The results of the pulse-echo measurements were analyzed using the damage detection algorithm discussed in Chapter 4. The results for the absolute difference and percent difference are shown in Figure 6.12. Because a thorough evaluation of the baseline variations had not been performed, no threshold limit was available for determining the presence of damage. However, the reflection from the pipe clamps was so strong that its presence was very apparent in the plot of

the absolute difference between the wavelet coefficients of the baseline and damage case measurement.

The estimated time of arrival for the reflection from flange B was 0.76-ms, which corresponded to a group velocity of 1.84 x 10^4-ft/sec. The estimated time of arrival for the reflection from the damage was 0.37-ms. Using the group velocity and time of arrival for the damage reflection, the estimated location of the damage was 3.4-ft (1.0-m) from flange A, which was a 2.8% difference from the actual damage location. Therefore, this set of measurements demonstrated that the same MFC patch used for making impedance measurements to detect joint damage could also be used for Lamb wave measurements to detect damage in the main body of the pipe.

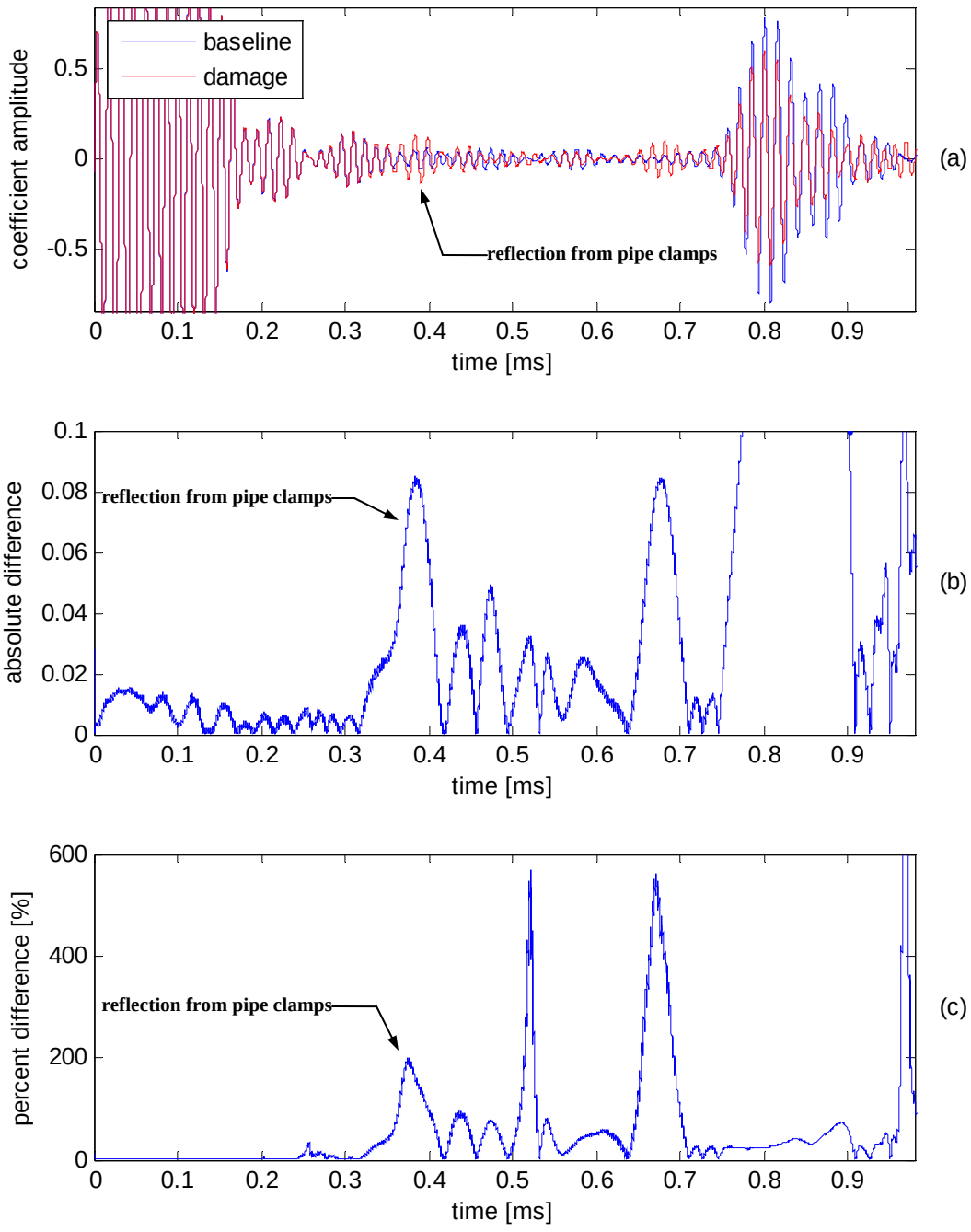

Figure 6.12: (a) Wavelet coefficients for a damage-case (2 pipe clamps) and a baseline measurement (b) difference between the signal envelopes (c) percent difference between the signal envelopes

6.5.4 Discussion

The brief set of Lamb wave measurements presented here involved the use of pulse-echo measurements to successfully detect and locate damage to the main body of the pipeline structure. The same MFC patches used for the pulse-echo measurements here were also used for the impedance measurements for detecting damage in the flanged joints, as presented at the beginning of this chapter. The successful implementation of Lamb wave methods with the same sensors shows that the dual use of the MFC patches is indeed possible. This ability is extremely important to the success of the proposed monitoring methods. In order to monitor the structural health of both the flanged joints and the body of the pipe, both impedance methods and Lamb wave methods are required. The localized nature of impedance measurements makes them insensitive to cracks and corrosion damage located near the opposite end of the pipe. However, the results presented above show that the impedance measurement were very effective at monitoring damage to the bolted joints. On the other hand, Lamb wave measurements were insensitive to damage to the bolted joints at the flanges. However, the pulse-echo measurements presented in the previous section show that they were very capable of detecting and locating cracks and corrosion damage along the entire length of the body of the pipe.

By implementing the flexible nature of MFC patches which enables them to be bonded directly to the curved surface of the pipe, the same set of transducers can be effectively used to evaluate both joint connection and corrosion damage. The importance of this approach cannot be over-emphasized. By enabling a single transducer to perform multiple tasks, the required number of transducers is reduced, which in turn reduces the cost to employ such a system. In addition, maintenance costs will decrease, and post-event assessments can occur rapidly using

the proposed methods. Therefore, the entire monitoring process can be simplified with the application of MFC patches to pipeline structures.

Chapter 7 Detecting deposits inside pipes

7.1 Overview

This chapter is a demonstration of the potential for monitoring the accumulation of fatty deposits on the interior surface of pipes. Previous types of damage addressed in the research of this thesis deal with structural defects such as cracks and corrosion. These types of damage involve defects which occur directly in the material of the pipe itself. Because such damage yields relatively strong reflections, the previous chapters demonstrated the use of pulse-echo methods to detect and locate the presence of damage. Another type of damage that also poses a threat to the functionality of a pipeline system is deposits on the interior surfaces. If left untreated, the accumulation of deposits can eventually lead to partial or complete clogging of flow through the pipe. Serious and costly problems can result from such clogging, including fire hazards and process interruption. Therefore, monitoring the accumulation of deposits inside pipelines can prove just as useful as monitoring the health of the pipeline itself.

Two techniques, Lamb wave methods and impedance methods, were implemented for the detection of the fatty deposits in this study. Because deposits on the surface of have much weaker reflections than cracks or corrosion, pitch-catch measurements were used rather than pulse-echo measurements. The presence of fatty deposits on the tube's surface was expected to change the characteristics of the propagated Lamb waves. These changes in the response signal could then be used to identify the presence of fatty deposits on the structure. However, the absence of strong reflections prevents the use of pulse-echo measurements and, therefore, the ability to locate the damage. As discussed in previous chapters, pitch-catch measurements can only indicate that the damage is located somewhere between the actuator and sensor.

As demonstrated with the bolted joints on the previous pipeline structure, the impedance method monitors the variations in structure's mechanical impedance, which is coupled with the electrical impedance of the MFC patch. The presence of fatty deposits on the surface of the pipe affects the mechanical impedance of the structure. These changes in the structure's mechanical impedance can also be used to identify the presence of deposits on the surface of the structure.

7.2 Apparatus

A copper tube was used as the test structure for detecting fatty deposits. The actual apparatus can be seen in the photograph in Figure 7.1. The tube was 32-in (81-cm) long with an outside diameter of 2-in (5-cm) and with a wall thickness of 1/16-in (1.6-mm). Two MFC patches were mounted to the tube, one near each end, and the copper tube was placed on closed-cell foam supports. Both MFC patches were mounted at the same circumferential location. A detailed view of one of the MFC patches can be seen in Figure 7.2. To simulate damage, which in this case was fatty deposits on the interior surface of the structure, a layer of vegetable shortening was applied to a portion of the tube's exterior surface. The exterior surface, rather than the interior surface, was used for ease of application.

Figure 7.1: Copper tube used as test structure

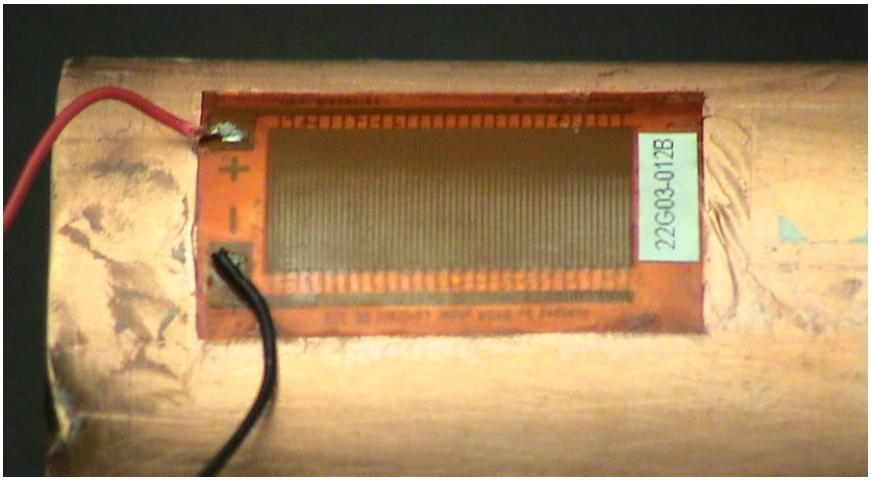

Figure 7.2: MFC patch, as mounted to the test structure

7.3 Experimental Procedure

In an effort to apply varying degrees of damage, the shortening was applied over various lengths of the pipe and at various thicknesses. The first damage case was a layer that was 1/8-in (3-mm) thick and 2-in (5-cm) long. The layer was centered along the axis of the tube. The second damage case was the same but with an increase in the thickness to 3/8-in (10-mm). The third damage case was 1/8-in (3-mm) thick and 6-in (15-cm) long. Again, the layer was centered along the axis of the tube. The fourth damage case was the same but with an increase in the thickness to 3/8-in (10-mm). Finally, the fifth and sixth damage cases were 3/8-in (10-mm) thick in lengths of 10 and 14-in (25 and 36-cm), respectively. These damage cases are summarized in Table 7.1 below, and a photograph of damage case 3 can be seen in Figure 7.3.

damage case	length of vegetable shortening [in (cm)]	thickness of vegetable shortening [in (mm)]
1	2 (5)	1/8 (3)
2	2 (5)	3/8 (5)
3	6 (15)	1/8 (3)
4	6 (15)	3/8 (5)
5	10 (25)	3/8 (5)
6	14 (36)	3/8 (5)

Table 7.1: Damage cases used for measurements

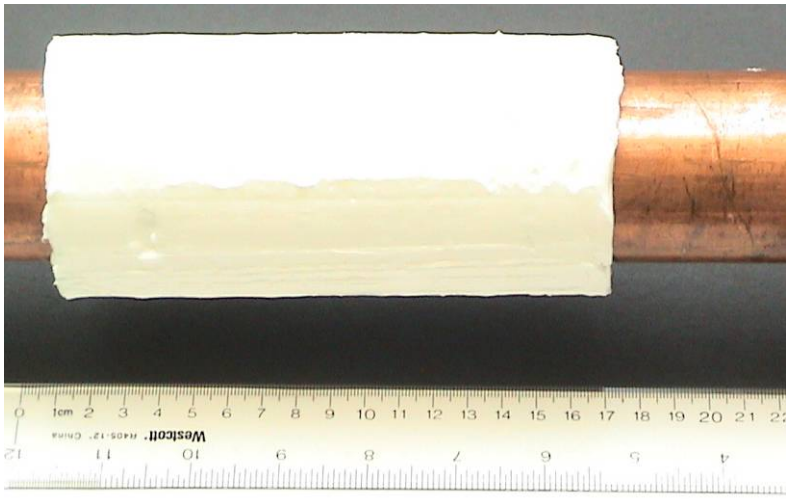

Figure 7.3: Layer of vegetable shortening for damage case 3

Before applying any of the damage cases, several baseline measurements for both Lamb wave and impedance methods were first taken to record the characteristics of the copper tube in a damage-free condition. These measurements provided a basis for the comparison of the subsequent damage cases. Once the baseline measurements were completed, vegetable shortening was applied to the exterior surface of the pipe according to the damage cases described above. Lamb wave and impedance measurements were then taken at the various stages of damage with each damage case.

7.4 Impedance measurements and analysis

For the impedance measurements, the MFC patch at the left end of the tube in the photograph in Figure 7.4 was used as both the actuator and sensor. An impedance analyzer, shown in Figure 7.4, was used to measure the electrical impedance of the MFC patch in the frequency range of 95 to 100-kHz. This range was chosen based upon the optimal response of the system as observed during initial setup of the experiment. The piezoelectric properties of the MFC patch made its electrical impedance coupled to the mechanical impedance of the structure.

Because the damage affected the mechanical impedance of the structure, the impedance measurements could be used to identify the presence of damage.

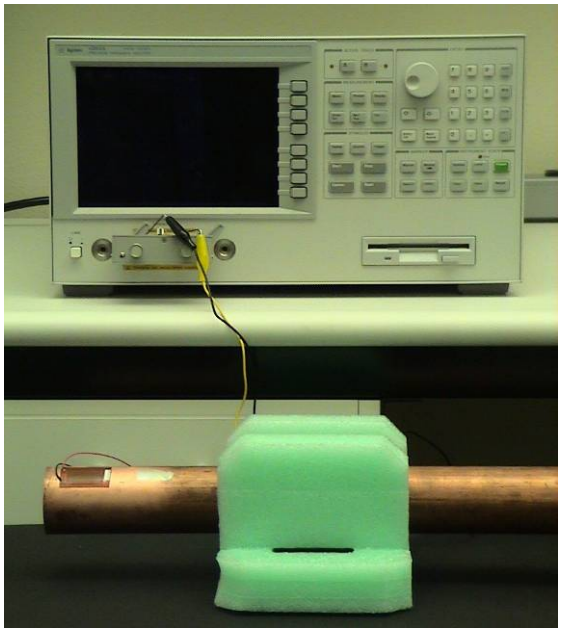

Figure 7.4: Test configuration for impedance measurements

The results of the impedance measurements over the full frequency range used for testing can be seen in Figure 7.5. To get a more detailed view of the results, a section of the data at the resonance near 96.9 and near 99.4-kHz can be seen in Figure 7.6 and Figure 7.7, respectively. In both of these figures the differences between the baseline measurement and the damage cases were much more apparent than in Figure 7.5. One can see that the magnitude of the real part of the impedance decreased as the relative amount of damage increased. Furthermore, the resonant frequencies decreased as the thickness and length of the shortening increased. The layer of vegetable shortening added mass to the system, which caused a decrease in the frequency of the resonances. This phenomenon, known as mass loading, was expected. The reduction in the response level seen in the damage cases was most likely caused by an increase in the damping in the system. The increase in damping was caused by the application of the vegetable shortening, which had a relatively high viscosity compared to the tube material.

Because the impedance measurements were made at relatively high frequency ranges, the changes in damping and mass loading were more easily identified than in conventional modal analysis, which typically uses a much lower frequency range (i.e. 5-Hz to 10-kHz). Furthermore, at such high frequency ranges, research has shown that the operational vibrations of the structure introduce no impact on the measured impedance, which is a clear advantage of the impedance method. (Wait, et al. 2005) Once the baseline data were available with the real structure, the impedance technique could correctly quantify the level of damage present in the system and warn to the operator whether a predetermined threshold limit has been reached. Experimental data from the actual system under known, preset conditions would be needed in order to determine this threshold limit.

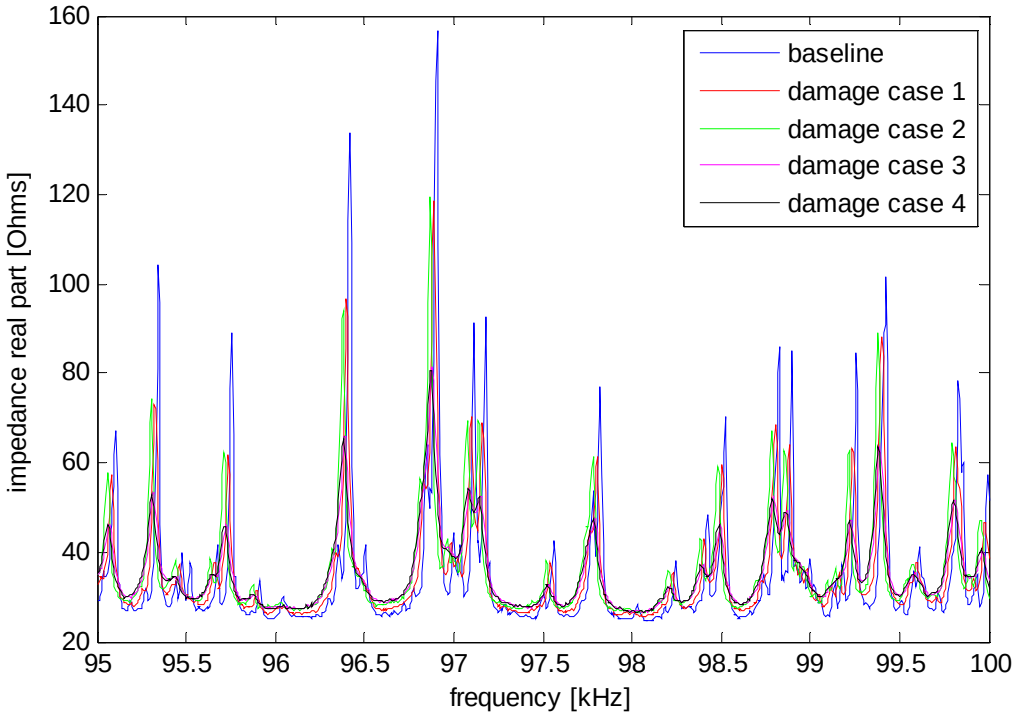

Figure 7.5: Impedance results for full frequency range measurements

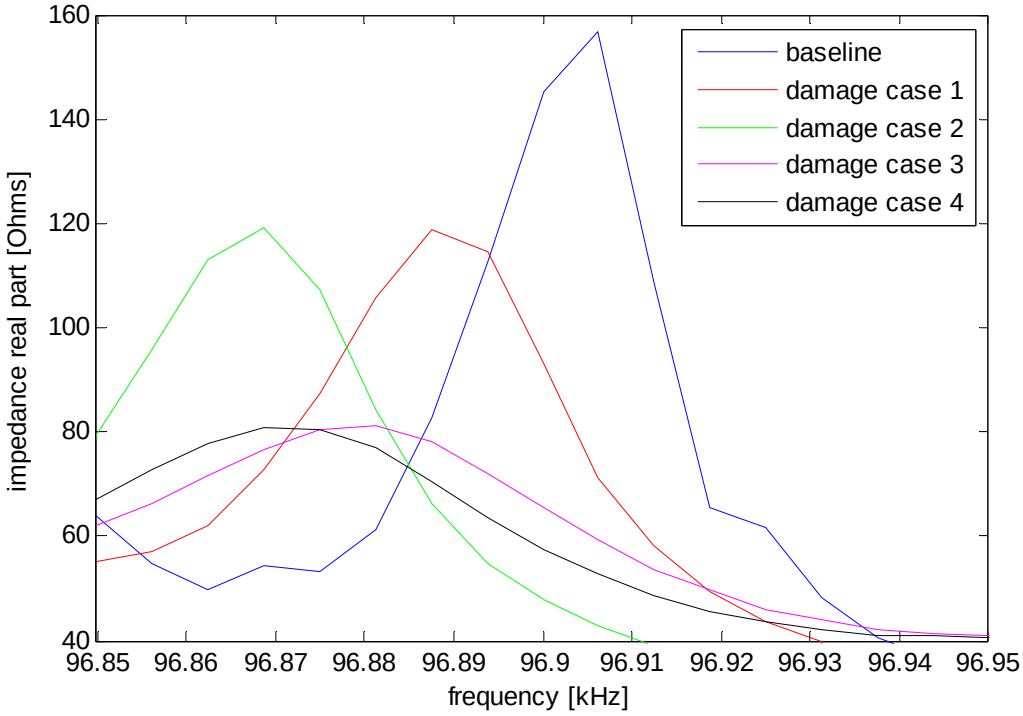

Figure 7.6: Detailed view of impedance measurements near resonance at 96.9-kHz

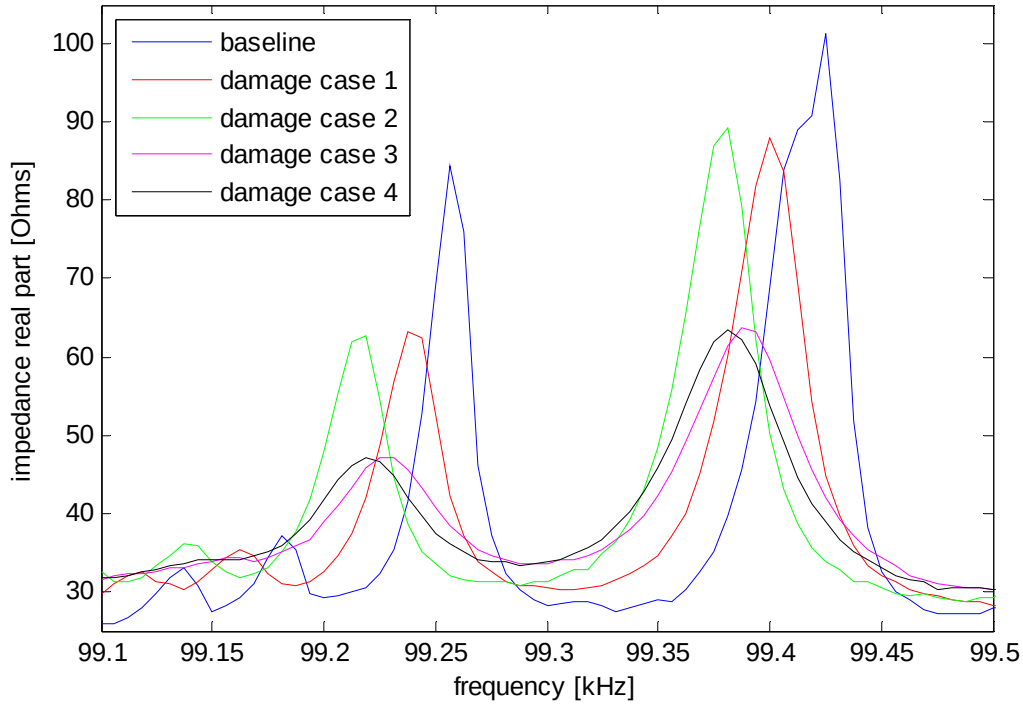

Figure 7.7: Detailed view of impedance measurements near resonance at 99.4-kHz

7.5 Pitch-catch measurements and analysis

For the Lamb wave measurements, the MFC patch at the left end of the tube in Figure 7.8 was the actuator, and the MFC patch at the right end of the tube was the sensor. The test configuration is shown in Figure 7.8, including the data acquisition system and an external signal amplifier. The actuator excited Lamb waves in the wall of the tube, and the sensor measured the corresponding response to the Lamb waves as they traveled down the length of the tube. The effect of the damage on the attenuation of the Lamb waves was then used to identify the presence of damage.

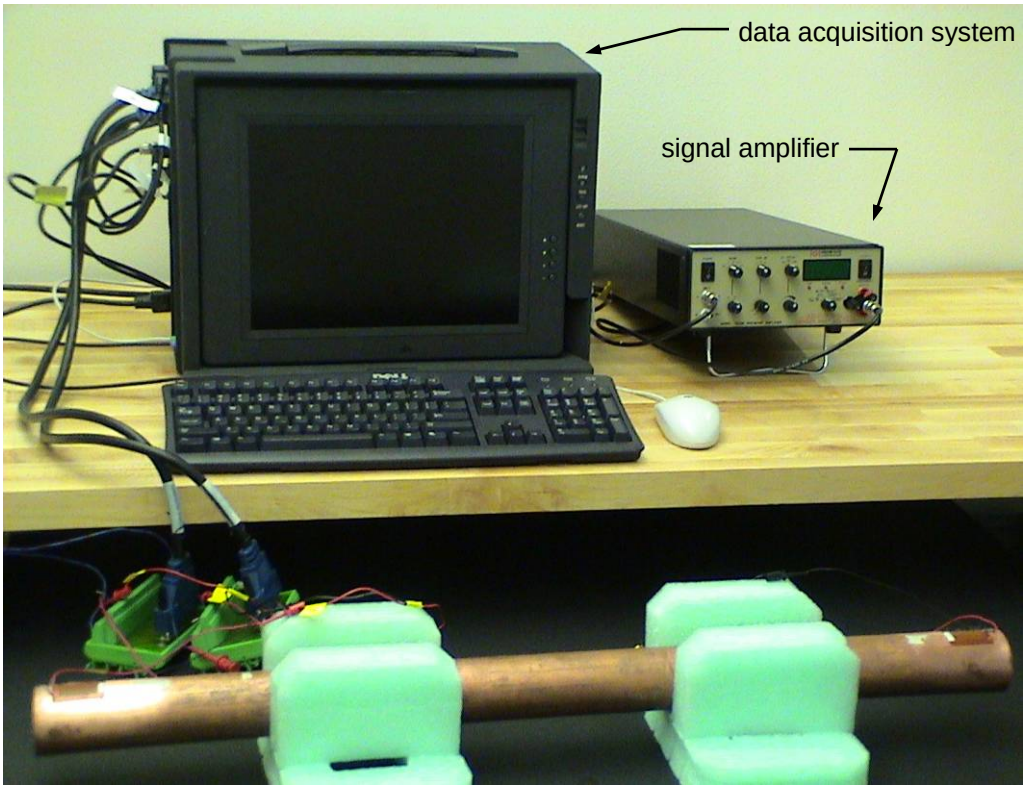

Figure 7.8: Test configuration for Lamb wave measurements

In Figure 7.9, the first arrival of Lamb waves, which corresponded to the mode with the highest group velocity, arrived at the sensor MFC at about 0.2-ms. Because the MFC patches were located very near each of the pipe ends, the sensor location and the reflection boundary are

considered to be the same. Several other modes arrived right after this mode. The first arrival showed distinct attenuation from the induced damage, which happened to be damage case 6 in this figure. After reflecting from both ends of the tube, this same mode from the first arrival arrived at the sensor MFC once again after 0.6-ms. The attenuation in the second arrival, however, was much more apparent than in the first arrival. The reason for the increase in attenuation was that the Lamb waves arriving at 0.7-ms had actually passed through the damaged section of pipe three times, where the Lamb waves in the first arrival had only passed through the damaged section once. A diagram of the paths traveled by the first and second arrivals can be seen in Figure 7.10.

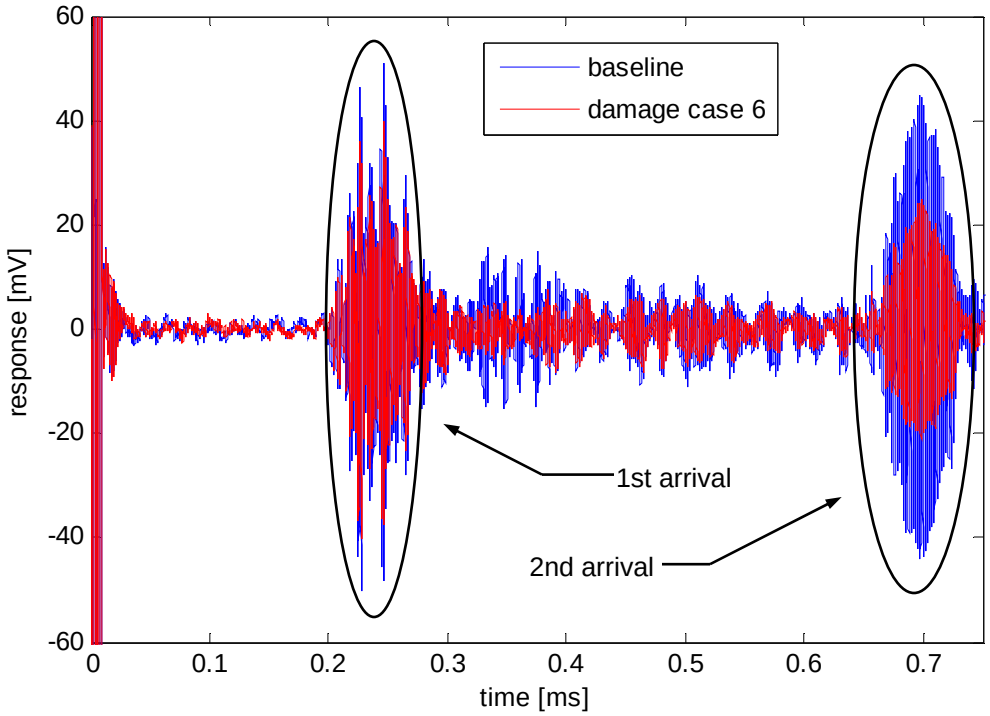

Figure 7.9: First and second arrivals for 500-kHz excitation

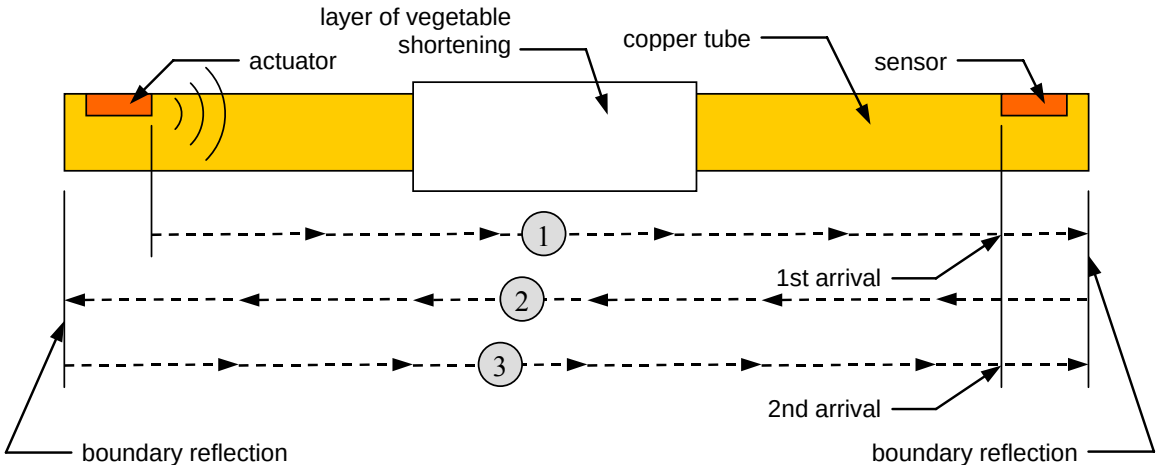

Figure 7.10: Diagram of Lamb wave propagation along tube, including reflections at boundaries

For the first four damage cases, an excitation frequency of 210-kHz was used. From visual inspection of the time histories from the responses, this frequency range did not seem to detect as significant of an amount of attenuation as one would expect from the relatively large amount of damping observed in the impedance measurements. An example from damage case 4 can be seen in Figure 7.11. For this reason, the excitation frequency was changed from 210-kHz to 500-kHz during measurements for damage case four. At 500-kHz the attenuation became much more apparent, as seen around 0.7-ms in Figure 7.12. Damage cases 5 and 6 were then measured at 500-kHz only.

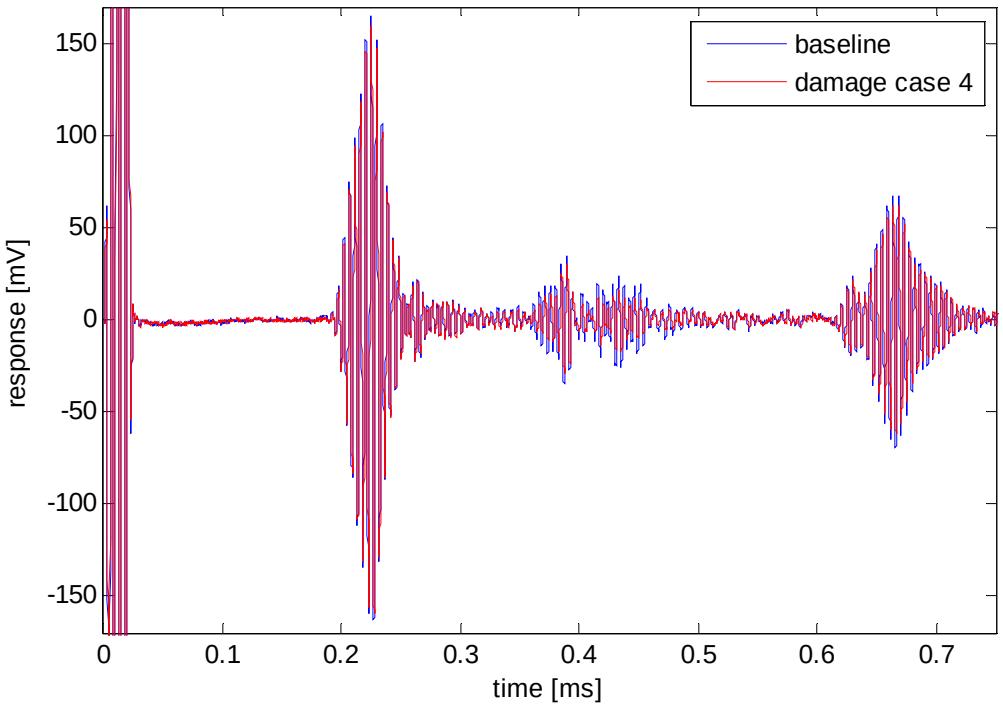

Figure 7.11: Lamb wave measurement for damage case 4 with 210-kHz excitation

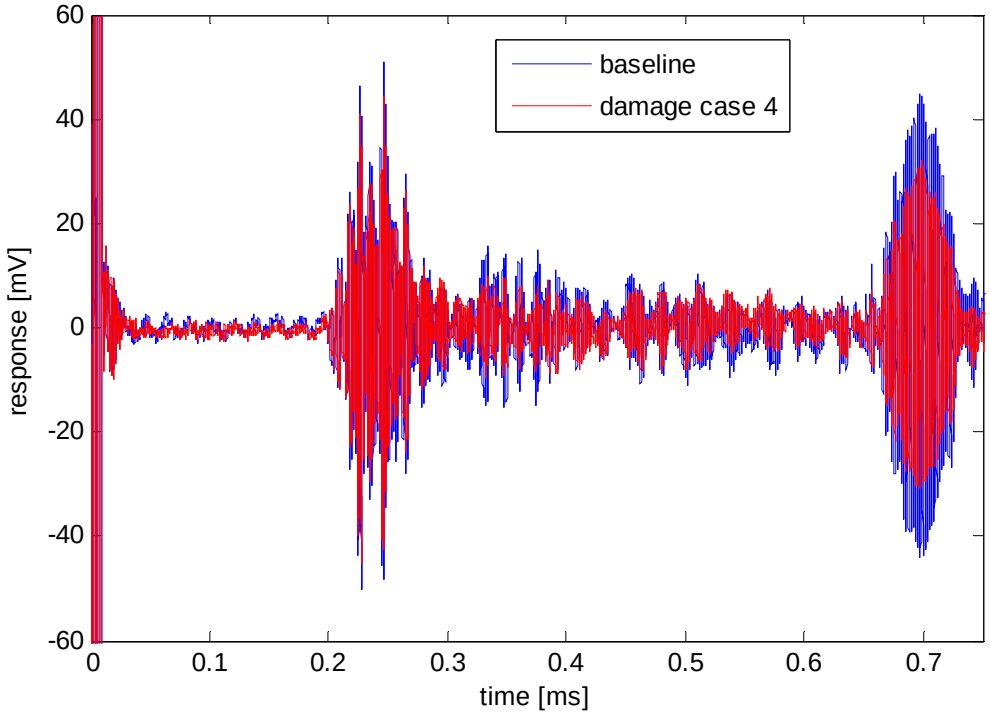

Figure 7.12: Lamb wave measurement for damage case 4 with 500-kHz excitation

From visual inspection of the time histories from the Lamb wave measurements, changes in the system caused by the damage were not as pronounced as in the results from the impedance methods. Therefore, the wavelet-based signal processing technique developed in Chapter 4 was applied to analyze the data. In this process, the wavelet transform was first used to obtain coefficients for the baseline signal. The coefficients corresponding to the input frequency, 210 or 500-kHz in this case, were extracted for additional signal processing. By looking at this filtered view of the transmitted energy from the actuator to the sensor at the input frequency, one can gain an insight into how the intensities of the input energy had been affected as a result of damage. This procedure was then repeated for a tested signal. Because pitch-catch measurements were used here, there were no reflections to be used for determining the location of the damage. Rather, only the attenuation characteristics in each of the arrivals were used to evaluate the presence of damage. Therefore, the Hilbert transform was not implemented as in Chapter 4. Instead, a damage metric based upon the ratio of the test signal's energy to that of the baseline signal's energy was used for evaluation. The range of damage metric was 0 to 1. Note that the value of damage metric was zero when there was no attenuation of the test signal when compared to the baseline signal, implying that no damage was present in the system. In addition, the value of the damage metric increased as the test signal attenuated more as a result of damage. This procedure was only performed over the time points that corresponded to the second arrival of Lamb waves, which was where the attenuation feature was the most pronounced, as discussed above. The results of this analysis for the 210 and 500-kHz measurements are shown in the following figures.

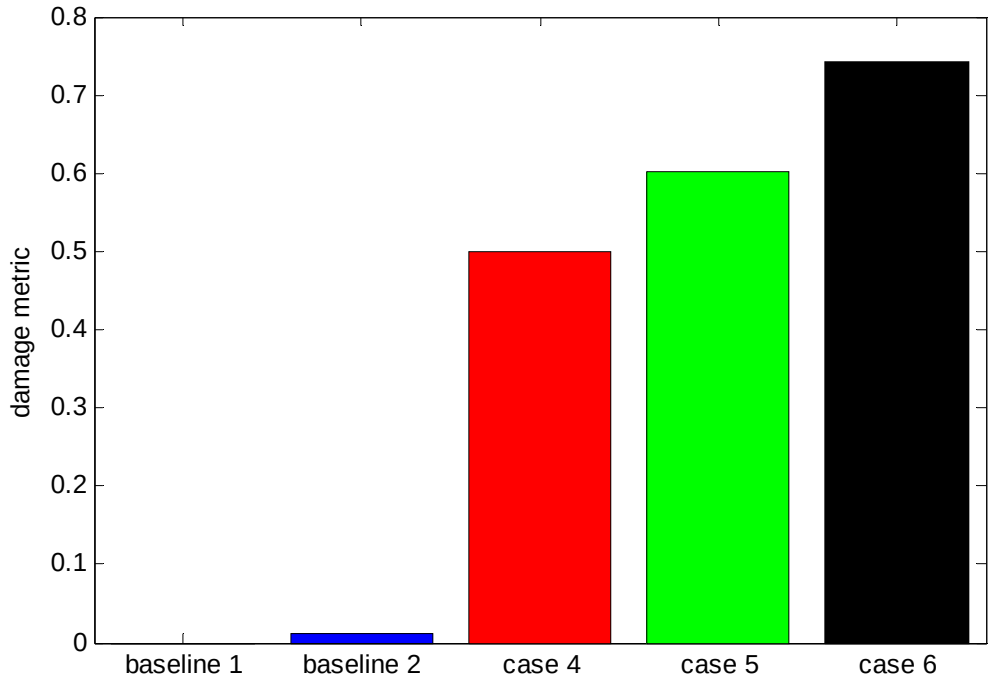

Figure 7.13: Damage metric for 500-kHz Lamb wave measurements

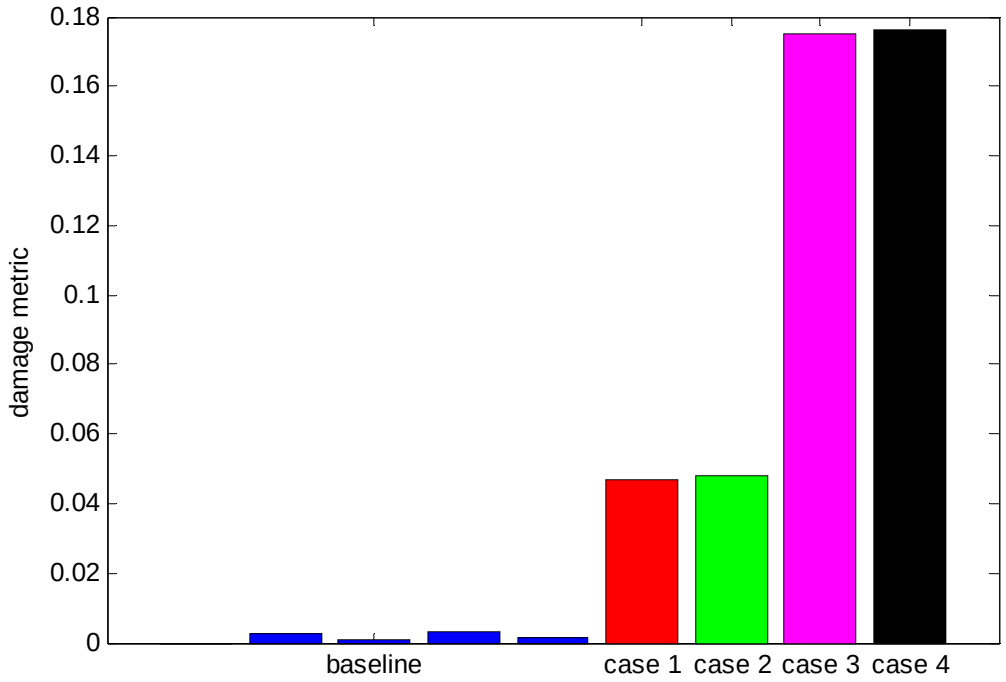

Figure 7.14: Damage metric for 210-kHz Lamb wave measurements

Because the baseline measurements were measured before any damage was introduced, they were very similar and, therefore, show only slight variation. Once damage was present in the system, however, the damage metric increased. Note that this increase in the damage metric was significantly larger in magnitude than the variation present in the baseline measurements. In addition, increasing levels of damage in a given measurement correlated to an increase in the value of the damage metric calculated for that measurement. The attenuation in the response was directly caused by the presence of damage, which in this case was the deposit of the vegetable shortening. The vegetable shortening affected the parameters of the system, slightly altering the propagation of the Lamb waves in the tube. The attenuation in the response can best be attributed to the increased damping that the vegetable shortening added to the system.

For damage case 1 in the 210-kHz measurement, in which a 2-in (5-cm) length of the tube was covered by the shortening, the damage metric was about 6 times greater than that of the baselines. When damage case 3, in which the length was increased to 6-in (15-cm), the damage metric was about 25 times greater than that of the baselines. This correlation shows that the Lamb wave technique correctly quantified the level of damage present in the system. However, increasing the thickness of the shortening did not have nearly as great of an affect on the Lamb waves, as shown by the relatively slight changes between case 1 and case 2 and between case 3 and case 4. This lack of effect was primarily caused by the fact that the shortening used in this study had very low stiffness. Hence, the increase in thickness did not necessarily affect the damping characteristics in the structure. The mass-loading effects, however, enabled the increase in thickness to be detected by the impedance measurements.

For the Lamb wave measurements with 500-kHz excitation, the changes between the damage cases and the baselines were at much higher levels than the changes seen in the 210-kHz

measurements. Again, the damage metric increased significantly as the length of the tube covered by the shortening increased. Most importantly, the overall levels of the damage metric in the 500-kHz measurements were much higher than those in the 210-kHz measurements. As a direct comparison, the damage metric for damage case 4 for the 500 and 210-kHz measurements was 0.74 and 0.17, respectively.

7.6 Discussion

The methods presented here demonstrate the capability to detect fatty deposits on the surface of a pipe. The impedance and Lamb wave techniques can correctly quantify the level of damage present in the system and warn the operator whether a predetermined threshold limit has been reached. The two techniques can be used in combination to detect the presence of deposits in a pipe and potentially quantify the thickness of the deposits. The impedance method was more sensitive to the thickness of the deposits than the Lamb wave method was, but the Lamb wave method was more sensitive to the area covered by the deposits than the impedance method. Because the same sensors are used for both methods, a combination of the two methods could easily be integrated for an effective detection system.

Chapter 8 Concluding remarks

8.1 Accomplishments

The research of this thesis has successfully demonstrated the benefit and feasibility of a structural health monitoring (SHM) system for pipeline networks. The economy of the United States is heavily dependent upon a vast network of pipelines for transportation of energy resources. As this network continues to age, monitoring and maintaining its structural integrity is of utmost importance. Although a few methods of nondestructive evaluation (NDE) are currently used in industry to perform this task, numerous accidents over the past several years have led to significant costs and fatalities, indicating that NDE techniques may not be sufficient. The implementation of a SHM system would enable pipeline operators to continuously monitor the structural integrity of their networks. By continuously monitoring the pipeline networks, the risks of catastrophic failure can be significantly reduced. In particular, damage which occurs over short time durations, such as that caused by excavation or earthquake events, can be tested immediately following the event to check if the pipeline's integrity was affected.

The ability of the proposed methods to effectively detect and locate damage demonstrates that a SHM system for pipelines is feasible. The proposed SHM system relies upon the deployment of macro-fiber composite (MFC) patches for the entirety of the sensor array. Two damage detection techniques, guided wave and impedance methods, are implemented using the MFC patches, avoiding the necessity for two separate sensor arrays. Because MFC patches are flexible and resilient, they can potentially be permanently bonded to the curved surface of a pipeline's main body. This permanent installation allows for the continuous monitoring of the

pipeline system and reduces the costs associated with implementing NDE techniques, such as excavation to gain direct access to the pipeline.

With the presented guided wave methods, Lamb wave techniques demonstrated the ability to correctly identify and locate the presence of damage in the main body of the pipeline system. Various forms of damage were used to simulate actual damage which might occur in an industrial setting. In particular, a saw cut was used to simulate a partial circumferential crack. An area of surface grinding was used to simulate corrosion or excavation damage. Finally, an electrolytic process was used to created actual corrosion on the pipe's surface. With the proposed damage detection algorithm, the Lamb wave methods were able to successfully detect and locate each of these forms of damage. With the presented impedance methods, active-sensing techniques demonstrated the ability to correctly identify and locate the presence of damage in the flanged joints of the pipeline system. Damage to the flanged joints of the pipeline was simulated by loosening one or more bolts on the flanges. With the proposed damage index, the impedance methods were able to successfully detect and locate deterioration of a particular flanged joint. The two proposed techniques are combined to assess the structural integrity of the entire pipeline system.

8.2 Thesis contribution

The primary contribution of this thesis is a first attempt at developing a SHM system for pipeline structures. Two damage detection techniques, guided wave and impedance methods, were implemented in the proposed system. Although previous research has developed and demonstrated the capabilities of these techniques for nondestructive evaluation (NDE), these techniques have not been successfully adapted to SHM applications involving pipeline systems.

While future issues still remain, the research of this thesis demonstrates the feasibility of commercially implementing a SHM system for pipeline structures.

Another contribution of this thesis is the use of MFC patches for a SHM system, particularly involving pipeline applications. The flexible nature of the MFC patch enables it to be mounted directly to the curved surface of the pipeline's main body. This transducer location allows the proposed system to exploit the dual purpose of the MFC patches for both guided wave and impedance methods. Therefore, the proposed SHM system can be used to monitor the structural integrity of the pipeline's main body and flanged joints.

8.3 Future work

Although the research of this thesis has proven the feasibility of a SHM system for pipeline structures, there are still a few future research issues which require attention before any commercial applications can be realized. First, the proposed damage detection methods need to be tested on a larger scale structure under real-world conditions. All experimental procedures presented in this thesis were performed in a laboratory environment. The suspension method used for each test apparatus simulated free-free boundary conditions. Further research is needed to assess the performance of the proposed methods under real-world boundary conditions and temperature variations. In addition, testing must be performed on a larger structure to determine the longest length of pipe which can be effectively monitored from a single pulse-echo array of MFC patches with Lamb wave methods. This length will help determine the density of the required sensor array for the overall SHM system.

A second issue which needs to be addressed is a method of self-diagnostics for MFC patches. If MFC patches are permanently bonded to a pipeline, then the performance of each individual MFC patch must be monitored to ensure that it is functioning properly. Over time, the

bonding condition between an MFC patch and the host structure will deteriorate. This deterioration will inevitably affect the performance of the particular MFC patch. If not properly identified and monitored, this altered performance could be falsely identified as damage to the pipeline structure. Therefore, the overall performance of the SHM system is dependent upon a reliable method of sensor self-diagnostics for each individual MFC patch.

Third, the proposed Lamb wave methods need to be refined to ensure that all potential damage types can successfully be detected and located. For example, the research of this thesis did not test the performance of the proposed methods for detecting cracks in the axial direction. The detection of such cracks may require the use of the torsional modes. Because no effective method for simulating a axial crack was available, no attempt was made to assess the performance of the proposed system with such damage. Also, the use of directional methods, such as phasing techniques, are needed to control the propagation direction. Without this control, the exact location of a reflection source cannot be specified if the transducer array is near the center of a relatively long section of pipe. In addition, the ability to extract mode properties from received signals may be required for sensing the mode conversions caused by certain types of damage, such as damage to the welded seams of the pipeline. Further, the proposed techniques can be developed to characterize the damage present in the pipeline system. With this information, an effort could then be made to estimate the remaining useful life, if any, of the damaged area. The proper measures for repairing the damaged section could then be determined.

Finally, the proposed SHM system is still a research topic. No effort has been made to commercialize this system. Before any industrial application of the proposed system can be realized, the techniques must be developed into a commercial package. Some of the steps

required include the development of a user friendly software interface and a standalone hardware arrangement. In addition, a better installation method for MFC patches is needed. The vacuum bagging process used in the research of this thesis for mounting the MFC patches to the various test articles is far too tedious for any manufacturing process. A more efficient method is needed which can be incorporated into the actual manufacturing process of the individual pipeline sections. With these additions, the proposed SHM system can provide the pipeline operator with the means to monitor and maintain the structural integrity of the pipeline network.

References

1. Achenbach, J. D. *Wave Propagation in Elastic Solids*. North-Holland Publishing Co., New York, 1984.
2. Alleyne, D. N., "The Excitation of Lamb Waves in Pipes Using Dry Coupled Piezoelectric Transducers." *Journal of NDE*. Vol. 15, No. 1: 11-20, 1996.
3. Alleyne, D. N., B. Pavlakovic, M.J.S. Lowe, P. Cawley. "Rapid Long-Range Inspection of Chemical Plant Pipework." *Insight: Non-Destructive Testing and Condition Monitoring*. Vol. 43, No. 2: 93-96, February, 2001.
4. Alleyne, D. N., M. J. S. Lowe, P. Cawley. "The inspection of chemical plant pipework using Lamb waves: Defect sensitivity and field experience." *Review of Progress in Quantitative NDE*. Vol. 15: 1859-1866, 1996.
5. Alleyne, D. N., M. J. S. Lowe, P. Cawley. "Reflection of guided waves from circumferential notches in pipes." *Journal of Applied Mechanics*. Vol. 65: 635-641, American Society of Mechanical Engineers, 1998.
6. Aristégui, C., M. J. S. Lowe, P. Cawley. "Guided Waves in Fluid-Filled Pipes Surrounded by Different Fluids." *Ultrasonics*. Vol. 39, No. 5: 367-375, 2001.
7. Barshinger, J., J. L. Rose, M. J. Avioli, Jr. "Guided Wave Resonance Tuning for Pipe Inspection." *Journal of Pressure Vessel Technology*. Vol. 124, No. 3: 303-310, August, 2002.
8. Brown, T. L., H. E. LeMay, Jr., B. E. Bursten. *Chemistry, the Central Science, Seventh Edition*. Prentice Hall, New Jersey, 1997.

9. Cawley, P., M. J. S. Lowe, D. N. Alleyne, B. Pavlakovic, P. Wilcox. "Practical Long Range Guided Wave Testing: Applications to Pipes and Rail." *Materials Evaluation*. Vol. 61, No. 1: 66-74, January, 2003.

10. Demma, A., P. Cawley, M. J. S. Lowe, A. G. Roosenbrand. "The Reflection of the Fundamental Torsional Mode from Cracks and Notches in Pipes." *Journal of the Acoustical Society of America*. Vol. 114, No. 2, August, 2003.

11. Demma, A., P. Cawley, M. J. S. Lowe, A. G. Roosenbrand. "The Reflection of Guided Waves from Notches in Pipes: A Guide for Interpreting Corrosion Measurements." *NDT&E International*. Vol. 37, No. 3: 167-180, 2004.

12. Doebling, S.W., C.R. Farrar, M.B. Prime. "A Summary Review of Vibration-Based Damage Identification Methods." *Shock and Vibration Digest*. Vol. 30: 91-105, 1998.

13. Farrar, C.R.., N.A.J. Lieven, M.T. Bement. "An Introduction to Damage Prognosis." *Damage Prognosis for Aerospace, Civil and Mechanical Systems*. Edited by D.J. Inman, C.R. Farrar, V. Lopes, Jr., V. Steffen, Jr. John Wiley and Sons Ltd, West Sussex, England, 2005.

14. Graff, K. F. *Wave Motion in Elastic Solids*. Dover Publications, Inc., New York, 1991.

15. Kessler, S. S. *Piezoelectric-based In-situ Damage Detection of Composite Materials for Structural Health Monitoring Systems*. Ph.D. Dissertation, Massachusetts Institute of Technology, Massachusetts, 2002.

16. Lamb, Horace. "On Waves in an Elastic Plate." *Proceedings of the Royal Society of London*. 1917.

17. Liang, C., F.P. Sun, C.A. Rogers. "Coupled Electromechanical Analysis of Adaptive Material Systems – Determination of the Actuator Power Consumption and System Energy Transfer." *Journal of Intelligent Material Systems and Structures*. Vol. 5: 12-20, 1994.

18. Lowe, M. J. S., D. N. Alleyne, P. Cawley. "Defect Detection in Pipes Using Guided Waves." *Ultrasonics*. Vol. 36, No. 1-5: 147-154, 1998.

19. Lowe, M. J. S., D. N. Alleyne, P. Cawley. "The Mode Conversion of a Guided Wave by a Part-Circumferential Notch in a Pipe." *Journal of Applied Mechanics*. Vol. 65, No. 3: 649-56, September, 1998.

20. Lu, C.J., Y.T. Hsu. "Application of wavelet transform to structural damage detection." *Shock and Vibration Digest*. Vol. 32, No. 1: 50, 2000.

21. Miklowitz, J. *The Theory of Elastic Waves and Waveguides*. North-Holland Publishing Co., New York, 1978.

22. National Transportation Safety Board. *Natural Gas Pipeline Rupture and Fire Near Carlsbad, New Mexico, August 19, 2000*. Pipeline Accident Report NTST/PAR-03/01. Washington, D.C., February, 2003.

23. National Transportation Safety Board. *Pipeline Rupture and Subsequent Fire in Bellingham, Washington, June 10, 1999*. Pipeline Accident Report NTSB/PAR-02/02. Washington, D.C., October, 2002.

24. Office of Pipeline Safety. "Frequently Asked Questions." <http://primis.phmsa.dot.gov/comm/FAQs.htm>. Pipeline and Hazardous Materials Safety Administration, 2005.

25. Office of Pipeline Safety. "Pipeline Failure Causes." <http://primis.phmsa.dot.gov/comm/FailureCauses.htm>. Pipeline and Hazardous Materials Safety Administration, 2005.

26. Office of Pipeline Safety. "Pipeline Statistics." <http://ops.dot.gov/stats/stats.htm>. Pipeline and Hazardous Materials Safety Administration, 2005.

27. Park, G., H. Cudney, D.J. Inman. "Impedance-Based Health Monitoring Technique for Massive Structures and High-Temperature Structures." *Proceedings of Smart Structures and Materials 1999: Sensory Phenomena and Measurement Instrumentation for Smart Structures and Materials*. Vol. 3670: 461-469, The International Society for Optical Engineering (SPIE), 1999.

28. Park, G., H. Sohn, C.R. Farrar, D.J. Inman. "Overview of Piezoelectric Impedance-Based Health Monitoring and Path Forward." *The Shock and Vibration Digest*. Vol. 35, No. 6: 451-463, November, 2003.

29. Park, G., H.H. Cudney, D.J. Inman. "Feasibility of using impedance-based damage assessment for pipeline structures." *Earthquake Engineering and Structural Dynamics*. Vol. 30: 1463-1474. 2001.

30. Posakony, G.J., V.L. Hill. "Assuring the integrity of natural gas transmission pipelines." Topical Report, Gas Research Institute, GRI-91/0366, November, 1992.

31. Rose, J. L. "A Baseline and Vision of Ultrasonic Guided Wave Inspection Potential." *Journal of Pressure Vessel Technology*. Vol. 124. American Society of Mechanical Engineers, August, 2002.

32. Rose, J. L. *Ultrasonic Waves in Solid Media*. Cambridge University Press, 1999.

33. Seco, F., J. M. Martín, A. Jiménez, J. L. Pons, L. Calderón, R. Ceres. "PCDISP: A Tool for the Simulation of Wave Propagation in Cylindrical Waveguides." *Proceedings of the 9th International Congress on Sound and Vibration*. July, 2002.

34. Silk, M. G., K. F. Bainton. "The propagation in metal tubing of ultrasonic wave modes equivalent to Lamb waves." *Ultrasonics*. Vol. 17, No. 1: 11-19, January, 1979.

35. Spanos, P.D., G. Failla. "Wavelets: Theoretical concepts and vibrations related applications." *Shock and Vibration Digest*. Vol. 35: 359-375. 2005.

36. Staszewski, W.J. "Structural and mechanical damage detection using wavelets." *Shock and Vibration Digest*. Vol. 30: 457-472, 1998.

37. Stokes, J.P. and G.L. Cloud. "The Application of Interferometric Techniques to the Nondestructive Inspection of Fiber-Reinforced Materials." *Experimental Mechanics*. Vol. 33: 314-319, 1993.

38. Sun, F.P., Z. Chaudhry, C. Liang, C.A. Rogers. "Truss Structure Integrity Identification Using PST Sensor-Actuator." *Journal of Intelligent Material Systems and Structures*. Vol. 6: 134-139, 1995.

39. Tucker, Raymond W., Stephen W. Kercel, Venugopal K. Varma. "Characterization of gas pipeline flaws using wavelet analysis." *Proceedings of the Sixth International Conference on Quality control by Artificial Vision*. Vol. 5132: 485-493, The International Society for Optical Engineering (SPIE), 2003.

40. United States National Energy Policy Development Group. *Reliable, Affordable, and Environmentally Sound Energy for America's Future: Report of the National Energy Policy Development Group*. Technical Report Number 061-000-00955-8. Washington, D.C., May, 2001.

41. Wait, J.R., G. Park, C.R. Farrar. "Integrated Structural Health Assessment using Piezoelectric Active Sensors." *Shock and Vibration Digest*, accepted for publication, 2005.

42. Wilkie, W.K., R.G. Bryant, J.W. High, et al. "Low-Cost Piezocomposite Actuator for Structural Control Applications." *Proceedings of the SPIE 7th Annual International Symposium on Smart Structures and Materials*. Newport Beach, CA, 2000.

43. Williams, R.B. *Nonlinear Mechanical and Actuation Characterization of Piezo-ceramic Fiber Composites*. Ph.D. Dissertation, Virginia Polytechnic Institute and State University, Virginia, 2004.

44. Worden, K., J. M. Dulieu-Barton. "An Overview of Intelligent Fault Detection in Systems and Structures." *Structural Health Monitoring*. Vol. 3, No. 1: 85-98, 2004.

45. Worlton, D.C. "Experimental Confirmation of Lamb Waves at Megacycle Frequencies." *Journal of Applied Physics*. Vol. 32, No. 6: 967-971, 1961.

Appendix A Damage detection algorithm for Lamb wave methods

As discussed in Chapter 4, the damage detection algorithm for Lamb wave methods is based upon the Wavelet and Hilbert transforms. Though the general theory of the algorithm has already been discussed, a detailed explanation of the actual algorithm is given in this appendix.

The damage detection algorithm was used to compare a current measurement from a damage case to a previous measurement from a baseline, or undamaged, state. In the algorithm, the data from each measurement were treated identically. The algorithm begins with the time history data from two measurements, one baseline and one damage case. First, the Continuous Wavelet Transform (CWT) was used to de-noise each of the signals. (Spanos et al. 2005; Lu and Hsu, 2000; Staszewski, 1998) Because of its similarity in shape to the excitation signal, the Morlet wavelet was used as the mother wavelet in the CWT. The wavelet coefficients corresponding to the excitation frequency of 100-kHz were then extracted (NOTE: The actual wavelet scale is dependent upon the sampling frequency). Second, the amplitude of each of the signals was normalized. To assure a proper amplitude, the peak of the immediate reflection from the near end of the pipe was used for normalization because none of the damage cases implemented in this research involved the area of the pipe between axial location #1 and the near end. Third, the Hilbert transform was used to find the envelope of each of the normalized signals. The magnitude of the complex Hilbert coefficients was used to determine the signal envelope.

Once the signal envelope of each measurement was found, the two were then compared to each other to determine the signal difference. Two comparison methods were used. The first method was based on the absolute difference between the two signal envelopes. The absolute

difference was formulated by subtracting the damage case signal envelope at each time point from the baseline signal envelope at the same time point and then finding the absolute value of the difference. The second method was based on the percent difference between the two signal envelopes. The percent difference was formulated by dividing the absolute difference at each time point by the magnitude of the baseline signal envelope at the same time point. A flow chart for the damage detection algorithm is given in Figure A.1.

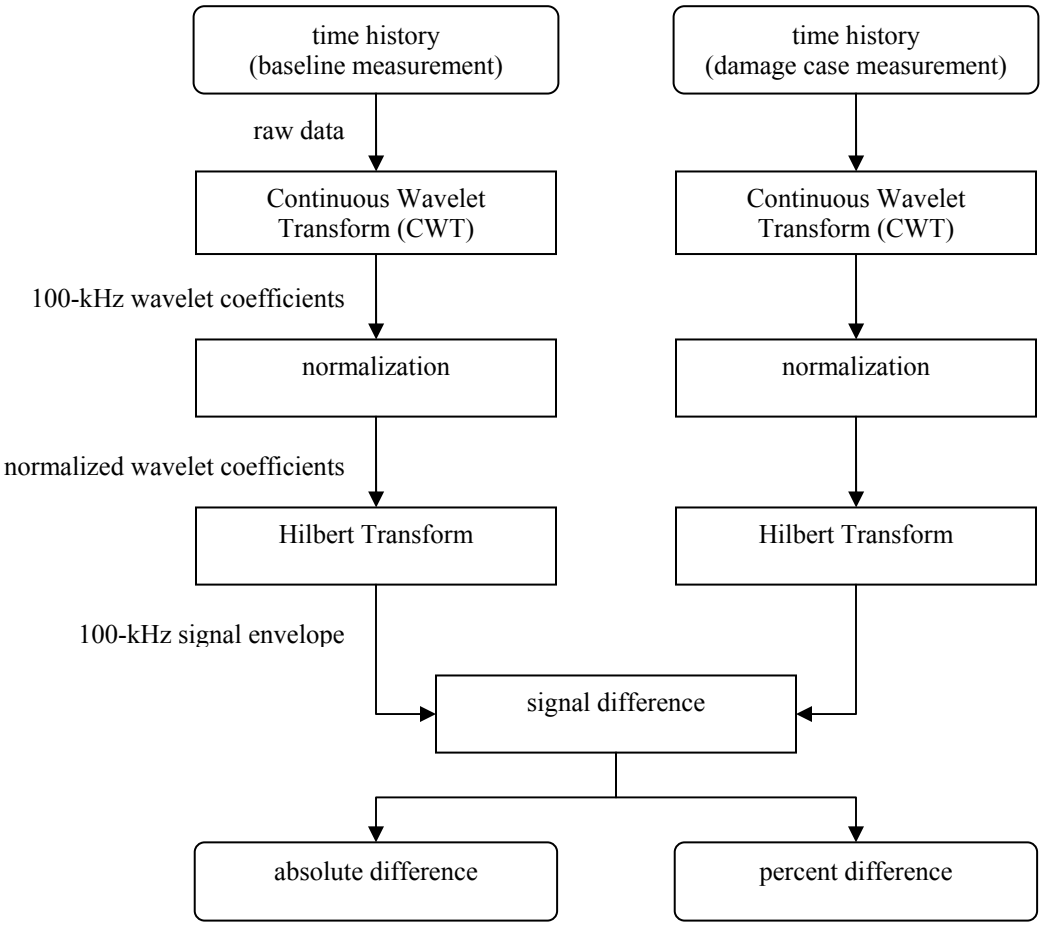

Figure A.1: Flow chart for damage detection algorithm